The white paper

I. G. Aznauryan,[1,2] V. Braun,[3] S. J. Brodsky,[4,5] V. Burkert,[2] Ian C. Cloët,[6] Robert G. Edwards,[2] M.M. Giannini,[7,8] R. W. Gothe,[9] Huey-Wen Lin,[10] P. Kroll,[11,3] T.-S. H. Lee,[12] V. Mokeev,[2,13] M. T. Peña,[14,15] G. Ramalho,[14] Craig D. Roberts,[12] E. Santopinto,[8] F. De Teramond,[16] K. Tsushima,[6] and David J. Wilson[12]

[1]*Yerevan Physics Institute, Yerevan, Armenia*
[2]*Thomas Jefferson National Accelerator Facility, Newport News, USA*
[3]*Institut für Theoretische Physik, Universität Regensburg, 93040 Regensburg, Germany*
[4]*Stanford National Accelerator Laboratory, Stanford University, Stanford, USA*
[5]*CP3-Origins, Southern Denmark University, Odense, Denmark*
[6]*CSSM and CoEPP, School of Chemistry and Physics University of Adelaide, Adelaide SA 5005, Australia*
[7]*Dipartimento di Fisica, Università di Genova, Italy*
[8]*Istituto Nazionale di Fisica Nucleare, Sezione di Genova, Italy*
[9]*University of South Carolina, Columbia, USA*
[10]*Department of Physics, University of Washington, Seattle, WA 98195, USA*
[11]*Fachbereich Physik, Universitĺat Wuppertal, 42097 Wuppertal, Germany*
[12]*Physics Division, Argonne National Laboratory, Argonne IL 60439 Department of Physics, Illinois Institute of Technology, Chicago, Illinois 60616*
[13]*Skobeltsyn Institute Nuclear Physics at Moscow State University, 119899 Moscow, Russia*
[14]*CFTP, IST, Universidade Tecnica de Lisboa, Portugal*
[15]*Physics Dept., Universidade Tecnica de Lisboa, Portugal*
[16]*Universidad de Costa Rica, San José, Costa Rica*

I. INTRODUCTION AND MOTIVATION

The studies of electromagnetic amplitudes for the transitions between ground and excited nucleon states, the so-called $\gamma_v NN^*$ electrocouplings, and their evolution with photon virtualities Q^2 represent an important avenue in the broad adventure to explore the strong interaction in the non-perturbative regime [1–5, 263]. The strong interaction dynamics in the non-perturbative domain represents the most important sector of the Standard Model we have to explore. We need to study the non-perturbative strong interaction in order to understand how QCD generates the real world of mesons, baryons, and atomic nuclei, as well as how their color-neutral strong interactions emerge from QCD. More than 98% of hadron masses are generated non-perturbatively, while the Higgs mechanism only accounts for less than 2% of the light-quark baryon masses. Higgs mechanism is almost irrelevant for the bulk of hadronic mass in the universe.

The studies of the non-perturbative strong interaction represent an enormous challenge. Never before having hadron structure studies we been confronted with the matter whose elementary components, current quarks and gauge gluons, are not these degrees-of-freedom accessible in experiment. Dressing of current quarks and gauge gluons with a cloud of virtual gluons and qq-bar pairs in the regime of large quark-gluon coupling generates so-called dressed quarks and gluons with momentum (distance) dependent dynamical mass and structure. The non-perturbative interaction of dressed quarks and gluons becomes very complex and entirely different than in the pQCD regime. In the evolution of the strong interaction from pQCD regime of almost pointlike and weakly coupled, massless quarks and gluons (distances $< 10^{-15}$ cm) to the non-perturbative regime, where dressed quarks and gluons acquire dynamical mass and structure (distances $\approx 10^{-13}$ cm), two major non-perturbative phenomena emerge: a) quark-gluon confinement and b) Dynamical Chiral Symmetry Breaking (DCSB). They both are completely outside of the pQCD scope and can not be described within any order of a pQCD expansion. How the confinement and the DCSB emerge from QCD remains a challenging problem of the contemporary hadron physics, which is being addressed in the studies of the $\gamma_v NN^*$ electrocouplings.

Non-perturbative strong interaction is responsible for the formation of hadrons as bound systems of quarks and gluons. Experimental studies of hadron structure at different distances carried out in close connection with QCD-based theory offer a promising way to access the essence of strong interaction in non-perturbative regime. Particularly the extraction of $\gamma_v NN^*$ electrocouplings from the data on meson electroproduction off nucleons [7–9] help to promote these efforts.

In a first round a very productive experiments with CLAS detector at Jefferson Lab (JLAB)in the broad area of hadron spectroscopy and hadron structure has been completed successfully. The experimental results obtained with CLAS provide for the first time information on inclusive, semi-inclusive, and fully exclusive reactions off nucleons and nuclei, which extends enormously the capabilities to explore confinement and DCSB in both mesons and baryons. The CLAS detector is a unique large-acceptance instrument that was designed for the comprehensive exploration of exclusive meson electroproduction off nucleons. It offered excellent opportunities to study the electroexcitation of nucleon resonances in detail and with precision. The CLAS detector has provided the dominant portion to the world data set on meson electroproduction in the resonance excitation region [7, 8, 12–14, 275, 276]. The electroexcitation amplitudes for the low-lying resonances $P_{33}(1232)$, $P_{11}(1440)$, $D_{13}(1520)$, and $S_{11}(1535)$ were determined over a wide range of Q^2 in independent analyses of $\pi^+ n$, $\pi^0 p$, and $\pi^+\pi^- p$ electroproduction channels [25, 26]. They are complemented by the preliminary results on electrocouplings of high-lying resonances with masses above 1.6 GeV [27]. The $\pi^+ n$, $\pi^0 p$, and $\pi^+\pi^- p$ exclusive channels are major contributors to the meson electroproduction in the resonance excitation region. The non-resonant mechanisms

in single- and double-pion exclusive channels are completely different, while $\gamma_v NN^*$ electrocouplings should be the same in all exclusive channels. Therefore, a successful description of measured observables in all aforementioned exclusive channels with the same $\gamma_v NN^*$ electrocouplings values confirms that they can be reliably determined in independent analyses of the experimental data on different exclusive electroproduction channels [25, 26]. A resonance electrocoupling extraction in a combined multi- channel analysis of the $N\pi$, $N\eta$, and KY channels within the framework of the advanced EBAC-DCC coupled channel approach is in progress [28, 29].

The CLAS data on the $P_{33}(1232)$, $P_{11}(1440)$, $D_{13}(1520)$ and $S_{11}(1535)$ electrocouplings, when compared to the predictions of relativistic light front quark models [17, 18] and the results on the N^* meson-baryon dressing amplitudes from the advanced EBAC-DCC coupled channel analysis [19] shed light on the relevant components in the structure of N^*-states at different distance scales. It was found that the structure of nucleon resonances in the mass range M $<$ 1.6 GeV is determined by contributions from both: a) an internal core of three dressed quarks and b) an external meson-baryon cloud. As an example, these contributions to the structure of the $P_{11}(1440)$ and $D_{13}(1520)$ states are shown in Fig. 1. The absolute values of meson-baryon dressing amplitudes are maximal at $Q^2 < 1.0$ GeV^2. They decreases with Q^2 and in the region $Q^2 > 1.0$ GeV^2 a gradual transition to the dominance of quark degrees of freedom occurs, as indicated by the better description of the $P_{11}(1440)$ and $D_{13}(1520)$ electrocouplings within the framework of quark models.

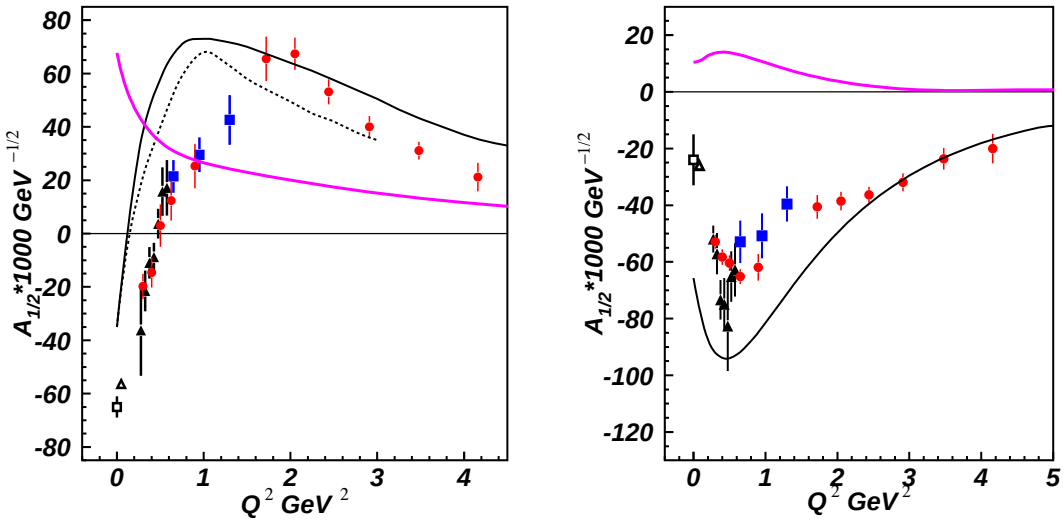

FIG. 1: (color online) (Left) The $A_{1/2}$ electrocoupling of the $P_{11}(1440)$ state from the analyses of the $N\pi$ electroproduction data [25] (circles), $\pi^+\pi^- p$ electroproduction data [275] (triangles), and preliminary results from the $\pi^+\pi^- p$ electroproduction data at Q^2 from 0.5 to 1.5 GeV^2 [276] (squares). The photocouplings are taken from RPP [15] (open square) and the CLAS data analysis [284] (open triangle). Predictions from relativistic light front quark models [17, 18] are shown by black solid and dashed lines, respectively. Absolute values of meson-baryon cloud amplitudes from the EBAC-DCC coupled channel analysis [19] are shown by magenta thick solid line. (Right) The $A_{1/2}$ electrocoupling of the $D_{13}(1520)$ state. The data symbols are the same as in the left panel. The results of the hypercentral constituent quark model [20] and absolute values of meson-baryon dressing amplitudes [19] are presented by the black thin and magenta thick solid lines, respectively.

At photon virtualities $Q^2 > 5.0$ GeV^2 the quark degrees of freedom are expected to dominate the N^* structure [5]. Analyses of available CLAS data [25, 26] strongly suggest that photons of high virtualities should penetrate the external meson-baryon cloud and interact mostly with the internal quark core. This expectation is supported by the high Q^2-behavior of $\gamma_v p N^*$ electrocouplings shown in Fig. 2, where the electrocoupling values scaled with the power of Q expected from constituent counting rules are plotted. The possible onset of scaling seen at $Q^2 > 3.0$ GeV^2 is likely related to the preferential interaction of the photon with dressed quarks, while the meson-baryon cloud causes strong deviations from this scaling behavior at smaller photon virtualities.

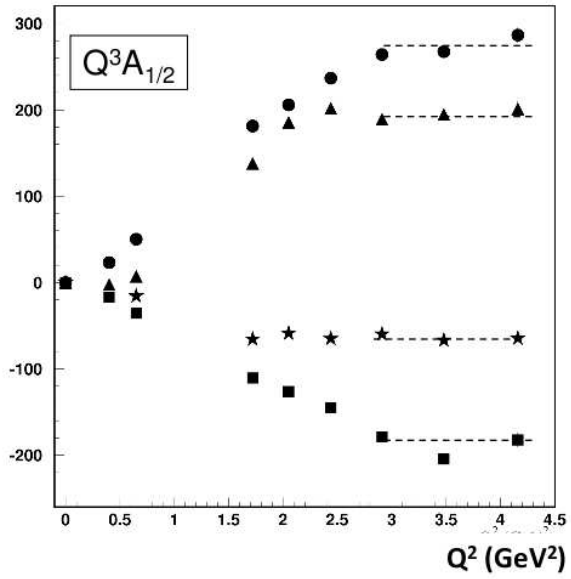

FIG. 2: The $A_{1/2}$ electrcouplings of $P_{11}(1440)$ (triangles), $D_{13}(1520)$ (squares), $S_{11}(1535)$ (circles), and $F_{15}(1685)$ (stars) scaled with Q^3 from the CLAS data analysis [25].

Therefore, in the $\gamma_v p N^*$ electrocoupling studies at $Q^2 > 5.0$ GeV^2, quark degrees of freedom in the N^* structure will be for the first time accessible directly from the experiment under small or even negligible contributions from the external meson-baryon cloud. This is a new and fully unexplored regime in the electroexcitation of nucleon resonances.

A dedicated experiment E12-09-003 on the N* studies in exclusive meson electroproduction off protons with the CLAS12 detector is scheduled within the first five years of running after the completion of the JLab 12-GeV Upgrade Project [263]. By measuring the differential cross sections for the electroproduction of exclusive single-meson and double-pion off protons, this experiment seeks to extract the electrocouplings of all prominent N^*-states in the still unexplored domain of photon virtualties up to 12 GeV^2. As an example, the projected $A_{1/2}$ electrocouplings of $P_{11}(1440)$ at photon virtualities from 5 GeV^2 to 12 GeV^2 are shown in the right panel of Fig 3. Similar quality of the results is expected for electrocouplings of all other prominent N^*-states. The available reaction models for extraction of the resonance electrocouplings have to be extended toward these high photon virtualities with the goal to reliably extrac $\gamma_v p N^*$ electrocouplings from the new data on meson electroproduction off protons. In particular, the new reaction models have to account for a gradual transition from meson-baryon to quark degrees of freedom in the reaction mechanisms. The current status and the prospects of the reaction model developments are

discussed in the Chapter V

The anticipated results will provide the world's only foreseen the information on electrocouplings of prominent N*-states extracted from meson electroproduction channels with an unprecedented coverage of photon virtualities (5.0-12.0 GeV^2). The $\gamma_v pN^*$ electrocouplings measured at these photon virtualities offer access to the non-perturbative strong interaction of dressed quarks, which are responsible for the resonance formation and will map out the transition towards perturbative QCD. Furthermore, these results will also allow access the parton distributions in excited nucleon states.

Up to date our knowledge on parton distributions in baryons is limited to the ground state nucleons only. Advances in tLight Cone Sum Rules approaches opened up the prospects to constrain theoretical expectations for the quark distribution amplitudes (DA) in N^* states by employing the information on the Q^2-evolution of $\gamma_v NN^*$ electrocouplings (see Chapter II **??**). The extension of the covered area of photon virtualities up to 12 GeV^2 will enhance considerably the capabilities to explore partonic degrees of freedom of excited proton states. A particular interest is how different the quark DA are for the N^*-states that belong to parity doublets as N and $S_{11}(1535)$, $P_{33}(1232)$ and $D_{33}(1700)$, etcetera. These differences are closely related to the manifestation of DCSB in baryons. The data on $\gamma_v pN^*$ electrocouplings at high Q^2 will also allow us to further develop the GPD concept making it applicable for the transition between the ground and excited nucleon states and offering opportunities to map out the $N \to N^*$ transition densities in the 3D space.

In general, the studies of the N^* structure at high Q^2 address most the fundamental issues of the contemporary hadron physics:

1. What is confinement?

2. How is it tied with dynamical chiral symmetry breaking, the origin of more than 98% of all visible mass in the universe?

The data on $\gamma_v pN^*$ electrocouplings at 5.0 GeV$^2 < Q^2 <$ 12 GeV^2 offer a unique opportunity to explore the transition between confinement and pQCD regimes. Currently two conceptually different approaches, a) Lattice QCD (LQCD) and b)Dyson-Schwinger Equation of QCD, can be employed in order to interpret the experimental results on resonance electrocouplings starting from the first principles of QCD. Recent progress and the prospects of these approaches in the studies of the N^* structure are outlined in the Chapters I-III**??**.

The dressed quark mass as a functions of momenta running over quark propagator as calculated from DSE of QCD [21] and LQCD [22] is shown in Fig. 3 (left). The sharp increase from the mass of almost undressed current quarks (p $>$ 2.GeV) to dressed constituent quarks (p $<$ 0.4 GeV) clearly demonstrates that the dominant part of dressed quark and consequently hadron masses is generated by strong interactions non-perturbatively. Bulk of the dressed quark mass arises from a cloud of low momentum gluons attaching themselves to the current-quark in the regime where running quark-gluon coupling is large and which is completely outside of the pQCD scope. The region where the dressed quark mass increase stromgest, also represents the transition domain from pQCD (p $>$ 2. GeV) to confinement (p $<$ 0.4 GeV). A solution of the DSE gap-equation [23] shows the propagator pole in confinement regime leave real momentum axis, and the momentum squared p^2 of dressed quark becomes substantially different than the dynamical mass squared M(p)^2. This means, that the dressed quark in the confinement regime will never be on-shell as it is required for a free particle when it propagates in the space-time. Dressed quarks have to be strongly bound and locked inside the nucleon. Aforementioned dressing mechanisms are also responsible for DCSB.

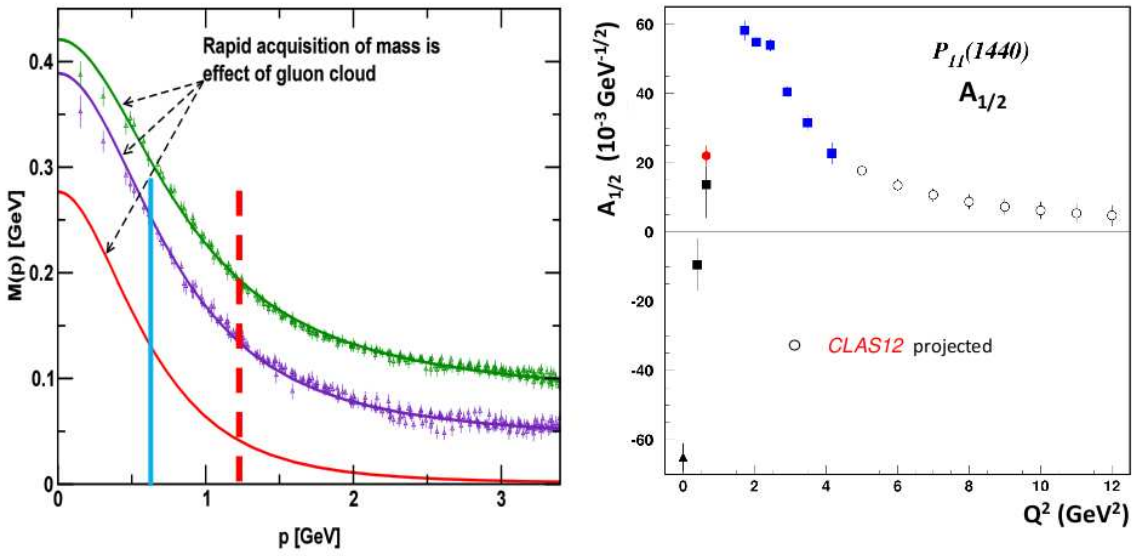

FIG. 3: (color on line) (Left) The mass function for the s-quark evaluated within the framework of LQCD [22] (points with error bars) and DSEQCD [21] (solid lines) for two values of bare masses: 70 MeV and 30 MeV, and shown in green and magenta, respectively. The chiral limit of zero bare quark mass, which is close to the bare masses of u and d quarks, is shown in red. Momenta p $<$ 0.4 GeV correspond to the confinement, while those at p $>$ 2. GeV corresponds to the regime which is close to pQCD. The areas accessible for mapping of the dressed quark mass function by the $\gamma_v NN^*$ electrocoupling studies with 6 GeV and 11 GeV electron beam are shown on the left of blue solid and red dashed lines, respectively. (Right) Available (filled symbols) and projected CLAS12 [263] (open symbols) $A_{1/2}$ electrocouplings of the $P_{11}(1440)$ state.

Studies of the transition area from confinement to pQCD via the Q^2-evolution of resonance electrocouplings are of prime importance in order to explore how confinement and DCSB emerge from fundamental QCD. The data on the $\gamma_v NN^*$ electrocouplings of all prominent N^* states that are accessible for the first time with the CLAS12 at photon virtualities from 5.0 to 12 GeV^2, will allow us to map out the momentum dependence of dressed quark masses, as well as their dynamical structure and to explore their interactions in the transition area from confinement to pQCD. The DSEQCD studies [2, 23] demonstrate that quark core contribution to the electromagnetic transition amplitudes from the ground to excited nucleon states are determined by the processes shown in Fig. 4. The momentum dependent dressed quark mass affects all quark propagators shown in Fig. 4. The virtual photon interaction with the dressed quark electromagnetic currents accesses the dynamical quark structure. The Schwinger interaction of virtual photon to the transition currents between di-quark and two-quarks states elucidates the details of strong interactions between dressed quarks. The value of momentum carried out by a single quark can be roughly estimated assuming equal sharing of the virtual photon momentum between all three dressed quarks. Under this assumption it is straightforward to see that the measurements of $\gamma_v NN^*$ electrocouplings at 5. GeV^2 $< Q^2 <$ 12. GeV^2 will be able to cover almost the entire area of quark momenta, where the transition from the confinement to the pQCD occurs, as it is shown in Fig. 3. Therefore, the data on $\gamma_v NN^*$ electrocouplings expected from CLAS12 will offer a unique way to explore the nature

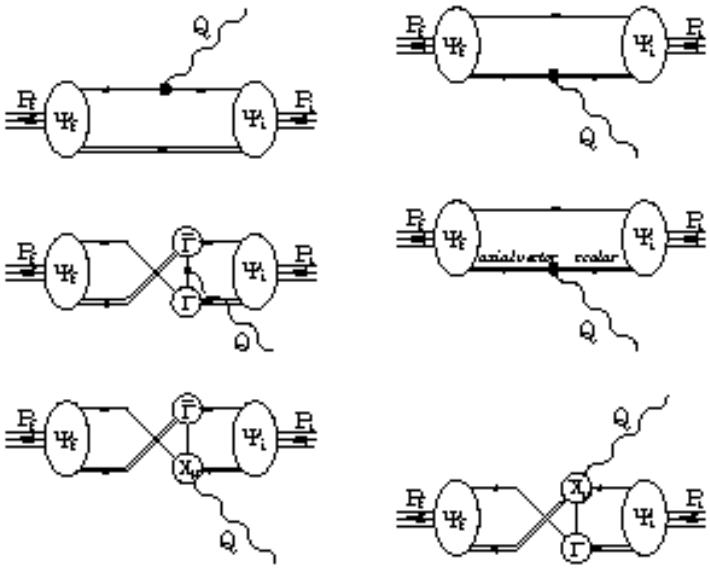

FIG. 4: The dressed quark interactions for the quark core contribution to the electromagnetic transition amplitudes ($\gamma_v NN^*$ electrocouplings) from the ground nucleon state of four-momentum P_i to excited nucleon states of four-momentum P_f in the DSEQCD approach [23]. Solid lines and double-solid lines stand for dressed quarks and the superposition of scalar and axial-vector di-quark propaggator, respectively. The Γ verticies describe the transition amplitudes between two-quark and di-quark states, while the X-verticies stand for the Schwinger interaction of virtual photon to the transition current between the di-quark and two-quark states. The ψ_i and ψ_f amplitudes describe the transitions between the intermediate di-quark quark states and the initial nucleon and final N^*-states, respectively.

of quark-gluon confinement based on QCD and how more than 98% of the nucleon resonance masses are generated non-perturbatively from almost massless current quarks via DCSB.

Lattice QCD (LQCD) opens up another conceptually different avenue to interpret $\gamma_v NN^*$ electrocouplings starting from the QCD Lagrangian. The current status and prospects of the LQCD for high level theoretical analysis of the data on $\gamma_v NN^*$ electrocouplings are discussed in Chapters I,II**??**. Recent LQCD advances clearly demonstrate the promising potential in describing the resonance $\gamma_v NN^*$ electrocouplings from first principles of QCD. Exploratory results on Q^2-evolution of the $F_1^{P_{11}}(Q^2)$ and $F_2^{P_{11}}(Q^2)$ form factors for the transition from the ground proton to the excited $P_{11}(1440)$ state have recently become available employing unquenched LQCD evaluations [24] and are shown in Fig. 5. Experimental values of the $F_1^{P_{11}}(Q^2)$ and $F_2^{P_{11}}(Q^2)$ form factors were computed from CLAS results [25] on the $\gamma_v pP_{11}(1440)$ electrocouplings. Despite the simplified basis of the projection operators used in these computations and relatively large pion mass ≈ 400 MeV, a reasonable description of experimental data from CLAS [25, 26] was achieved. In the future, when the LQCD evaluation of $\gamma_v NN^*$ electrocouplings will become available when a realistic basis of the projection operators in a box of relevant size is employed and the physical pion mass is approached, the comparison between LQCD and the experimental electrocoupling results for all prominent N^* states will allow us to answer the most challenging question: whether

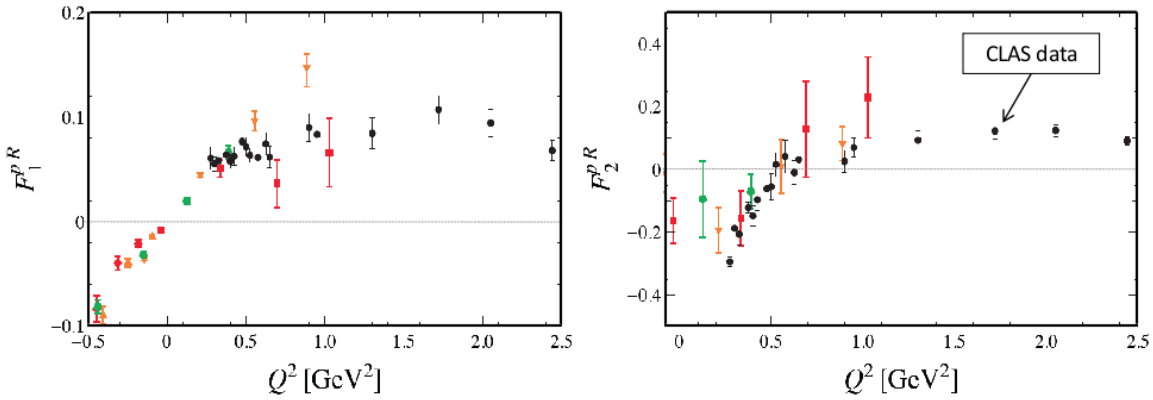

FIG. 5: (color on line) Exploratory evaluation of the $F_1^{P_{11}}(Q^2)$ and $F_2^{P_{11}}(Q^2)$ form factors for the transition from the ground proton to the excited $P_{11}(1440)$ state carried out within the framework of unquenched LQCD [24] in comparison with the experimental data from CLAS (filled black circles) [25]. LQCD results shown by green diamonds, red squares, and golden triangles are obtained for pion masses of 390 MeV, 450 MeV, and 875 MeV, respectively.

QCD is in fact the fundamental theory of strong interaction, which is capable to account for the full complexity of non-perturbative mechanisms which generate ground and excited hadron states from quarks and gluons.

Consistent results on $\gamma_v NN^*$ electrocouplings obtained within the framework of two conceptually different but QCD based approaches DSEQCD and LQCD will offer compelling evidence for the reliable prediction of resonance electrocoupling behaviors as they should be expected from the first principles of QCD.

In order to develop credible approaches, which are capable of relating information on $\gamma_v NN^*$ electrocouplings to dressed quark mass functions, structure, and eventually to the QCD Lagrangian, the data on electrocouplings of all prominent N^* states of different masses, spin and parity quantum numbers are of particular importance. Moreover, resonance electrocouplings and detailed information on nucleon ground state structure, expected from the measurements of elastic form factors, GPD's and TMD, should be analyzed collectively. The studies of nucleon ground and excited state structures carried out within the framework of conceptually different approaches strongly indicate the need to explore all prominent N^* state electrocouplings in order to fully access the complexity of the quark interactions, which are responsible for each nucleon resonance formation. The structure of the nucleon ground and excited states is generated by the common non-perturbative quark-gluon interaction. However, the resonance structure strongly depends on the quantum numbers of the excited state, and hence the information on $\gamma_v NN^*$ electrocouplings of all prominent N^* states is needed.

The DSEQCD studies revealed the $\gamma_v NN^*$ electrocoupling sensitivity to the di-quark correlations in baryons. These correlations are produced by the specific interaction within pairs of dressed quark in baryons. Similar interactions between quark anti-quark pairs generate mesons. In th case of baryons the effect of such interactions is the correlated motion of qq-pair, which can be described effectively by quasi-particles of final size - scalar and axial-vector di-quarks. It turns out that the relative contributions of the possible di-quark components strongly depend on the N^*

state quantum numbers. Furthermore, the shown amplitudes in Fig 4, which describe the transitions between the intermediate di-quark-quark state and the initial ground ψ_i or the final N^* state ψ_f, are strongly dependent on the quantum numbers of both the initial nucleon and the final N^* states. Here again the information on electrocouplings of as many N^*-states as possible is needed in order to fully explore the aforementioned mechanisms in nucleon resonance electroexcitations, and to gain access to the dressed quark mass function as well as the dynamical structure from the data on the Q^2-evolution of resonance electrocouplings.

The recent LQCD studies of the N^* spectrum and structure [3] also demonstrated the need for photo- and electrocoupling data of the full excited nucleon spectrum. For the first time LQCD results on the full spectrum of excited proton states have become available. However, they were obtained with pion mass larger than 380 MeV, which remains far from the physical pion mass. Consequently the N^* masses estimated in [3] are larger than those observed in experiments. Despite this and several other simplifications, the pattern of the N^* spectrum is reproduced, and the computed LQCD states can be matched to physical N^* states observed in experiment. The excited proton state structure was also determined in terms of contributing three quark configurations, which represents the vectors of irreducible SU$_{sf}$(6)·O(3) group representations. It was found that the structure of N^*-states with masses less than 1.75 GeV is dominated by not more than two SU$_{sf}$(6)·O(3) configurations. However, the structure high lying nucleon excitations (M $>$ 1.75 GeV) represent a su[erposition of many different configurations. Another clear evidence that both low and high lying resonance electrocouplings have to be measured.

Furthermore, LQCD results [3] predict the contributions of particular configurations to the resonance structure, that should strongly couple to glue. The N^* states with dominant contribution of such configurations would represent the baryon hybrids. The proposed in [9], the search for hybrid N^*'s opens up another avenue in the N^* program with the CLAS/CLAS12 detectors. Based on the LQCD results [3], the hybrid N^* masses are expected to be heavier than 1.9 GeV. The hybrid states may be seen as overpopulation of the SU$_{sf}$(6)·O(3) mutiplets. However, the hybrid N^*s should have the same quantum numbers as regular N^*s, thus only the the particular Q^2-evolution of $\gamma_v pN^*$ electrocouplings which is a consequence of a specific configuration structure can prove the hybrid nature of state. The study of $\gamma_v pN^*$ electrocouplings of high lying resonances offers a promising way to elucidate the role of gluons in the formation process of the excited nucleon states. The area of high Q^2 is of particular interest, since there the contribution from quark and gluon degrees of freedom to the N^* structure is expected to dominate.

Substantially different manifestations of confinement mechanisms in electrocouplings of different nucleon resonances is also strongly supported by the quark models discussed in the Chapter IV**??**. The expectations of different quark models and the experimental CLAS results on the $\gamma_v pP_{11}(1440)$ electrocouplings [25] are shown in Fig. 6. The quark model predictions were obtained with the parameters that are tuned to the data on elastic nucleon form factors, and all these models offer equally reasonable description of nucleon elastic form factors. The data on elastic nucleon form factors are unable to discriminate between particular features of the nucleon structure modeling within the framework of the different quark models. Instead, the data on $\gamma_v pP_{11}(1440)$ electrocouplings [25] are very sensitive to the particular quark model ingredients, as demonstrated by the comparison of the quark model expectations and the CLAS results in Fig. 6. Therefore, a combined study of ground and different excited nucleon state electrocouplings are critical in order to explore the evolution of the quark core contributions to the N^* structure for the states of different quantum numbers. Most quark models do not account for the resonance meson-baryon dressing, hence the data on $\gamma_v pN^*$ electrocouplings at high Q^2 provided a unique opportunity to make credible comparison of the quark model expectations with the experimental results for the

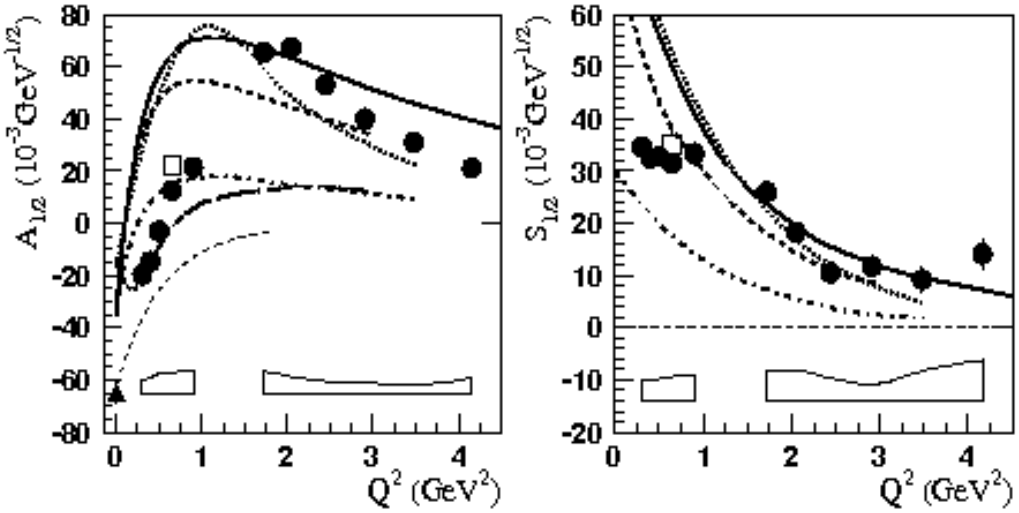

FIG. 6: Expectations of different quark models (different curves) in comparison with the CLAS results [25] on the $P_{11}(1440)$ electrocouplings (symbols). The quark models are outlined in [18].

first time.

The aforementioned studies of hadron structure have clearly demonstrated that even the most detailed information on the nucleon ground state structure, including elastic form factors, available/foreseen results on the GPD and TMD structure functions, remains insufficient in order to access the full complexity of non-perturbative interactions which generate nucleons from quarks and gluons. Instead, a combined studies of ground and all prominent N^*-states open up an exciting prospects to explore most challenging areas in the contemporary hadron physics confinement and DCSB in baryons. The CLAS12 detector offer a unique worldwide opportunity to observe how both these fundamental non-perturbative phenomena come from QCD based on experimental data for the first time obtained in the transition area from confinement to pQCD regimes.

Comprehensive studies of this transition area require joint efforts in different branches of hadron physics. The transition area can be also explored in measurements of the pion electromagnetic form factor in approved JLab experiments [35] for the 12 GeV Upgrade. The information on the pion structure offers valuable input for the understanding of qq correlations in nucleon ground and excited states. Vice versa, the information on these correlations available from the data on $\gamma_v NN^*$ electrocouplings can be used to interpret the data on the pion electromagnetic form factor. The detailed studies of the meson spectrum proposed in the CLAS12 experiment [36] offer another important source of information on qq-correlations in N^* states. JLab@12 GeV is the only foreseen facility worldwide that will be capable of delivering information on $\gamma_v NN^*$ electrocouplings, elastic nucleon [30–34], and pion electromagnetic form factors [35] with an unprecedented coverage of photon virtualities ever achieved complemented by deep insight into the meson spectrum. High level theoretical analyses of all these results combined are critical for exploration of the transition from confinement to pQCD.

A strong collaboration between experimentalists and theorists is required and have been initiated in order to achieve aforementioned challenging objectives in the N^* studies at high photon virtualities. Two topical Workshops [37, 38] were organized by Hall-B and Theory Center at Jefferson Lab to foster these efforts and create opportunities to facilitate and stimulate further growth

in this field. This document is prepared based on presentations and discussions at the II Workshop on "Nucleon Resonance Structure in Exclusive Electroproduction at High Photon Virtualities with the CLAS 12 Detector", May 16 2011, JLab, Newport News,VA with a goal of developing:

1. reaction models for the extraction of the $\gamma_v pN^*$ electrocouplings from the data on single meson and double pion electroproduction off protons at photon virtualities from 5.0 to 12.0 GeV^2, incorporating the transition from meson-baryon to quark degrees of freedom into the reaction mechanisms;

2. approaches for the theoretical interpretation of $\gamma_v pN^*$ electrocouplings, which are capable to explore how N^* states are generated non-perturbatively by strong interaction and how these processes emerge from the QCD.

II. ANALYSIS APPROACHES FOR EVALUATION OF NUCLEON RESONANCE ELECTROCOUPLINGS FROM THE CLAS DATA: STATUS AND PROSPECTS

A. Introduction

Dedicated experiment with the primary objective of determining $\gamma_v NN^*$ electrocouplings from the data on exclusive $\pi^+ n$, $\pi^0 p$, and $\pi^+\pi^- p$ meson electroproduction off protons, that will be obtained in the future measurements with the CLAS12 detector [263], was approved by PAC for 40 days running time in the first five years after completion of the JLAB 12 GeV Upgrade Project in 2015. The CLAS12 is the only foreseen worldwide detector that will be capable to perform experiments to determine $\gamma_v NN^*$ electrocouplings of prominent excited proton states listed in the Table I at highest photon virtualities ever achieved in N^* studies from 5.0 to 10.0-12.0 GeV^2, where upper boundary of photon virtualities depends on the mass of excited proton state. The proposed experiment represents the first step in extension of current N* Program with the CLAS detector [264, 265], employing new opportunities offered by 11 GeV continuous electron beam.

Analysis of the CLAS results on $\gamma_v NN^*$ electrocouplings [96, 97, 164, 266] carried out within the framework of the quark models [76, 152, 246, 267, 268], and employing the advanced coupled-channel approach recently developed by the Excited Baryon Analysis Center (EBAC) in Theory Center at JLAB [43, 49] demonstrated that the structure of excited proton states with masses less than 1.6 GeV at photon virtualities $Q^2 < 5.0$ GeV^2 is determined by a combined contributions from inner core of dressed quarks and from external meson-baryon cloud. Relative contributions from quark core increases with Q^2, and at $Q^2 > 5.0$ GeV^2 these contributions are expected to play a major role in resonance structure [246, 267]. Therefore, the planned studies of $\gamma_v NN^*$ electrocouplings with the CLAS12 detector [263] for the first time will open up almost direct access to quark degrees of freedom in N^* structure, allowing us to explore dynamical quark masses and structure, as well as their non-perturbative strong interaction, that are responsible for N^* formation, and how they emerge from the QCD. These studies are of particular importance in order to understand origin of quark/gluon confinement in baryon sector from the first principles of the QCD [129].

The data on $\pi^+ n$, $\pi^0 p$, and $\pi^+\pi^- p$ electroproduction channels play a key role in evaluation of $\gamma_v NN^*$ electrocouplings. The $N\pi$ and $\pi^+\pi^- p$ exclusive channels combined account for $\approx 90\%$ of the total meson electroproduction cross section in resonance excitation region $W < 2.0$ GeV. Both single and charge double pion electroproduction channels are sensitive to N^* contributions, as it can be seen from the Table I. Furthermore, they offer complementary opportunities for N^* studies.

For extraction of $\gamma_v NN^*$ electrocouplings we are planning to employ independent analyses of single and charged double pion electroproduction data within the framework of different phenomenological reaction models. Reliable separation of resonant and non-resonant contributions becomes critical for evaluation of $\gamma_v NN^*$ electrocouplings within the framework of these approaches. The $\pi^+ n$, $\pi^0 p$ and $\pi^+\pi^- p$ exclusive electroproduction channels have different non-resonant mechanisms, while $\gamma_v NN^*$ electrocouplings determined in independent analyses of these channel data should be the same. Resonance electroproduction and hadronic decay amplitudes can not affect each other, being separated in space-time by resonant propagators. Therefore, successful description of a large body of observables measured in $\pi^+ n$, $\pi^0 p$ and $\pi^+\pi^- p$ electroproduction reactions, achieved with consistent values of $\gamma_v NN^*$ electrocouplings will demonstrate reliable extraction of these fundamental quantities.

Furthermore, the $N\pi$ and $\pi^+\pi^- p$ electroproduction channels are strongly coupled by the final

N^*, Δ^* states	Branching fraction $N\pi$ %	Branching fraction $N\pi\pi$ %	Prominent in $N\pi$ exclusive channels	Prominent in $\pi^+\pi^-p$ exclusive channel
$P_{33}(1232)$	100	0	*	
$P_{11}(1440)$	60	40	*	*
$D_{13}(1520)$	60	40	*	*
$S_{11}(1535)$	45	<10	*	
$S_{31}(1620)$	<25	75		*
$S_{11}(1650)$	75	<15	*	
$F_{15}(1680)$	65	35	*	*
$D_{33}(1700)$	<15	85		*
$P_{13}(1720)$	<15	>70		*
$F_{35}(1905)$	<10	90		*
$F_{37}(1950)$	40	>25	*	*

TABLE I: $N\pi$ and $N\pi\pi$ branching fractions for decays of excited proton states that have prominent contributions to the exclusive single and/or charged double pion electroproduction channels. The values are taken from [124] or from the CLAS data analyses [164, 266]. Symbols * mark most suitable exclusive channel(s) for the studies of particular N* state.

state interactions. The data of experiments with hadronic probes showed that the $\pi N \to \pi\pi N$ reactions are the second biggest exclusive contributors to inclusive πN interactions. Therefore, the data on mechanisms contributing to single and charged double pion electroproduction off protons are needed for development of global multi channel analyses for extraction of $\gamma_v NN^*$ electrocouplings within the framework of coupled-channel approaches. Consistent description of hadronic interactions between the πN and $\pi\pi N$ asymptotic states is critical for reliable extraction of $\gamma_v NN^*$ electrocouplings within the framework of coupled-channel approaches. Most of available worldwide coupled-channel approaches have substantial difficulties in describing complexity of these interactions. Advanced coupled-channel approach EBAC-DCC [269] is currently under development. It will allow us for the first time to account consistently for hadronic interactions between single and double pion electroproduction channels. This approach will be used for extraction of $\gamma_v NN^*$ electrocouplings from the data of experiment on N^* studies with the CLAS12 detector [263] along with independent analyses of $N\pi$ and $\pi^+\pi^-p$ electroproduction channels. The progress achieved in development of the EBAC-DCC approach is outlined in the Chapter ...

In this Chapter we review the current status and prospects for development of phenomenological reaction models with a primary objective of determining $\gamma_v NN^*$ electrocouplings in independent analyses of π^+n, π^0p and $\pi^+\pi^-p$ electroproduction data.

B. Approaches for independent analyses of the CLAS data on single and charged double pion electroproduction off protons

Phenomenological reaction models [164, 197, 201, 266, 270] were developed for evaluation of $\gamma_v NN^*$ electrocouplings in independent analyses of the data on π^+n, π^0p, and $\pi^+\pi^-p$ electroproduction off protons and used successfully for analyses of the CLAS data [264, 265]. These reaction models allowed us to access resonant amplitudes fitting all available observables in each

channel independently and within the framework of different reaction models. Eventually $\gamma_v NN^*$ electrocouplings and theirs $N\pi$, $N\pi\pi$ hadronic decay widths have been determined, employing the Breit-Wigner parametrization of resonant amplitudes.

1. Development of approaches for analysis of single pion electroproduction off protons

The CLAS data considerably extended information on $\pi^+ n$, $\pi^0 p$ electroproduction off protons. A total of nearly 120000 data points on unpolarized differential cross sections, longitudinally polarized beam asymmetries, and longitudinal target and beam-target asymmetries were obtained with almost complete coverage of the accessible phase space [164]. The data were analyzed within the framework of two conceptually different approaches: a) the unitary isobar model (UIM), and b) a model, employing dispersion relations [201, 270]. All well established N^* states in the mass range $M_{N^*} < 1.8$ GeV were incorporated into the $N\pi$ channel analyses.

The UIM follows the approach of ref. [59]. The $N\pi$ electroproduction amplitudes are described as a superposition of N^* electroexcitation in s-channel and non-resonant Born terms. A Breit-Wigner ansatz with energy-dependent hadronic decay widths [271] is employed for the resonant amplitudes. Non-resonant amplitudes are described by a gauge invariant superposition of nucleon s- and u-channel exchanges, and π, ρ, and ω t-channel exchanges. The latter are reggeized in order to better describe the data in the second and the third resonance regions, while at $W < 1.4$ GeV the role of regge trajectory exchanges becomes insignificant. The Regge-pole amplitudes were constructed using prescription of [272, 273] allowing us to preserve gauge invariance of non-resonant amplitudes.

The final state interactions are treated as πN rescattering in the K-matrix approximation [270].

In another approach, the real and imaginary parts of invariant amplitudes, that describe $N\pi$ electroproduction, are related in a model-independent way by dispersion relations [270]. The analysis showed that the imaginary parts of amplitudes are dominated by resonant contributions at $W > 1.3$ GeV. In this kinematical region, they are described by resonant contributions only. At smaller W values, both resonant and non-resonant contributions to the imaginary part of amplitudes are taken into account based on analysis of πN elastic scattering and employing Watson theorem and dispersion relations.

The Q^2-evolution of non-resonant amplitudes in both approaches is determined by behavior of hadron electromagnetic form factors at different photon virtualities. The s- and u- channel nucleon exchange amplitudes depend on proton and neutron electromagnetic form factors, respectively. The t-channel π, ρ, ω exchanges depend on pion electromagnetic form factors and $\rho(\omega) \to \pi\gamma$ transition form factors. Parametrization of mentioned above electromagnetic form factors as a function of Q^2 employed in analyses of the CLAS single pion electroproduction data can be found in [164]. These analyses demonstrated that at photon virtualities $Q^2 > 0.9$ GeV^2, reggezation of the Born amplitudes becomes insignificant in resonance region at $W < 1.9$ GeV. Consequently, at these photon virtualities the background of UIM was built just from the nucleon exchanges in the s- and u-channels and t-channel π, ρ and ω exchanges. In addition, in the approach based on dispersion relations we take into account Q^2-evolution of subtraction function $f_{sub}(Q^2, t)$. Subtraction function was determined using liner parametrization over Mandelstam variable t and fitting two parameters to the data in each bin of Q^2 [164]. Employing information on Q^2-evolution of hadron electromagnetic form factors from other experiments or from the CLAS data fit, we are able to predict Q^2-evolution of non-resonant contributions to single pion electroproduction in the area of Q^2, where meson-baryon degrees of freedom remain relevant.

The two approaches provide good description of the $N\pi$ data in the entire range covered by

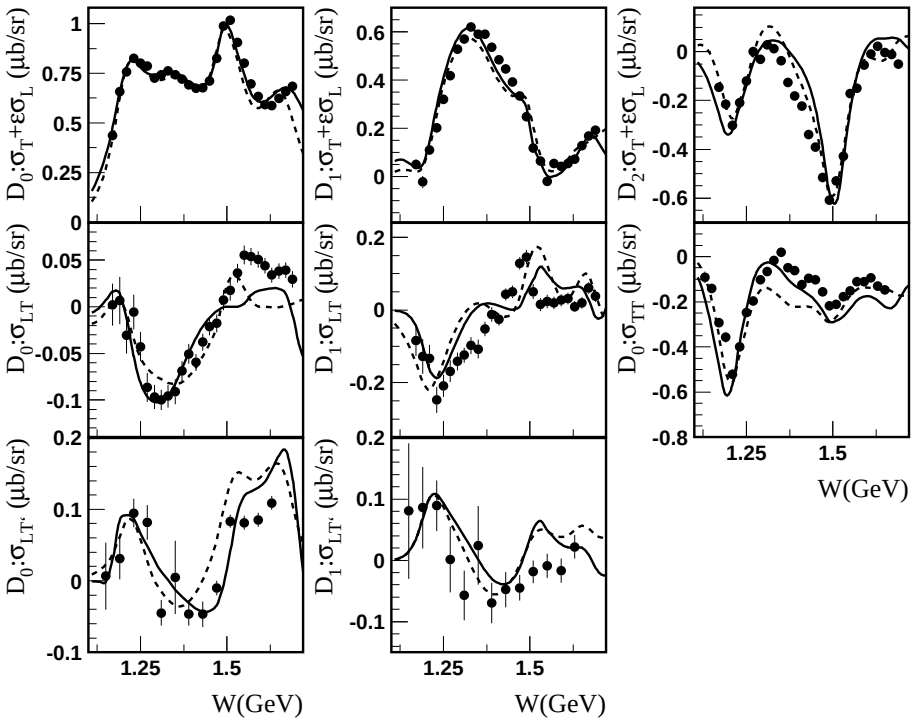

FIG. 7: Results for the Legendre moments of the $\vec{e}p \to en\pi^+$ structure functions in comparison with experimental data [274] for $Q^2 = 2.44$ GeV^2. The solid (dashed) curves correspond to the results obtained using DR (UIM) approach.

the CLAS measurements: $W < 1.7$ GeV and $Q^2 < 5.0$ GeV^2, resulting in χ^2/d.p. < 2.0 [164]. Example of the structure function description is shown in Fig. 7. The results of two approaches provide information for evaluation of systematical model uncertainties.

Consistent description of a large body of observables in the $N\pi$ exclusive channels achieved within the framework of two conceptually different approaches strongly suggest credible evaluation of resonant contributions.

2. Evaluation of $\gamma_v NN^*$ resonance electrocouplings from the data on charged double pion electroproduction off protons

The $\pi^+\pi^-p$ electroproduction data measured with the CLAS detector [275, 276] provide information on nine independent one-fold-differential and fully-integrated cross sections in a mass range $W < 2.0$ GeV, and at photon virtualities of $0.25 < Q^2 < 1.5$ GeV^2. Examples of available $\pi^+\pi^-p$ one-fold differential cross sections data in particular bins of W and Q^2 are shown in Figs. 8, 9. Analysis of these data allowed us to establish essential contributing mechanisms from their manifestation in measured cross sections. The peaks in invariant mass distributions provide evidence for presence of the channels $\gamma_v p \to Meson - Baryon \to \pi^+\pi^-p$ with unstable baryon or meson in the intermediate state. Pronounced dependences in angular distributions allow us to establish the relevant t- u- and s-channel exchanges. The mechanisms without pronounced kinematical dependences are identified via examination of their manifestations in various differential cross sections as a particular correlation pattern. Phenomenological reaction model JM

[197, 266, 281] was developed in collaboration between Hall B at Jefferson Lab and Skobeltsyn Nuclear Physics Institute in Moscow State University with the primary objective of determining $\gamma_v NN^*$ electrocouplings and theirs $\pi\Delta$ and ρp partial hadronic decay widths from fit of all measured observables of $\pi^+\pi^- p$ electroproduction channel.

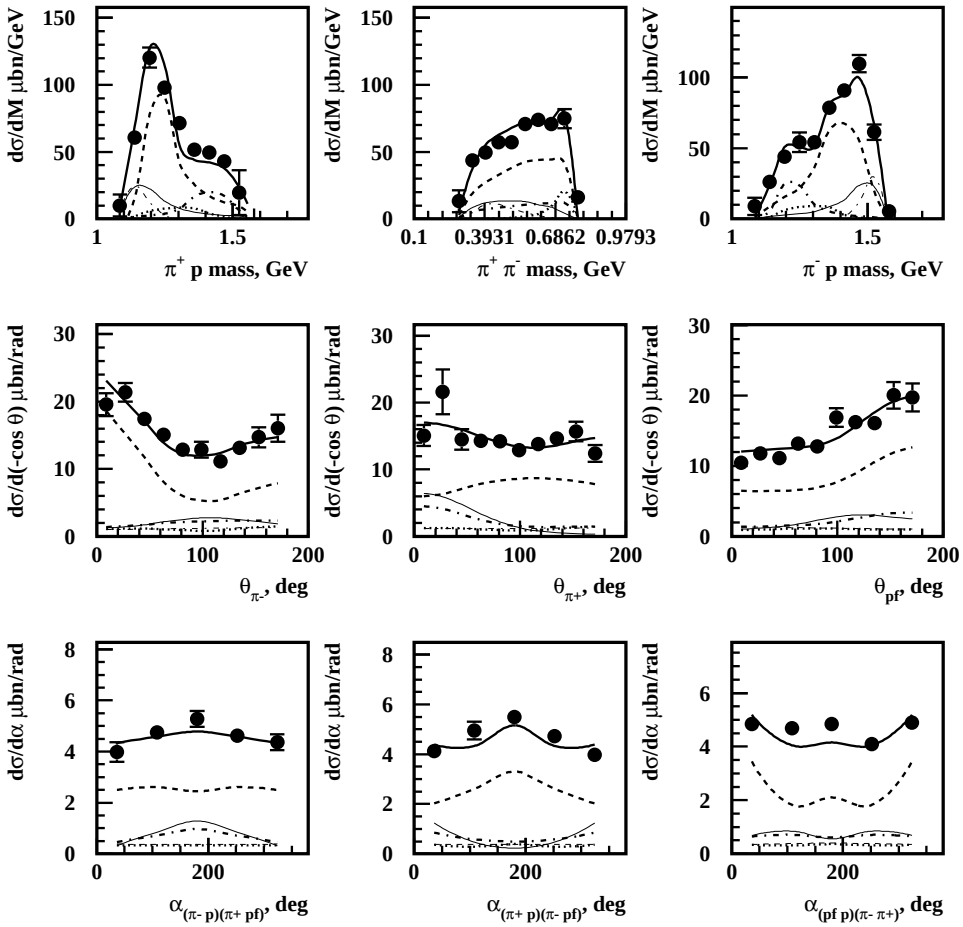

FIG. 8: Fit of the CLAS $ep \to e'\pi^+\pi^- p$ data [276] within the framework of JM model [97, 197, 266] at W = 1.71 GeV and Q^2=0.65 GeV^2. Full model results are shown by thick solid lines together with the contributions from $\pi^-\Delta^{++}$ (dashed thick lines), ρp (dotted thick lines), $\pi^+\Delta^0$ (dash-dotted thick lines), $\pi^+ D^0_{13}(1520)$ (thin solid lines), $\pi^+ F^0_{15}(1685)$ (dash-dotted thin lines) isobar channels. The contributions from other mechanisms described in the Section II B 2 are comparable with the data error bars, and they are not shown in the plot.

The amplitudes of $\gamma_v p \to \pi^+\pi^- p$ reaction are described in the JM model as a superposition of $\pi^-\Delta^{++}$, $\pi^+\Delta^0$, ρp, $\pi^+ D^0_{13}(1520)$, $\pi^+ F^0_{15}(1685)$, $\pi^- P^{++}_{33}(1600)$ sub-channels with subsequent decays of unstable hadrons to the final $\pi^+\pi^- p$ state, and additional direct 2π production mechanisms, where the final $\pi^+\pi^- p$ state is created without formation of unstable hadrons in the intermediate states.

The JM model incorporates contributions from all well established N^* states to $\pi\Delta$ and ρp sub-channels only. We also included the $3/2^+(1720)$ candidate state, suggested in the analysis [276] of the CLAS $\pi^+\pi^- p$ electroproduction data. In the current 2011' JM model version, the resonant amplitudes are described by the unitarized Breit-Wigner ansatz proposed in Ref. [277], that was modified to make it consistent with the parametrization of individual N^* state contributions by relativistic Breit-Wigner ansatz with energy dependent hadronic decay widths [278] employed in the JM model. After unitarization, Breit-Wigner ansatz accounts for transitions between the same and different N^* states in dressed-resonant propagators, making resonant amplitudes consistent with unitarity condition. Quantum number conservation in strong interactions allows the transitions between $D_{13}(1520)/D_{13}(1700)$, $S_{11}(1535)/S_{11}(1650)$ and $3/2^+(1720)/P_{13}(1720)$ pairs of N^* states incorporated into the JM model and listed in the Table I. We found that use of the unitarized Breit-Wigner ansatz has a minor influence on the $\gamma_v NN^*$ electrocouplings, but may affect substantially the N^* hadronic decay widths determined from the CLAS data fit.

Non-resonant contributions to $\pi\Delta$ sub-channels incorporate a minimal set of current conserving Born terms [197, 278]. They consist of t-channel pion exchange, s-channel nucleon exchange, u-channel Δ exchange and contact terms. Non-resonant Born terms were reggeized preserving current conservation, as it was proposed in [272, 273]. The initial and final state interactions in $\pi\Delta$ electroproduction are treated in absorptive approximation with absorptive coefficients estimated from the data on πN scattering [278]. Non-resonant contributions to $\pi\Delta$ sub-channels also include the additional contact terms that have different Lorentz-invariant structures with respect to the contact terms in the sets of Born terms. These extra contact terms account effectively for non-resonant processes in $\pi\Delta$ sub-channels beyond the Born terms, as well as for the final state interaction effects, that are beyond those taken into account by absorptive approximation. Parametrizations of extra contact terms in the $\pi\Delta$ sub-channels are given in [197].

Non-resonant amplitudes in ρp sub-channel are described within the framework of diffractive approximation, taking into account the effects caused by ρ-line shrinkage [279]. The latter effects play a significant role in the N^* excitation region, in particular in near threshold and sub-threshold ρ-meson production at $W<$1.8 GeV. Even in this kinematics, when non-resonant parts of ρp sub-channel become small, the ρp sub-channel may affect one-fold differential cross sections due to the contributions from the nucleon resonances that decay to the ρp final states. Therefore, credible treatment of non-resonant contributions in ρp sub-channel becomes important for evaluation of electrocouplings and hadronic parameters of these resonances. Analysis of the CLAS data [275, 276] revealed presence of the ρp sub-channel contributions at W $>$ 1.5 GeV.

The $\pi^+ D^0_{13}(1520)$, $\pi^+ F^0_{15}(1685)$, $\pi^- P^{++}_{33}(1600)$ sub-channels are described in the JM model by non-resonant contributions only. The amplitudes of $\pi^+ D^0_{13}(1520)$ sub-channel were derived from the non-resonant Born terms of $\pi\Delta$ sub-channels, implementing an additional γ_5-matrix that account for opposite parities of Δ and $D_{13}(1520)$ [280]. The magnitudes of $\pi^+ D^0_{13}(1520)$ production amplitudes were fit to the data independently in each bin of W and Q^2. The contributions from $\pi^+ D^0_{13}(1520)$ sub-channel should be taken into account at $W >$ 1.5 GeV.

The $\pi^+ F^0_{15}(1685)$ and $\pi^- P^{++}_{33}(1600)$ sub-channel contributions are seen in the data [276] at $W >$ 1.6 GeV. These contributions are almost negligible at smaller W. The effective contact terms were employed in the JM model for parametrization of these sub-channel amplitudes [280, 281]. Magnitudes of the $\pi^+ F^0_{15}(1685)$ and $\pi^- P^{++}_{33}(1600)$ sub-channel amplitudes were fit to the data in each bin of W and Q^2.

A general unitarity condition for $\pi^+\pi^- p$ electroproduction amplitudes requires presence of so-called direct 2π production mechanisms, when the final $\pi^+\pi^- p$ state is created without formation of unstable hadrons in the intermediate states [282]. These processes are beyond the discussed

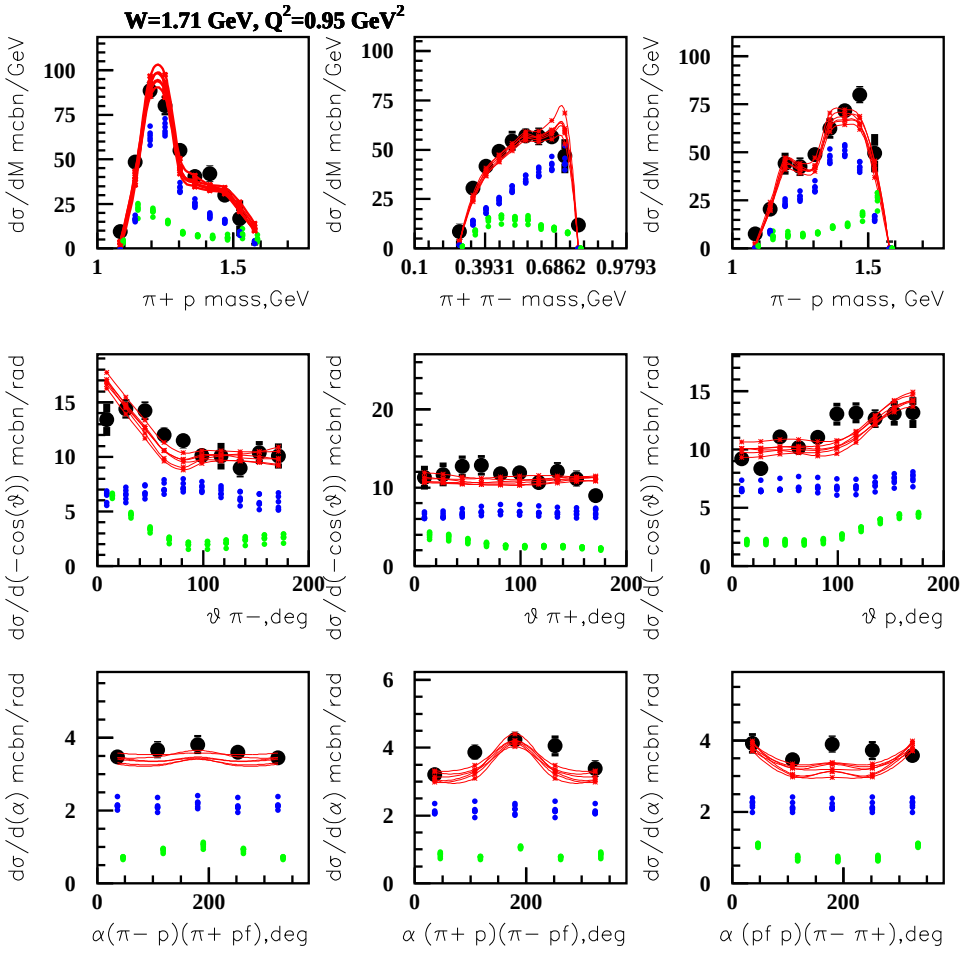

FIG. 9: (color online) Resonant (blue bars) and non-resonant (green bars) contributions to differential cross sections obtained from the CLAS data [276] fit within the framework of JM model at W= 1.71 GeV, Q^2=0.95 GeV^2. Red lines show the fit results.

above contributions from two-body sub-channels. Direct 2π production amplitudes were established for the first time in the analysis of the CLAS $\pi^+\pi^- p$ electroproduction data [197]. They are described in the JM model by a sequence of two exchanges in t- and/or u- channels by unspecified particles. The amplitudes of 2π production mechanisms are parametrized by Lorentz-invariant contraction between spin-tensors of the initial and final state particles, while two exponential propagators describe mentioned above exchanges by unspecified particles. Magnitudes of these amplitudes are fit to the data in each bin of W and Q^2. Recent studies of the correlations between the final hadron angular distributions allowed us to establish the phases of the 2π direct production amplitudes [283]. The contributions from 2π direct production mechanisms are maximal and substantial ($\approx$ 30%) at $W < 1.5$ GeV. They decrease with W and become negligible at $W >$ 1.6 GeV, where full $\pi^+\pi^- p$ electroproduction amplitudes are well described by superposition of two-body sub-channels. This transition to the dominance of two-body sub-channel amplitudes ob-

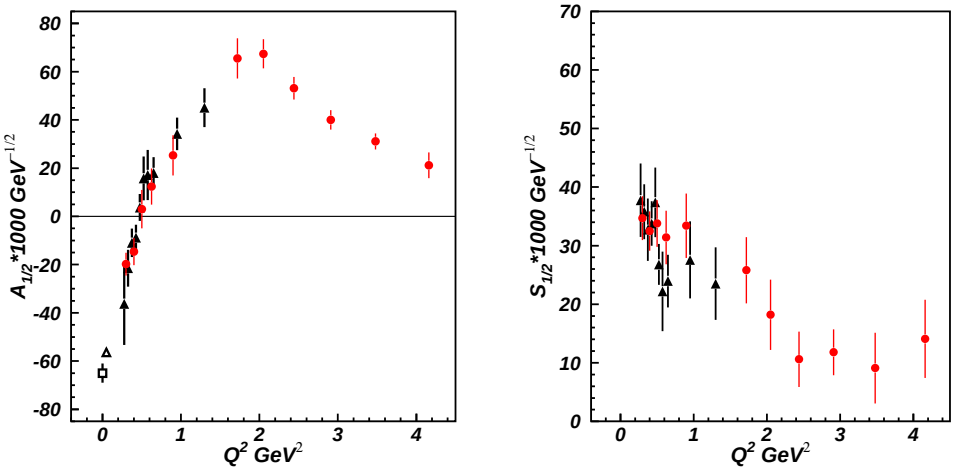

FIG. 10: $A_{1/2}$ (left) and $S_{1/2}$ (right) electrocouplings of the $P_{11}(1440)$ resonance determined in independent analyses of the CLAS data on $N\pi$ (circles) [164] and $\pi^+\pi^- p$ (triangles) [266] electroproduction off protons. Squares and triangles at Q^2=0 GeV^2 correspond to Nakamura:2010zzi [124] and the CLAS $N\pi$ [284] photoproduction results, respectively.

served in phenomenological analysis of the CLAS data is of particular interest for understanding of the coupled-channel effects in the $\pi^+\pi^- p$ final state.

The JM model provided reasonable description of $\pi^+\pi^- p$ differential cross sections at $W <$ 1.8 GeV and $Q^2 < 1.5$ GeV^2 with χ^2/d.p. < 3.0, accounting for statistical uncertainties of experimental data only. As a typical example, the model description of nine one-fold differential cross sections at W = 1.71 GeV and Q^2 = 0.65 GeV^2 is shown in Fig. 8 together with the contributions of individual mechanisms incorporated into the JM description. Each contributing mechanism has the distinctive shape of cross section in all shown in Fig. 8 observables. Furthermore, any contributing mechanism has substantially different shapes of cross sections in various observables, that are highly correlated by underlying reaction dynamics. Therefore, successful description of all nine one-fold differential cross sections combined allowed us to identify essential mechanisms contributing to the $\pi^+\pi^- p$ electroproduction off protons, and to access their dynamics.

A successful fit of the CLAS $\pi^+\pi^- p$ electroproduction data also allowed us to determine the resonant parts of cross sections. An example is shown in Fig 9. The resonant part uncertainties are comparable with those of the experimental data. It is a strong evidence for an unambiguous separation of resonant/non-resonant contributions. Credible resonance/background separation achieved in the CLAS data fit within the framework of the JM model is of particular importance for extraction of $\gamma_v NN^*$ electrocouplings, as well as for evaluation of their $\pi\Delta$ and ρp decay widths.

A special fitting procedure for extraction of resonance electrocouplings and their full and partial $\pi\Delta$ and ρp hadronic decay widths was developed, allowing us to obtain uncertainties of resonance parameters accounting for both experimental data uncertainties and for systematical uncertainties of the JM reaction model.

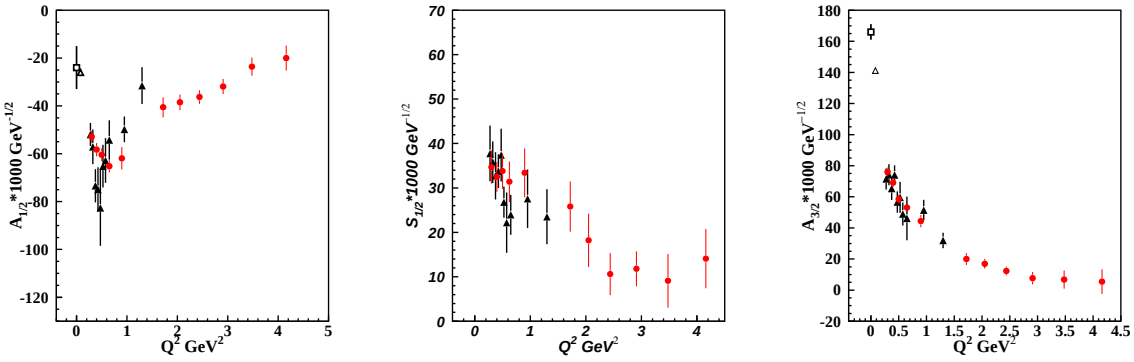

FIG. 11: $A_{1/2}$ (left), $S_{1/2}$ (middle), and $A_{3/2}$ (right) electrocouplings of the $D_{13}(1520)$ resonance determined in independent analyses of the CLAS data on $N\pi$ (circles) [164] and $\pi^+\pi^-p$ (triangles) [266] electroproduction off protons. Squares and triangles at Q^2=0 GeV^2 correspond to Nakamura:2010zzi [124] and the CLAS $N\pi$ [284] photoproduction results, respectively.

C. Resonance electrocouplings from the CLAS data on single and charged double pion electroproduction

Analyses of the CLAS data on single and charged double pion electroproduction off protons carried out within the framework of fixed-t dispersion relations, the UIM model, and the JM model described in the Sections II B 1,II B 2 for the first time provided information on electrocouplings of $P_{11}(1440)$, $D_{13}(1520)$, and $F_{15}(1685)$ resonances from independent analyses of π^+n, π^0p, and $\pi^+\pi^-p$ electroproduction channels [97, 266]. Electrocouplings of $P_{11}(1440)$ and $D_{13}(1520)$ resonances determined from these channels are shown in Figs. 10 , 52. They are consistent within uncertainties. Longitudinal $S_{1/2}$ electrocouplings of $D_{13}(1520)$, $S_{11}(1535)$, $S_{31}(1620)$, $S_{11}(1650)$, $F_{15}(1685)$, $D_{33}(1700)$, and $P_{13}(1720)$ excited proton states have become available from the CLAS data for the first time [97, 164, 266].

Consistent results on γ_vNN^* electrocouplings of $P_{11}(1440)$, $D_{13}(1520)$, and $F_{15}(1685)$ resonances determined in independent analyses of major π^+n, π^0p, and $\pi^+\pi^-p$ electroproduction channels with different backgrounds demonstrate reliable extraction of these fundamental quantities. Furthermore, this consistency also strongly suggests that the reaction models described in the Sections II B 1,II B 2 provide reliable evaluation of γ_vNN^* electrocouplings analyzing either single or charged double pion electroproduction data only. It makes possible to determine electrocouplings of all resonances that decay preferentially to the $N\pi$ and/or $N\pi\pi$ final states. The studies of $N\pi$ exclusive channels are the primary source of information on electrocouplings of the N^* states with masses below 1.6 GeV [164]. Analysis of the $\pi^+\pi^-p$ electroproduction off protons allows us to check the results of $N\pi$ exclusive channels for the resonances that have substantial decays to both $N\pi$ and $N\pi\pi$ channels, as $P_{11}(1440)$ and $D_{13}(1520)$. The charged double pion electroproduction channel is of particular importance for evaluation of high-lying resonance electrocouplings, since most N^* states with masses above 1.6 GeV decay preferentially via two pion emission (Table I). As it is shown in the Table I, most of well established resonances have substantial decays to either the $N\pi$ or $N\pi\pi$ final states. Therefore, the studies of $N\pi$ and $\pi^+\pi^-p$ electroproduction off protons allow us to determine electrocouplings of all prominent excited proton states.

In the mass range $1.4 < W < 1.6$ GeV only the $S_{11}(1535)$ resonance has minor hadronic de-

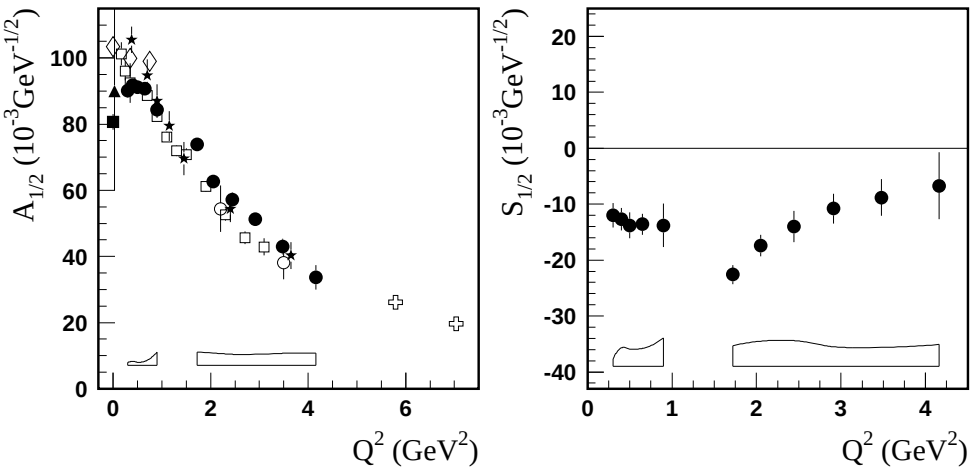

FIG. 12: Transverse electrocoupling $A_{1/2}$ of the $\gamma^* p \to S_{11}(1535)$ transition. The full circles are the electrocouplings extracted from $N\pi$ electroproduction data [164]. The electrocouplings extracted from $N\eta$ electroproduction data are: the stars [198], the open boxes [131], the open circles [199], the crosses [200], and the rhombuses [60, 201]. The full box and triangle at $Q^2 = 0$ correspond to Nakamura:2010zzi [124] and the CLAS $N\pi$ [284] photoproduction results, respectively.

cays to the $N\pi\pi$ final state (see Table I). Therefore, the studies of this very pronounced in $N\pi$ electroproduction resonance become problematic in the charged double pion electroproduction off protons. The $S_{11}(1535)$ resonance has large branching ratio to the πN and ηN channels and, starting in 1999, has been extensively studied at JLab in a wide range of Q^2 up to 4.5 and 7 GeV^2, respectively, in $N\pi$ and $N\eta$ electroproduction off protons (see Fig. 12). In $N\eta$ electroproduction, the $S_{11}(1535)$ strongly dominates the cross section at $W < 1.6$ GeV and is extracted from the data in a nearly model-independent way using a Breit-Wigner form for the resonance contribution [131, 198–200]. These analyses assume that the longitudinal contribution is small enough to have a negligible effect on the extraction of the transverse amplitude. This assumption is confirmed by the analyses of the CLAS $N\pi$ electroproduction data [164]. Accurate results were obtained in both reactions for the transverse electrocoupling $A_{1/2}$; they show a consistent Q^2 slope and allowed the determination of the branching ratios to the $N\pi$ and $N\eta$ channels [164]. Transverse $A_{1/2}$ electrocouplings of the $S_{11}(1535)$ extracted in independent analyses of $N\pi$ and $N\eta$ electroproduction channels are in a reasonable agreement, considering systematical uncertainties of the analysis [164]. Extension of the proposal [263] by the studies of $N\eta$ electroproduction at high Q^2 would enhance considerably our capabilities for extraction of reliable results on $S_{11}(1535)$ electrocouplings in independent analyses of $N\pi$ and $N\eta$ electroproduction channels.

Preliminary results on electrocouplings of $S_{31}(1620)$, $S_{11}(1650)$, $F_{15}(1685)$, $D_{33}(1700)$ and $P_{13}(1720)$ resonances were obtained from analysis of the CLAS $\pi^+\pi^- p$ electroproduction data [276] within the framework of the JM model [97, 266]. As an example, electrocouplings of the $D_{33}(1700)$ resonance determined from analysis of the CLAS $\pi^+\pi^- p$ electroproduction data are shown in Fig. 13 in comparison with previous world data taken from [285]. The $D_{33}(1700)$ resonance decays preferentially to the $N\pi\pi$ final states with the branching fraction > 80 %. Consequently, electrocouplings of this resonance determined from the $N\pi$ electroproduction channels have large uncertainties because of insufficient sensitivity of these exclusive channels to the contributions of $D_{33}(1700)$ resonance. The CLAS results improved considerably our knowledge on

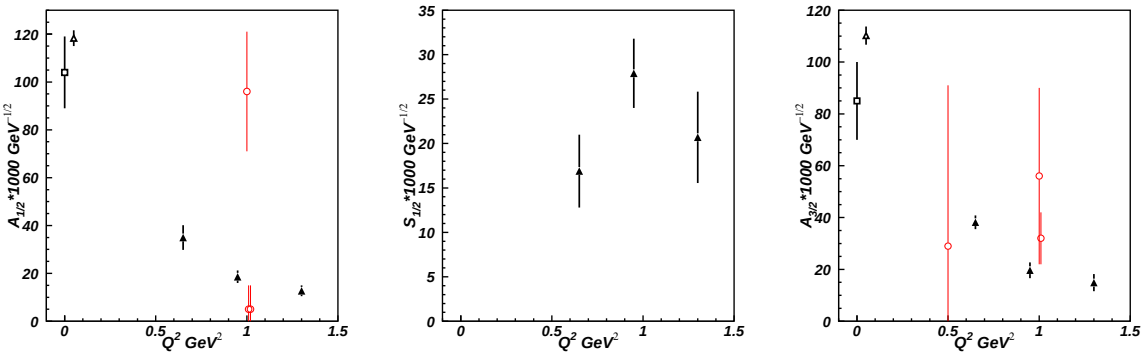

FIG. 13: Electrocouplings of $D_{33}(1700)$ resonance $A_{1/2}$ (left), $S_{1/2}$ (middle) and $A_{3/2}$ (right) determined in analyses the CLAS $\pi^+\pi^- p$ electroproduction data [197] and world data on $N\pi$ electroproduction off protons [285].

electrocouplings of $S_{31}(1620)$, $S_{11}(1650)$, $F_{15}(1685)$, $D_{33}(1700)$ and $P_{13}(1720)$ resonances. They provided accurate information on Q^2-evolution of transverse electrocouplings, while longitudinal electrocouplings of these states were determined for the first time. These preliminary results revealed particular feature in electroexcitation of the $S_{31}(1620)$ state, which is a dominance of longitudinal $S_{1/2}$ electrocoupling at $Q^2 > 0.5$ GeV^2.

III. FUTURE DEVELOPMENTS

New data from the CLAS detector keep continuously growing the outreach of the N* program, offering promising prospects for development of reaction models with the primary objective of $\gamma_v NN^*$ electrocoupling extraction at $Q^2 > 5.0$ GeV^2 from the data of future experiments on N^* studies with the CLAS12 detector [96].

Preliminary CLAS data on charged double pion electroproduction have recently become available [286]. The measurements cover an entire N^* excitation region and the area of photon virtualities $2.0 < Q^2 < 5.0$ GeV ^{2}. The data were obtained in 115 bins of W and Q^2. They consist of nine one-fold differential cross sections as those shown in Figs 8, 9. Extension of JM approach toward higher Q^2 values up to 5.0 GeV^2 covering an entire N^* excitation region is in progress and will be completed in one-two years.

After completion of this data analysis, electrocouplings of $P_{11}(1440)$ and $D_{13}(1520)$ resonances will become available from both the $N\pi$ and $\pi^+\pi^- p$ electroproduction channels at $0.2 < Q^2 < 5.0$ GeV^2. We will have reliable information on these state electrocouplings at full range of distances, that correspond to transition toward dominance of quark degrees of freedom in resonance structure. The $P_{11}(1440)$ and $D_{13}(1520)$ resonances become very attractive for high level theoretical interpretation of their electrocouplings from the first principles of the QCD, employing Lattice QCD and Dyson-Schwinger Equation of the QCD approaches, that were outlined in the Chapters... The studies of N^* meson-baryon dressing carried out by the EBAC [75] strongly suggest almost negligible contribution from meson-baryon cloud to the $A_{1/2}$ electrocouplings of $D_{13}(1520)$ resonance at $Q^2 > 1.5$ GeV^2. Therefore, theoretical interpretation of already available and future CLAS results on $A_{1/2}$ electrocouplings of $D_{13}(1520)$ resonance are of particular interest for approaches that are capable of describing quark content of resonances based on the QCD.

Analysis of the CLAS $\pi^+\pi^- p$ electroproduction data [286] within the framework of JM ap-

proach will deliver first information on electrocouplings of most high lying excited proton states (M $>$ 1.6 GeV) at 2.0 $< Q^2 <$ 5.0 GeV^2. This information will allows us to extend considerably our knowledge on how strong interactions create excited proton states of different quantum numbers. Analyses of available and future CLAS results on electrocouplings of prominent N^* states at $Q^2 >$ 2.0 GeV^2 within the framework of LCSR approach outlined in the Chapter.. will constrain quark distribution amplitudes of various N^* states. Access to quark distribution amplitudes in N^* structure is of particular importance, since they can be evaluated from the first principles of the QCD employing lattice calculations, as it was discussed in the Chapter...

Information on evolution of non-resonant mechanisms with Q^2 obtained from analyses of the CLAS data on single and charged double pion electroproduction at $Q^2 <$ 5.0 GeV^2 will serve as the starting point for the development of reaction models that make it possible to determine $\gamma_v N N^*$ electrocouplings from the fit of the future data at Q^2 area from 5.0 to 12.0 GeV^2.

Consistent description of a large body of observables in the $N\pi$ exclusive channels achieved within the framework of two conceptually different approaches outlined in the Section II B 1, and success of the JM model in describing of $\pi^+\pi^- p$ electroproduction off protons demonstrate that meson-baryon degrees of freedom employed in these approaches play a significant role at photon virtualities $Q^2 <$ 5.0 GeV^2. For analyses of these exclusive channel data, that will be measured with the CLAS12 detector at distances, where quark degrees of freedom are expected to be dominant, further development of reaction models is needed. The reaction models for description of $\pi^+ n$, $\pi^0 p$, and $\pi^+\pi^- p$ electroproduction off protons at $Q^2 >$ 5.0 GeV^2 should account explicitly for the contributions from quark degrees of freedom. Currently theory of hadron interactions is not in a position to offer any ready-to-go approach at these particular distance scales, that dominate by quark degrees of freedom but still correspond to non-perturbative strong interaction regime. In a such situation, we pursue a phenomenological way for evaluation of non-resonant mechanisms at high Q^2. We will explore the possibilities to implement different models, that employ quark degrees of freedom explicitly, and to confront the model predictions to the data. We will start from the models, that employ hand bag diagrams for parametrization of non-resonant single pion electroproduction, and at the next step to extend them for description of $\pi^+\pi^- p$ electroproduction off protons

For the kinematics accessible at the upgraded Jlab one reaches the region where a description of the processes of interest in terms of quark degrees of freedom applies. In this case the calculation of cross sections and other observables can be performed within the handbag approach which bases on QCD factorization of the scattering amplitudes in hard subprocesses, pion electroproduction off quarks, and in generalized parton distributions (GPDs) for $p \to p$ or $p \to N^*$ transitions.

In recent years the data on electroproduction of vector and pseudoscalar mesons have extensively been analyzed. In particular in [287–289] a systematic analysis of these processes in the kinematical region of large Q^2 (> 3 GeV^2) and W larger than about 4 GeV but small Bjorken-x (i.e. small skewness) lead to a set of GPDs ($H, E, \widetilde{H}, H_T, \cdots$) which respect all theoretical constraints - polynomiality, positivity, parton distributions and nucleon form factors. These GPDs are also in reasonable agreement with moments calculated within lattice QCD [290] and with data on deeply virtual Compton scattering in the mentioned kinematical region [291]. On the other hand, applications in the kinematical region accessible at the present Jlab which is characterized by rather large values of Bjorken-x and small W, do not lead to agreement with experiment in general. Predictions for ρ^0 electroproduction, for instance, fails by order of magnitude while ϕ works quite well, see Fig. **??**.

For the upgraded Jlab one can expect fair agreement between experiment and predictions for

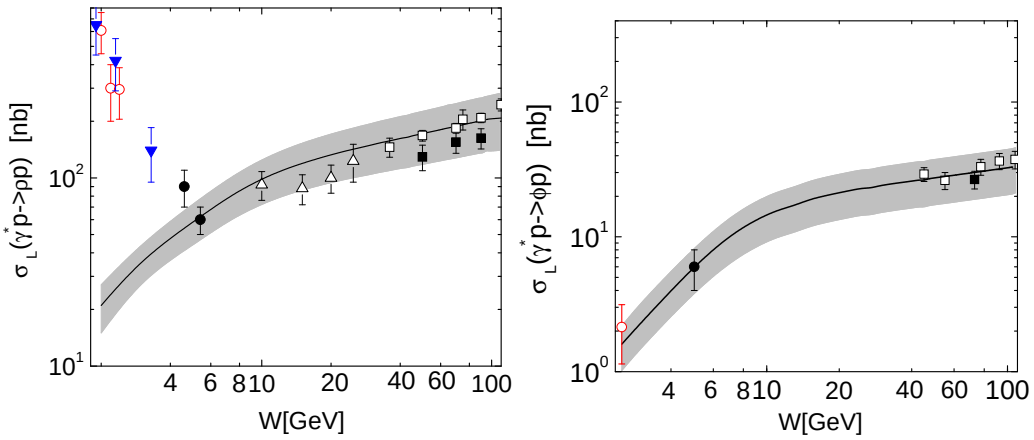

FIG. 14: Predictions of the longitudinal cross section of ρ^0 (left) and ϕ (right) production versus W at $Q^2 = 4\,\mathrm{GeV}^2$. For references to data see [287] and references therein.

meson electroproduction evaluated from the mentioned set of GPDs [1] .

For electroproduction of nucleon resonances one needs the $p \to N^*$ transition GPDs. In principle, these GPDs are new unknown functions. Straightforward predictions for reactions like $\gamma^* p \to \pi N^*$ are therefore not possible at present. In the large N_c limit, however, one can at least relate the $p \to \Delta^+$ GPDs to the flavor diagonal $p \to p$ ones since the nucleon and the Δ are eigenstates of the same object, the chiral soliton [292, 293]. The proton-proton GPDs occur here always in the isovector combination $F^{(3)} = F^u - F^d$ where F is a proton-proton GPD. With the help of flavor symmetry one can further relate the $p \to \Delta^+$ GPDs to all other octet-decuplet transitions. Using these theoretical considerations the observables for $\gamma^* p \to \pi N^*$ can be estimated. One should be aware, however, that the quality of the large N_c and $SU(3)_F$ relations are unknown; corrections of the order of 20 to 30% are to be expected. One also should bear in mind that for pion electroproduction transversely polarized virtual photons play an important role as has been shown in [288, 289]. Within the handbag approach the contributions from such photons are related to the transversity (helicity-flip) GPDs. Despite this complication an estimate of hard exclusive resonance production seems feasible.

Developed program on resonance studies at high photon virtualities [263] allow us to determine electrocouplings of several high lying N^* states with dominant $N\pi\pi$ decays (see the Table I) from the data on charged double pion electroproduction channel only. However, reliable extraction of these state electrocouplings should be supported by independent analyses of other exclusive electroproduction channels with different non-resonant mechanisms. The ηp, $K\Lambda$ electroproduction channels may improve our knowledge on electrocouplings of isospin 1/2 $P_{13}(1720)$ state, because of isospin filtering in these exclusive channels. The studies of $K\Sigma$ and $\eta\pi N$ electroproduction may offer an access to electrocouplings of $D_{33}(1700)$ and $F_{35}(1905)$ resonances. More detailed studies on feasibility to incorporate mentioned above additional exclusive channels for evaluation of high lying resonance electrocouplings are needed.

[1] . Tables of predictions for electroproduction of various mesons in this kinematical region can be obtained from the authors of [289] on request.

IV. STATUS AND PROSPECT OF EXCITED BARYON ANALYSIS CENTER (EBAC)

A. Introduction

One of the important problems in hadron physics is to understand the structure of the nucleon within Quantum Chromodynamics. Since the nucleon is a composite particle, its structure is closely related to the spectrum and structure of its excited states. For example, if the nucleon is dominanted by the quark-diquark configurations, the spectrum of its excited states will be different from the conventional constituent quark model. From the available data, we know that all of the excited nucleon states are unstable and couple strongly to the meson-baryon continuum states to form resonances in πN and γN reactions. Therefore, the extraction of nucleon resonances (called collectively as N^*) from data has been a well recognized important task in advancing our understanding of strong interactions.

With the experimental developments [39, 40] in the past two decades, very extensive high precision data of electromagnetic meson production reactions have now been obtained at Jefferson Laboratory (JLab), MIT-Bates, LEGS of Brookhaven National Laboratory, Mainz, Bonn, GRAAL, and Spring-8. The Excited Baryon Analysis Center (EBAC) was established at JLab in the Spring of 2006 for including these data to investigate nucleon resonances. In this paper, we report on the status and prospect of this 5-years research project.

The analysis at EBAC is based on a dynamical coupled-channel model (called EBAC-DCC from now on) developed in Ref.[41]. In the past few years, we have analyzed πN and γN reactions with πN[42–44] and $\pi\pi N$[45, 46] final states. The method for extracting the nucleon resonances within the EBAC-DCC model was developed in Ref.[47] with the results presented in Refs.[48–50]. The current focus is on extending these earlier efforts to perform a combined analysis of the $world$ data for $\pi N, \gamma N \to \pi N, \eta N, K\Lambda, K\Sigma$.

To explain the motivation of our approach, it is necessary to briefly describe here the procedures for extracting nucleon resonances from the data. It involves the following steps:

1. Perform complete measurements of all independent observables of the reactions considered. For pseudo-scalar meson photoproduction reactions $\gamma N \to \pi N, \eta N, K\Lambda, K\Sigma$ one needs to measure 8 observables[51] : differential cross sections, three single polarizations Σ, T and P, and four, such as G, H, E, and F, of 12 possible beam-target double polarization observables. For $\pi N \to \pi N, \eta N, K\Lambda, K\Sigma$, three observables must be measured[52] : differential cross section, target polarization P and one double polarization observable such as spin rotation R.

2. Determine the partial-wave amplitudes (PWA) from the data of complete measurements under the unitarity condition.

3. Extract the resonance parameters, defined at the poles of PWA on the unphysical sheets of the complex-energy plane, from the determined PWA. (A review of resonance extractions is given in Ref.[47].)

In reality, we still don't have complete measurements for practically all meson-nucleon reactions, while efforts are being made at JLab, Bonn, and Mainz to improve the situation. Even if the measurements are complete, the step 2 requires some model assumptions to solve the inverse bilinear problem in extracting PWA. This is easy to see by considering the simplest elastic scattering of two scalar mesons. This process has only one observable, differential cross section $d\sigma/d\Omega$, which is determined by a complex amplitude T :$d\sigma/d\Omega = |T_R + iT_i|^2$. Hence the data from

a "complete" experiment for this process can not determine the amplitude T unless its phase or magnitude is fixed by theoretical input. A study of the difficulty in determining PWA from data for the pseudo-scalar meson photoproduction reactions has recently been carried out in a EBAC-Hall B collaboration[53]. Thus, theoretical input is needed in step 2 to reduce the errors due to the lack of the complete data in step 1 and to remove the ambiguities in the determination of PWA. It is very difficult, if not impossible, to have model indepenent determinations of PWA from experimental data.

For step 3, all nucleon resonance extraction methods seem to assume that the resonance parameters can be extracted by using "any" analytic function to fit the determined partial-wave amplitudes, if the data are very accurate and cover the relevant energy region. It is possible that this may be true if the data cover all energy regions and "all" reaction channels. But such an ideal situation can never be realized in practice. Therefore it is not surprising to find that some of the extracted resonance parameters do depend sensitively on the resonance extraction method used in the analysis when the uncertainties in steps 1 and 2 are large.

In a phenomenological approach[54–63] the parametrizations of PWA are often written in terms of polynominal functions, the Briet-Wigner forms, tree-diagrams of phenomenological Lagrangians, or various combinations of them. The K-matrix method is commonly used in these analyses. The resulting functional forms allow a PWA with complex E for resonance extractions. In the EBAC-DCC model, the PWA on the unphysical sheets, where nucleon resonaces are located, of complex energy plane are defined by the dynamical coupled-channels integral equations with the driving terms defined by the well-studied meson-exchange mechanisms. A similar coupled-channel approach is also taken in the Juelich analysis[64]. Both approaches, as well as the earlier dyanmical models[65–71] for πN and γN reactions in the Δ (1232) region, are motivated by the success of the meson-exchange model of NN interactions[72]. As reviewed in Ref.[39], the K-matrix analysis models used in Refs.[57–63] can be derived from a dynamical formulation by taking the on-shell approximation , which greatly simplifes the numerical calculations, to evaluate meson-baryon propagators in the scattering equations. The analysis models of Refs.[54–57] also only involve solving algebraic equations.

Obviously, our approach and all dynamical models are much more complex and difficult than the other approaches[54–63]. Here we elebaorate two major reasons for taking a dynamical approach. First, it is desirable to fit the available data, which are often much less than what complete measurements can provide, within a reaction model which is constrained by the well-established physics. This will reduce the errors due to the lack of complete data in determining PWA and defining analytic functions for resonance extractions. In the dynamical approach, these analytic functions are constrainted by the the meson-exchange mechanisms. In the disperson-relations[73] approach, the determinations of PWA, which are then used to determine resonances by speed-plot methods, also need dyanmical assumptions, such as the choice of substraction terms, the input needed for crossing symmetry, and the asymptotic behavior of the amplitudes, to reduce the errors due to the lack of data in some kinematic regions.

The second motivation of developing dynamical models is to provide interpretations of the extracted resonance parameters in terms of the reaction mechanisms and the intrinsic excitations of the quark-gluon sub-structure of the nucleon. The extracted nucleon resonance poles and residues can in principle only be compared with the "exact" solutions of meson-baron reactions within QCD. Thus model interpretations of resonances, as provided by DCC models, are not needed if one can solve QCD exactly. However, the complex final state meson-baryon interactions make this extremely difficult, if not possible, in the forseen future. The results and interpretations from dynamical models can provide useful information for finding ways to solve QCD with good ap-

proximations, if not exactly. For example, the outcome of EBAC-DCC analysis are not only the positions and residues of resonance poles, but an effective Hamiltonian with the parameters determined in the fits to the data. A hadron structure calculation may try to see whether the parameters of this effective Hamiltonian, such as the bare masses and bare form factors, can be calculated from hadron models or LQCD. This two-steps procedure is similar to successful practices that have been used in Nuclear Physics for many years. For example, various nuclear reaction models[74] were first developed to interprete the nuclear reaction data in terms of optical potentials, form factors, spectroscopic factors etc. The many-body theory is then applied to derive these models from nuclear Hamiltonian to relate the model parameters to the basic two-nucleon and three-nucleon interactions. Attemps to calculate nuclear reactions, even the simplest proton-nucleus elastic scattering were not successful until very recent years. Thus many-years practical experience in nuclear physics (also in atmoic and molecular Physics) indicates that it is useful to take a similar programatic approach to understand hadron structure within the much more complex QCD by using information extracted from using dynamical models to analyze hadron reaction data. In fact, some advances along this two-step approach have been made in our understanding of the Δ (1232) resonaces by combing the dynamical model analyses of of Refs.[67, 68, 75] and hadron structure calculations based on the constinutent quark models[76, 77] and LQCD[78]. The P_{11} mass parameters extracted from our earlier EBAC-DCC analysis[42, 48] can be understood from the evolution of an excited state with a mass predicted by a Dyson-Schwinger-Equation model[79] to resonances determined by the coupling with meson-baryon scattering states, as required by the coupled-channels unitarity condition.

Here we note that the K-matrix models used in Refs.[57–63], which also include tree-diagram meson-exchange mechanisms can be derived , as reviewed in Ref.[39], from a dynamical formulation by taking the on-shell approximation. The on-shell approximation amounts to neglecting the influence of the reaction mecahnisms on the meson-baryon wavefunctions in the short-range region where we want to map out the quark-gluon sub-struture of N-N^* transitions. The analysis models of Refs.[54–57] also only involve on-shell matrix elements and do not have dynamical assumptions of reaction mechanisms. Accordingly, additional assumptions or theoretical efforts are needed to interpret resonance parameters extracted from the analysis based on these models.

To extract the nucleon resonance parameters and also develop interpretaions, the EBAC project has three components, as illustrated in in Fig.15. The first task is to perform a dynamical coupled-channels analysis of the *world* data of $\pi N, \gamma^* N \to \pi N, \eta N, 2\pi N, K\Lambda, K\Sigma, \pi\omega$ to determine the meson-baryon partial-wave amplitudes. The second step is to develop a procedure to extract the N^* parameters from the determined partial-wave amplitudes. The third step is to investigate the interpretations of the extracted N^* properties in terms of the available hadron models and Lattice QCD.

In section II, the dynamical coupled-channels model used in the EBAC analysis is briefly reviewed. Highlights of the analysis results are presented in section III. In section IV, we indicate the works need to be done to complete the EBAC project with conclusive results.

B. EBAC-DCC model

The EBAC analysis is based on a Hamiltonian formulation[41] within which the reaction amplitudes $T_{\alpha,\beta}(p, p'; E)$ in each partial-wave are calculated from the following coupled-channels

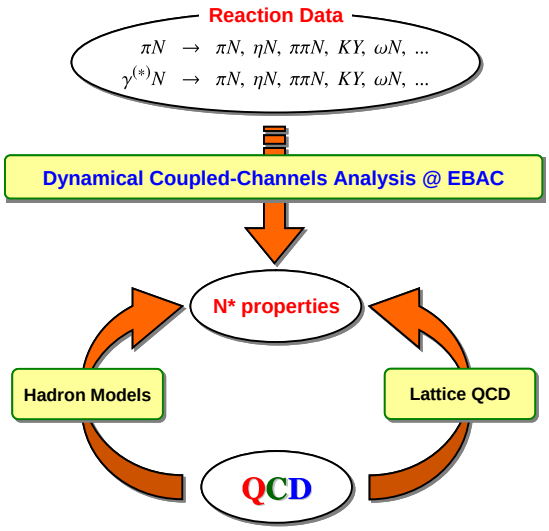

FIG. 15: The strategy of EBAC project.

integral equations

$$T_{\alpha,\beta}(p,p';E) = V_{\alpha,\beta}(p,p') + \sum_{\gamma} \int_0^{\infty} q^2 dq V_{\alpha,\gamma}(p,q) G_{\gamma}(q,E) T_{\gamma,\beta}(q,p',E)\,, \tag{1}$$

$$V_{\alpha,\beta} = v_{\alpha,\beta} + \sum_{N^*} \frac{\Gamma^{\dagger}_{N^*,\alpha}\Gamma_{N^*,\beta}}{E - M^*}\,, \tag{2}$$

where $\alpha,\beta,\gamma = \gamma N, \pi N, \eta N, KY, \omega N$, and $\pi\pi N$ which has $\pi\Delta, \rho N, \sigma N$ resonant components, $v_{\alpha,\beta}$ are meson-exchange interactions deduced from phenomenological Lagrangian, $\Gamma_{N^*,\beta}$ describes the excitation of the nucleon to a bare N^* state with a mass M^*, and $G_{\gamma}(q,E)$ is a meson-baryon propagator. The EBAC-DCC model, defined by Eqs.(1)-(2), satisfies two- and three-body unitarity conditions which are the most essential theoretical requirements. Compared with the approaches based on K-matrix or dispersion-relations, the EBAC-DCC approach has one distinct feature that the analysis can provide information on reaction mechanisms for interpreting the extracted nucleon resonances in terms of the coupling of the bare N^* states with the meson clouds generated by the meson-exchange interaction $v_{\alpha,\beta}$.

C. Development in 2006-2010

In order to determine the parameters associated with the strong-interactions parts of $V_{\alpha,\beta}$ of Eq.(2), the EBAC-DCC model was first applied to fit the πN elastic scattering up to invariant mass $W = 2$ GeV. For simplicity, KY and ωN channels were not included during this developing stage. The electromagnetic parts of $V_{\alpha,\beta}$ were then determined by fitting the data of $\gamma p \rightarrow \pi^0 p, \pi^+ n$ and $p(e,e'\pi^{0,+})N$.

The resulting 5-channels model was then tested by comparing the predicted $\pi N, \gamma N \rightarrow \pi\pi N$ production cross sections with the data. In parallel to analyzing the data, a procedure to analytically continue Eqs.(1)-(2) to the complex energy plane was developed to extract the positions an residues of nucleon resonances.

In the following subsections, we present the sample results from these efforts.

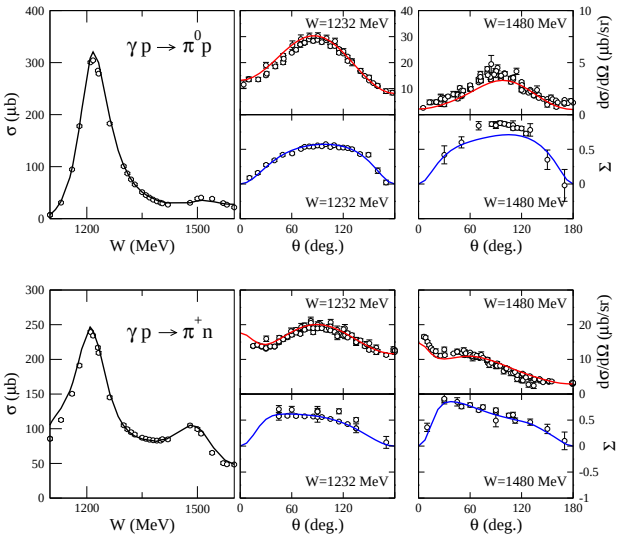

FIG. 16: The EBAC-DCC results[43] of total cross sections (σ), differential cross sections ($d\sigma/d\Omega$), and photon asymmetry (Σ) of $\gamma p \to \pi^0 p$ (upper parts), $\gamma p \to \pi^+ n$ (lower parts).

1. **Results for single pion production reactions**

In fitting the πN elastic scattering, we found that one or two bare N^* states were needed in each partial wave. The coupling strengths of the $N^* \to MB$ vertex interactions $\Gamma_{N^*,MB}$ with $MB = \pi N, \eta N, \pi\Delta, \rho N, \sigma N$ were then determined in the χ^2-fits to the data. Our results were given in Ref.[42].

Our next step was to determine the bare $\gamma N \to N^*$ interaction $\Gamma_{N^*,\gamma N}$ by fitting the $\gamma p \to \pi^0 p$ and $\gamma p \to \pi^+ n$ data. We found[43] that we were able to fit the data only up to invariant mass $W = 1.6$ GeV, mainly because we did not adjust any parameter which was already fixed in the fits to πN elastic scattering. Some of our results for total cross sections (σ), differential cross sections ($d\sigma/d\Omega$), and photon asymmetry (Σ) are shown in Fig.16.

The Q^2-dependence of the $\Gamma_{N^*,\gamma N}$ vertex functions were then determined[44] by fitting the $p(e,e'\pi^0)p$ and $p(e,e'\pi^+)n$ data up to $W = 1.6$ GeV and $Q^2 = 2$ (GeV/c)^2. Here we also did not adjust any parameter which was already fixed in the fits to πN elastic scattering. In Fig.17 we show four of our fits.

2. **Results for two-pions production reactions**

The model constructed from fitting the data of single pion production reactions was then tested by examining the extent to which the $\pi N \to \pi\pi N$ and $\gamma N \to \pi\pi N$ data can be described. It was found[45, 46] that the predicted total cross sections are in excellent agreement with the data in the near threshold $W \leq 1.4$ GeV. Our results for $\gamma p \to \pi^+\pi^- p, \pi^+\pi^0 n, \pi^0\pi^0 p$ are shown in Fig.**??**. In the higher W region, the predicted $\pi N \to \pi\pi N$ cross sections can describe to a very large extent the available data, as shown in Fig.**??**. Here the important role of the coupled-channel effects were also demonstrated. However the predicted $\gamma p \to \pi^+\pi^- p, \pi^0\pi^0 p$ cross sections were a factor of about 2 larger

than the data while the shapes of two-particles invariant mass distributions could be described very well.

3. Resonance Extractions

We follow the earlier works to define that the resonances are the eigenstates of the Hamiltonian with only outgoing waves of their decay channels. One then can show that the nucleon resonance positions are the poles M_R of meson-baryon scattering amplitudes calculated from Eqs.(1)-(2) on the unphysical sheets of complex E Riemann surface. The coupling of meson-baryon states with the resonances can be determined by the residues $R_{N^*,MB}$ at the pole positions. Our procedures for determining M_R and $R_{N^*,MB}$ and the results were presented in Refs.[47–50].

With our analytic continuation method[47, 49], we were able to analyze the dynamical origins of the extracted nucleon resonances. This was done by examining how the resonance positions move as the coupled-channels effects are gradually turned off. As illustrated in Fig.**??** for the P_{11} states, this exercise revealed that the two poles in Roper region and the next higher pole are associated with the same bare state.

The extracted residues $R_{N^*,MB}$ are complex which is the necessary mathematical consequences of any approach based on a Hamiltonian formulation. As an example, the extracted $N^* \to \gamma N$ form factors for the three P_{11} resonances indicated in Fig.**??** are shown in Fig.**??**. To complete the EBAC project, we must investigate how these results can be related to the current hadron models and LQCD.

D. Prospect

During the developing stage of EBAC in 2006-2010, the EBAC-DCC model parameters were determined by analyzing separately the following data: $\pi N \to \pi N$ [42]; $\gamma N \to \pi N$ [43], $N(e,e'\pi)N$ [44], $\pi N \to \pi\pi N$ [45], and $\gamma N \to \pi\pi N$[46]. The very extensive data of $K\Lambda$ and $K\Sigma$ production were not included in the analysis. To have a high precision extraction of nucleon

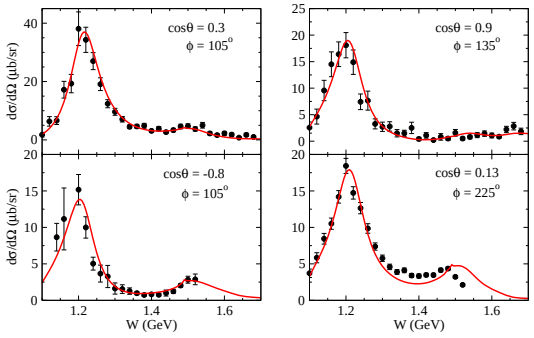

FIG. 17: The EBAC-DCC results[44] of the differential cross sections ($d\sigma/d\Omega$) of $p(e,e'\pi^0)p$.

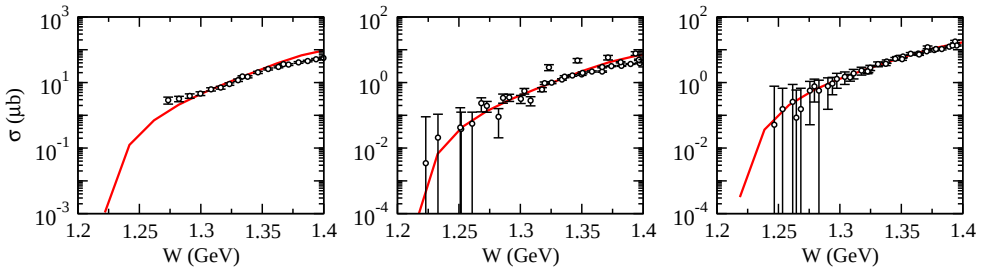

FIG. 18: The predicted[46] total cross sections of $\gamma p \to \pi^+\pi^0 n$ (left), $\pi^0\pi^0 p$ (center), $\pi^+\pi^- p$ (right) are compared with the data at $W < 1.4$ GeV.

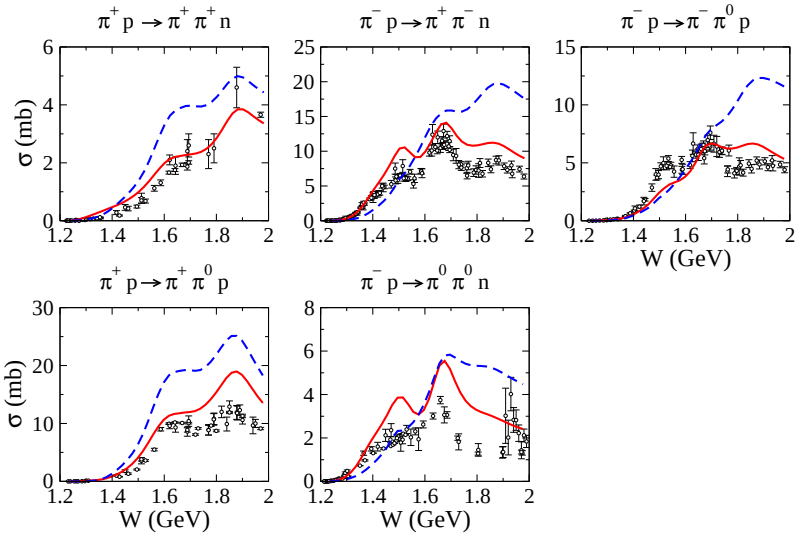

FIG. 19: The predicted[45] total cross sections of $\pi N \to \pi\pi N$ are compared with the data. The dashed-curves are obtained when the coupled-channel effects are turned off within the EBAC-DCC model.

resonances, it is necessary to perform a *combined* simultaneous coupled-channels analysis of all meson production reactions.

We have started the first combined analysis of *world* data of $\pi N, \gamma N \to \pi N, \eta N, K\Lambda, K\Sigma$ since the summer of 2010. Preliminary results have been obtained. As an example, we show in Fig. **??** the result for triple polarization observables $C_{z'}$ of $\gamma p \to K^+\Lambda$ from this combined analysis. We expect to complete this task in the Spring of 2012.

The combined analysis must be continued to also fit the $world$ data of meson electroproduction data for extracting $\gamma N \to N^*$ form factors up to sufficiently high Q^2. In addition, we should explore the interpretations of the extracted resonance parameters in terms of Lattice QCD and the available hadron models, such as the Dyson-Schwinger-Equation model and constituent quark model. This last step is needed to complete the EBAC project with conclusive results, as indicated in Fig.15. Anticipating the data from the 12 GeV upgrade of JLab, the Argonne-Osaka University collaboration will continue and extend this several years' effort to achieve this important milestone in the next decade.

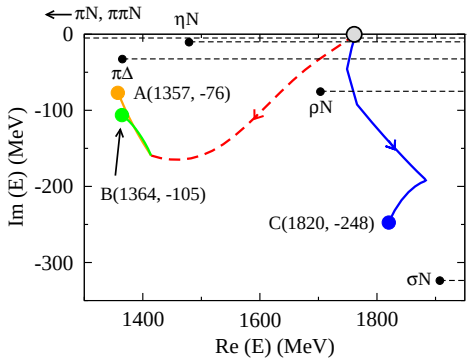

FIG. 20: The trajectories of the evolution of three nucleon resonances in P_{11} from the same bare N^* state. The results were from Ref.[48].

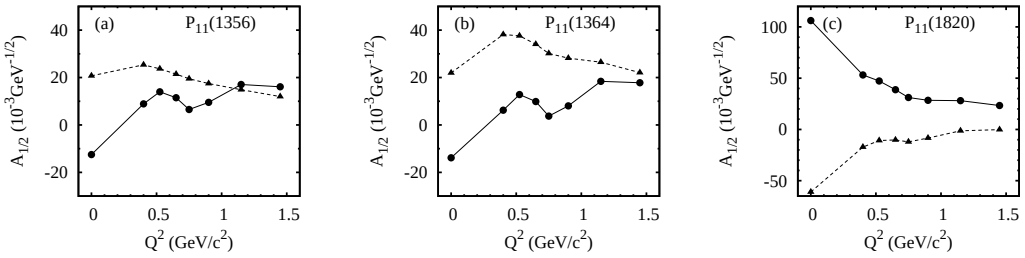

FIG. 21: The extracted[49] $\gamma N \rightarrow N^*$ form factors for the first three P_{11} nucleon resonances. Solid (dashed) curves are their real (imaginary) parts.

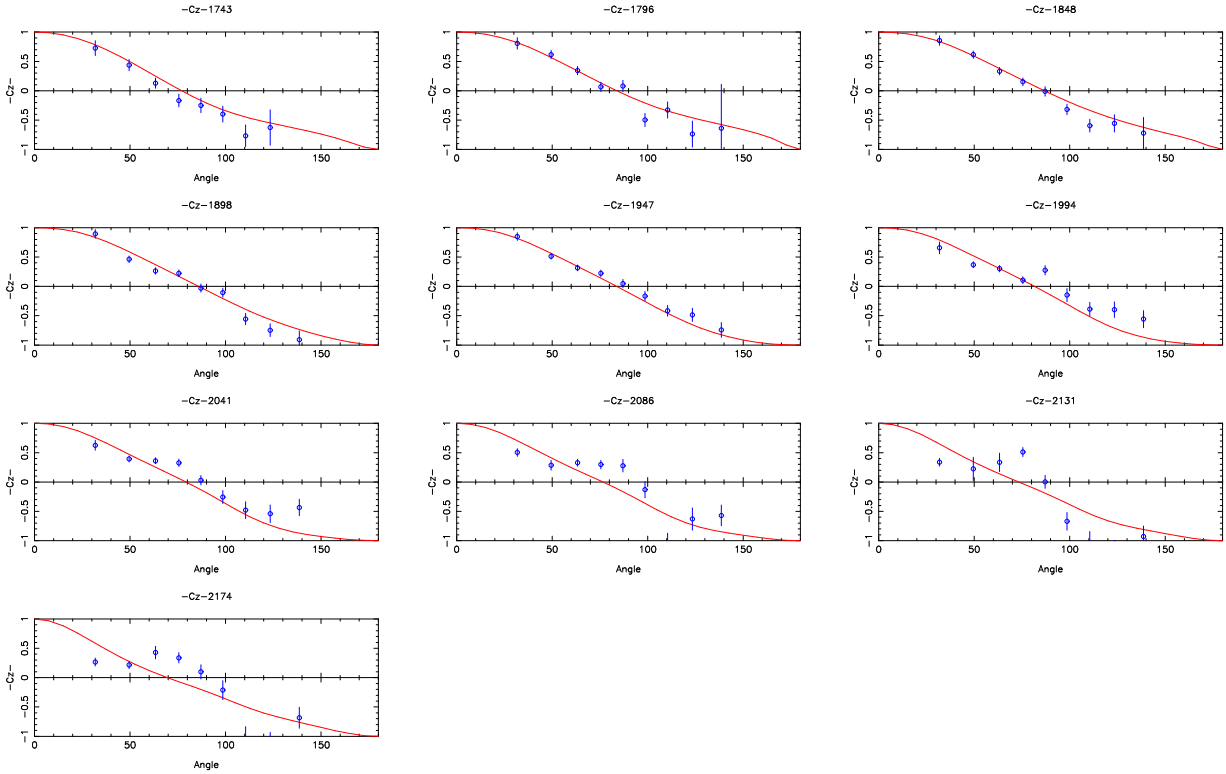

FIG. 22: Triple polarization observables $C_{z'}$ of $\gamma p \to K^+\Lambda$.

V. ILLUMINATING THE MATTER OF LIGHT-QUARK HADRONS

A. Heart of the problem

Quantum chromodynamics (QCD) is the strong-interaction part of the Standard Model of Particle Physics. Solving this theory presents a fundamental problem that is unique in the history of science. Never before have we been confronted by a theory whose elementary excitations are not those degrees-of-freedom readily accessible through experiment; i.e., whose elementary excitations are *confined*. Moreover, there are numerous reasons to believe that QCD generates forces which are so strong that less-than 2% of a nucleon's mass can be attributed to the so-called current-quark masses that appear in QCD's Lagrangian; viz., forces capable of generating mass *from nothing* (see Sec. V C). This is the phenomenon known as dynamical chiral symmetry breaking (DCSB). Elucidating the real-world predictions that follow from QCD is basic to drawing the map that explains how the Universe is constructed.

The need to determine the essential nature of light-quark confinement and dynamical chiral symmetry breaking (DCSB), and to understand nucleon structure and spectroscopy in terms of QCD's elementary degrees of freedom, are two of the basic motivations for an upgraded JLab facility. In addressing these questions one is confronted with the challenge of elucidating the role of quarks and gluons in hadrons and nuclei. Neither confinement nor DCSB is apparent in QCD's Lagrangian and yet they play the dominant role in determining the observable characteristics of real-world QCD. The physics of hadronic matter is ruled by *emergent phenomena*, such as these, which can only be elucidated and understood through the use of nonperturbative methods in quantum field theory. This is both the greatest novelty and the greatest challenge within the Standard Model. We must find essentially new ways and means to explain precisely via mathematics the observable content of QCD.

Building a bridge between QCD and the observed properties of hadrons is a key problem in modern science. The international effort focused on the physics of excited nucleons is at the heart of this program. It addresses the questions: Which hadron states and resonances are produced by QCD, and how are they constituted? The N^* program therefore stands alongside the search for hybrid and exotic mesons as an integral part of the search for an understanding of QCD.

B. Confinement

Regarding confinement, little is known and much is misapprehended. It is therefore important to state clearly that the static potential measured in numerical simulations of quenched lattice-QCD is not related in any known way to the question of light-quark confinement. It is a basic feature of QCD that light-quark creation and annihilation effects are fundamentally nonperturbative; and hence it is impossible in principle to compute a potential between two light quarks [80, 81]. Thus, in discussing the physics of light-quarks, linearly rising potentials, flux-tube models, etc., have no connection with nor justification via QCD.

A different take on confinement was laid out in Ref. [83] and exemplified in Sec. 2 of Ref. [84]. It draws on a long list of sources; e.g., Refs. [85–88], and, expressed simply, relates confinement to the analytic properties of QCD's Schwinger functions, which are often called Euclidean-space Green functions. For example, one reads from the reconstruction theorem that the only Schwinger functions which can be associated with expectation values in the Hilbert space of observables; namely, the set of measurable expectation values, are those that satisfy the axiom of reflection positivity [89]. This is an extremely tight constraint whose full implications have not yet been

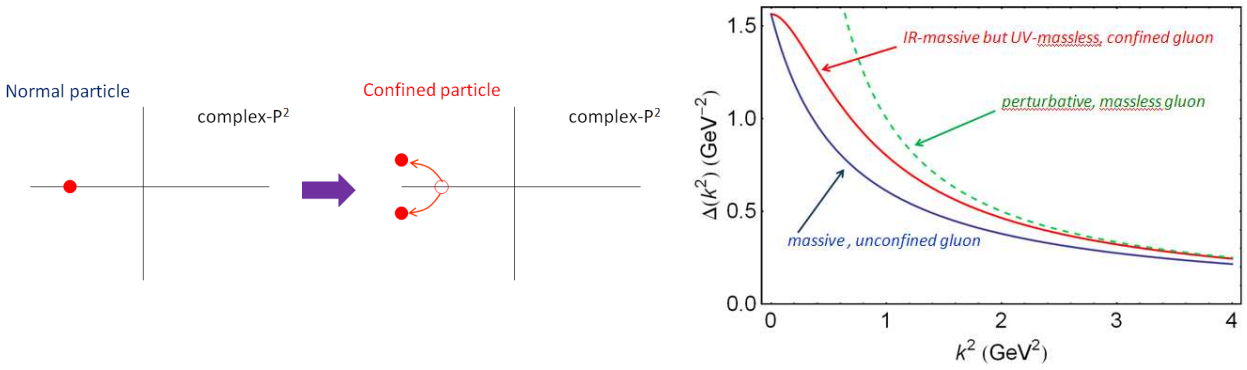

FIG. 23: *Left panel* – An observable particle is associated with a pole at timelike-P^2, which becomes a branch point if, e.g., the particle is dressed by photons. *Middle panel* – When the dressing interaction is confining, the real-axis mass-pole splits, moving into pairs of complex conjugate poles or branch points. No mass-shell can be associated with a particle whose propagator exhibits such singularity structure. *Right panel* – $\Delta(k^2)$, the function that describes dressing of a Landau-gauge gluon propagator, plotted for three distinct cases. A bare gluon is described by $\Delta(k^2) = 1/k^2$ (the dashed line), which is convex on $k^2 \in (0, \infty)$. Such a propagator has a representation in terms of a non-negative spectral density. In some theories, interactions generate a mass in the transverse part of the gauge-boson propagator, so that $\Delta(k^2) = 1/(k^2 + m_g^2)$, which can also be represented in terms of a non-negative spectral density. In QCD, however, self-interactions generate a momentum-dependent mass for the gluon, which is large at infrared momenta but vanishes in the ultraviolet [82]. This is illustrated by the curve labelled "IR-massive but UV-massless." With the generation of a mass-*function*, $\Delta(k^2)$ exhibits an inflexion point and hence cannot be expressed in terms of a non-negative spectral density.

elucidated. There is a great deal of mathematical background to this perspective. However, for a two-point function; i.e., a propagator, it means that a detectable particle is associated with the propagator only if there exists a non-negative spectral density in terms of which the propagator can be expressed. No function with an inflexion point can be written in this way. This is readily illustrated and Fig. 23 serves that purpose. The simple pole of an observable particle produces a propagator that is a monotonically-decreasing convex function, whereas the evolution depicted in the middle-panel of Fig. 23 is manifest in the propagator as the appearance of an inflexion point at $P^2 > 0$. To complete the illustration, consider $\Delta(k^2)$, which is the single scalar function that describes the dressing of a Landau-gauge gluon propagator. Three possibilities are exposed in the right-panel of Fig. 23. The inflexion point possessed by $M(p^2)$, visible in Fig. 24, entails, too, that the dressed-quark is confined.

With the view that confinement is related to the analytic properties of QCD's Schwinger functions, the question of light-quark confinement may be translated into the challenge of charting the infrared behavior of QCD's universal β-function. (The behavior of the β-function on the perturbative domain is well known.) This is a well-posed problem whose solution is a primary goal of hadron physics; e.g., Refs. [92–94]. It is the β-function that is responsible for the behavior evident in Figs. 23 and 24, and thereby the scale-dependence of the structure and interactions of dressed-gluons and -quarks. One of the more interesting of contemporary questions is whether it is possible to reconstruct the β-function, or at least constrain it tightly, given empirical information on the gluon and quark mass functions.

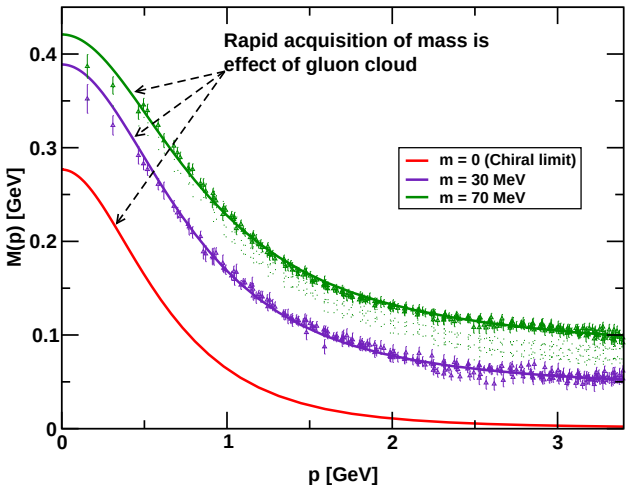

FIG. 24: Dressed-quark mass function, $M(p)$: *solid curves* – DSE results, [90], "data" – lattice-QCD simulations [91]. (NB. $m = 70\,$MeV is the uppermost curve. Current-quark mass decreases from top to bottom.) The constituent mass arises from a cloud of low-momentum gluons attaching themselves to the current-quark: DCSB is a truly nonperturbative effect that generates a quark mass *from nothing*; namely, it occurs even in the chiral limit, as evidenced by the $m = 0$ curve.

Experiment-theory feedback within the N^*-programme shows promise for providing the latter [95–97]. This is illustrated through Fig. 25, which depicts the running-gluon-mass, analogous to $M(p)$ in Fig. 24, and the running-coupling determined by analysing a range of properties of light-quark ground-state, radially-excited and exotic scalar-, vector- and flavoured-pseudoscalar-mesons in the rainbow-ladder truncation, which is leading order in a symmetry-preserving DSE truncation scheme [98]. Consonant with modern DSE- and lattice-QCD results [82], these functions derive from a gluon propagator that is a bounded, regular function of spacelike momenta, which achieves its maximum value on this domain at $k^2 = 0$ [94, 99, 100], and a dressed-quark-gluon vertex that does not possess any structure which can qualitatively alter this behaviour [101, 102]. In fact, the dressed-gluon mass drawn here produces a gluon propagator much like the curve labelled "IR-massive but UV-massless" in the right-panel of Fig. 23.

Notably, the value of $M_g = m_g(0) \sim 0.7\,$GeV is typical [99, 100]; and the infrared value of the coupling, $\alpha_{RL}(M_g^2)/\pi = 2.2$, is interesting because a context is readily provided. With nonperturbatively-massless gauge bosons, the coupling below which DCSB breaking is impossible via the gap equations in QED and QCD is $\alpha_c/\pi \approx 1/3$ [103–105]. In a symmetry-preserving regularisation of a vector $\times$ vector contact-interaction used in rainbow-ladder truncation, $\alpha_c/\pi \approx 0.4$; and a description of hadron phenomena requires $\alpha/\pi \approx 1$ [106]. With nonperturbatively massive gluons and quarks, whose masses and couplings run, the infrared strength required to describe hadron phenomena in rainbow-ladder truncation is unsurprisingly a little larger. Moreover, whilst a direct comparison between α_{RL} and a coupling, α_{QLat}, inferred from quenched-lattice results is not sensible, it is nonetheless curious that $\alpha_{QLat}(0) \lesssim \alpha_{RL}(0)$ [94]. It is thus noteworthy that with a more sophisticated, nonperturbative DSE truncation [107, 108], some of the infrared strength in the gap equation's kernel is shifted from the gluon propagator into the dressed-quark-gluon vertex. This cannot materially affect the net infrared strength required to explain observables but does reduce the amount attributed to the effective coupling. (See, e.g., Ref. [108], wherein $\alpha(M_g^2) = 0.23\,\pi$ explains important features of the meson spectrum.)

C. Dynamical chiral symmetry breaking

Whilst the nature of confinement is still debated, Fig. 24 shows that DCSB is a fact. This figure displays the current-quark of perturbative QCD evolving into a constituent-quark as its momentum becomes smaller. Indeed, QCD's dressed-quark behaves as a constituent-like-quark or a current-

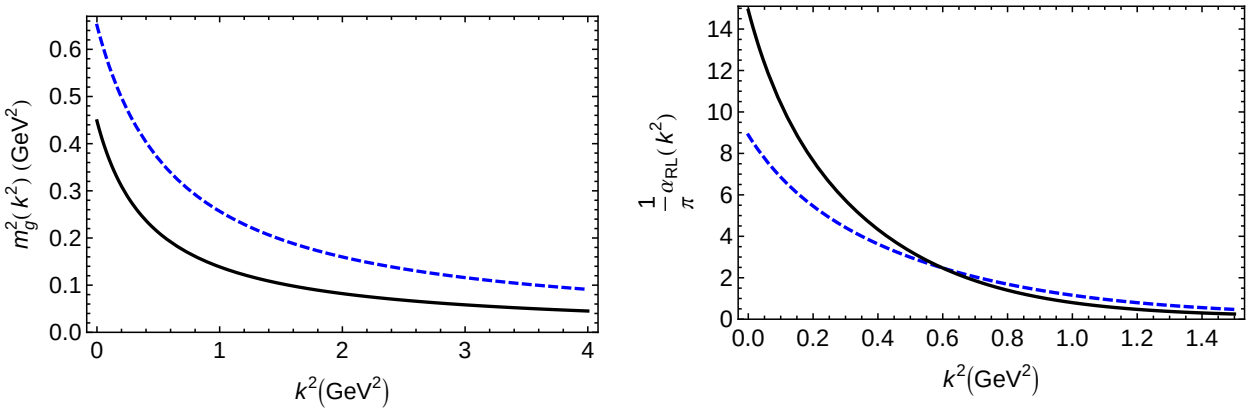

FIG. 25: *Left panel* – Rainbow-ladder gluon running-mass; and *right panel* – rainbow-ladder effective running-coupling, both determined in a DSE analysis of properties of light-quark mesons. The dashed curves illustrate forms for these quantities that provide the more realistic picture [92, 109]. (Figures drawn from Ref. [92].)

quark, or something in between, depending on the momentum with which its structure is probed.

Dynamical chiral symmetry breaking is the most important mass generating mechanism for visible matter in the Universe. This may be illustrated through a consideration of the nucleon. The nucleon's σ-term is a Poincaré- and renormalisation-group-invariant measure of the contribution to the nucleon's mass from the fermion mass term in QCD's Lagrangian [110]:

$$\sigma_N \stackrel{K^2=0}{=} \tfrac{1}{2}(m_u + m_d)\langle N(P+K)|J(K)|N(P)\rangle \approx 0.06\, m_N, \tag{3}$$

where $J(K)$ is the dressed scalar vertex derived from the source $[\bar{u}(x)u(x) + \bar{d}(x)d(x)]$ and m_N is the nucleon's mass. Some have imagined that the non-valence s-quarks produce a non-negligible contribution but it is straightforward to estimate [81, 111]

$$\sigma_N^s = 0.02 - 0.04\, m_N\,. \tag{4}$$

Based on the strength of DCSB in for heavier quarks [110], one can argue that they do not contribute a measurable σ-term. It is thus plain that more than 90% of the nucleon's mass finds its origin in something other than the quarks' current-masses.

The source is the physics which produces DCSB. As we have already mentioned, Fig. 24 shows that even in the chiral limit, when $\sigma_N \equiv 0 \equiv \sigma_N^s$, the massless quark-parton of perturbative QCD appears as a massive dressed-quark to a low-momentum probe, carrying a mass-scale of approximately $(1/3)m_N$. A similar effect is experienced by the gluon-partons: they are perturbatively massless but are dressed via self-interactions, so that they carry an infrared mass-scale of roughly $(2/3)m_N$, see Fig. 25. In such circumstances, even the simplest symmetry-preserving Poincaré-covariant computation of the nucleon's mass will produce $m_N^0 \approx 3\, M_Q^0$, where M_Q^0 is the infrared mass-scale associated with the chiral-limit dressed-quark mass-function. The details of real-world QCD fix the strength of the running coupling at all momentum scales. That strength can, however, be varied in models; and this is how we know that if the interaction strength is reduced, the nucleon mass tracks directly the reduction in M_Q^0 (see Fig. 26 and Sec. V D). Thus, the nucleon's mass is a visible measure of the strength of DCSB in QCD. These observations are an up-to-date expression of the notions first expressed in Ref. [112].

It is worth noting in addition that DCSB is an amplifier of explicit chiral symmetry breaking. This is why the result in Eq. (3) is ten-times larger than the ratio $\hat{m}/m_N$, where $\hat{m}$ is

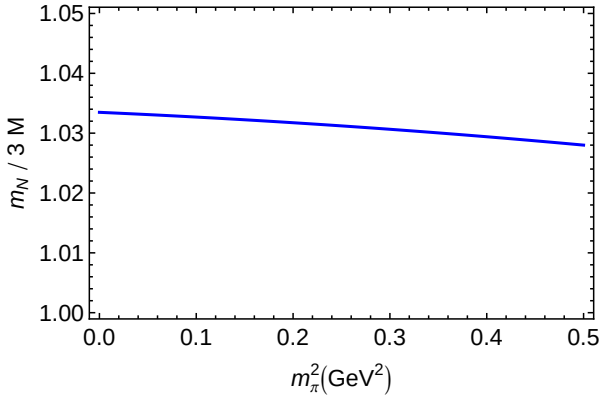

FIG. 26: Evolution with current-quark mass of the ratio $m_N/[3M]$, which varies by less-than 1% on the domain depicted. The calculation is described in Ref. [79]. NB. The current-quark mass is expressed through the computed value of m_π^2: $m_\pi^2 = 0.49\,\mathrm{GeV}^2$ marks the s-quark current-mass.

the renormalisation-group-invariant current-mass of the nucleon's valence-quarks. The result in Eq. (4) is not anomalous: the nucleon contains no valence strangeness. Following this reasoning, one can view DCSB as being responsible for roughly 98% of the proton's mass, so that the Higgs mechanism is (almost) irrelevant to light-quark physics.

The behavior illustrated in Figs. 23–25 has a marked influence on hadron elastic form factors. This is established, e.g., via comparisons between Refs. [113–117] and Refs. [106, 118, 119]. Owing to the greater sensitivity of excited states to the long-range part of the interaction in QCD, we expect this influence to be even larger in the Q^2-dependence of nucleon-to-resonance electrocouplings, the extraction of which, via meson electroproduction off protons, is an important part of the current CLAS program and studies planned with the CLAS12 detector [96, 97]. In combination with well-constrained QCD-based theory, such data can potentially therefore be used to chart the evolution of the mass function on $0.3 \lesssim p \lesssim 1.2$, which is a domain that bridges the gap between nonperturbative and perturbative QCD. This can plausibly assist in unfolding the relationship between confinement and DCSB.

In closing this subsection we re-emphasize that the appearance of running masses for gluons and quarks is a quantum field theoretic effect, unrealizable in quantum mechanics. It entails, moreover, that: quarks are not Dirac particles; and the coupling between quarks and gluons involves structures that cannot be computed in perturbation theory. Recent progress with the two-body problem in quantum field theory [107] has enabled these facts to be established [120]. One may now plausibly argue that theory is in a position to produce the first reliable symmetry-preserving, Poincaré-invariant prediction of the light-quark hadron spectrum [108].

D. Mesons and Baryons: Unified Treatment

Owing to the importance of DCSB, it is only within a symmetry-preserving, Poincaré-invariant framework that full capitalization on the results of the N^*-program is possible. One must be able to correlate the properties of meson and baryon ground- and excited-states within a single, symmetry-preserving framework, where symmetry-preserving means that all relevant Ward-Takahashi identities are satisfied. This is not to say that constituent-quark-like models are worthless. As will be seen in this White Paper, they are of continuing value because there is nothing better that is yet providing a bigger picture. Nevertheless, such models have no connection with quantum field theory and therefore not with QCD; and they are not "symmetry-preserving" and hence cannot veraciously connect meson and baryon properties.

An alternative is being pursued within quantum field theory via the Faddeev equation. This analogue of the Bethe-Salpeter equation sums all possible interactions that can occur between three dressed-quarks. A tractable equation [121] is founded on the observation that an interaction which

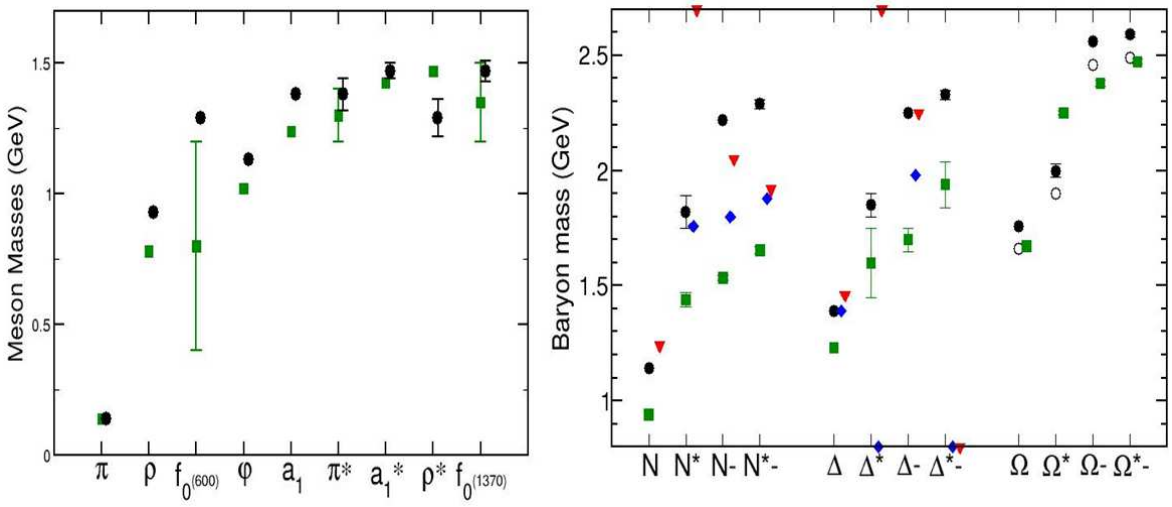

FIG. 27: Comparison between DSE-computed hadron masses (*filled circles*) and: bare baryon masses from the Excited Baryon Analysis Center (EBAC), [48] (*filled diamonds*) and Jülich,[123] (*filled triangles*); and experiment [124], *filled-squares*. For the coupled-channels models a symbol at the lower extremity indicates that no associated state is found in the analysis, whilst a symbol at the upper extremity indicates that the analysis reports a dynamically-generated resonance with no corresponding bare-baryon state. In connection with Ω-baryons the *open-circles* represent a shift downward in the computed results by $100\,$MeV. This is an estimate of the effect produced by pseudoscalar-meson loop corrections in Δ-like systems at a s-quark current-mass.

describes color-singlet mesons also generates nonpointlike quark-quark (diquark) correlations in the color-antitriplet channel [122]. The dominant correlations for ground state octet and decuplet baryons are scalar (0^+) and axial-vector (1^+) diquarks because, e.g., the associated mass-scales are smaller than the baryons' masses and their parity matches that of these baryons. On the other hand, pseudoscalar (0^-) and vector (1^-) diquarks dominate in the parity-partners of those ground states [79]. This approach treats mesons and baryons on the same footing and, in particular, enables the impact of DCSB to be expressed in the prediction of baryon properties.

Building on lessons from meson studies [125], a unified spectrum of u, d-quark hadrons has been obtained using a symmetry-preserving regularization of a vector $\times$ vector contact interaction [79]. This study simultaneously correlates the masses of meson and baryon ground- and excited-states within a single framework. In comparison with relevant quantities, the computation produces $\overline{\text{rms}}$=13%, where $\overline{\text{rms}}$ is the root-mean-square-relative-error/degree-of freedom. As evident in Fig. 27, the prediction uniformly overestimates the PDG values of meson and baryon masses [124]. Given that the employed truncation deliberately omitted meson-cloud effects in the Faddeev kernel, this is a good outcome, since inclusion of such contributions acts to reduce the computed masses.

Following this line of reasoning, a striking result is agreement between the DSE-computed baryon masses [79] and the bare masses employed in modern coupled-channels models of pion-nucleon reactions [48, 123], see Fig. 27. The Roper resonance is very interesting. The DSE study [79] produces a radial excitation of the nucleon at $1.82 \pm 0.07\,$GeV. This state is predominantly a radial excitation of the quark-diquark system, with both the scalar- and axial-vector diquark correlations in their ground state. Its predicted mass lies precisely at the value determined in the analysis of Ref. [48]. This is significant because for almost 50 years the "Roper resonance" has

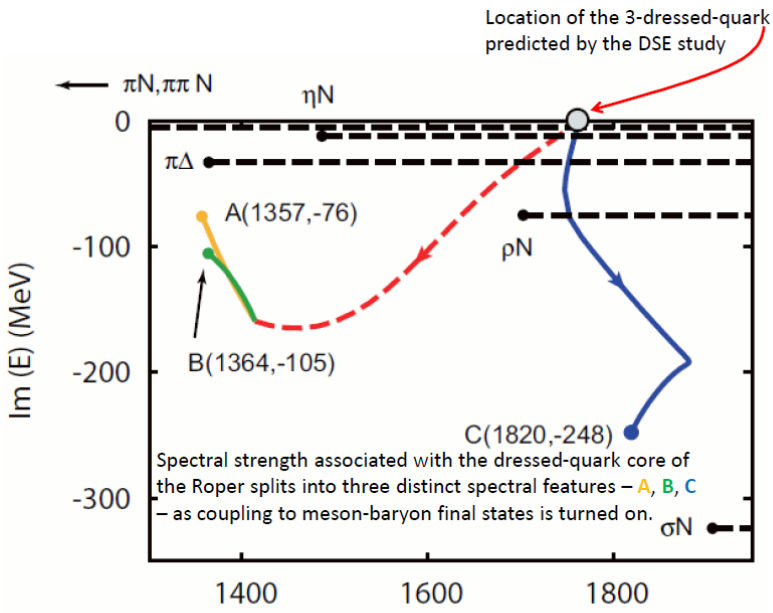

FIG. 28: EBAC examined the P_{11}-channel and found that the two poles associated with the Roper resonance and the next higher resonance were all associated with the same seed dressed-quark state. Coupling to the continuum of meson-baryon final states induces multiple observed resonances from the same bare state. In EBAC's analysis, all PDG-identified resonances were found to consist of a core state plus meson-baryon components. (Adapted from Ref. [48].)

defied understanding. Discovered in 1963, it appears to be an exact copy of the proton except that its mass is 50% greater. The mass was the problem: hitherto it could not be explained by any symmetry-preserving QCD-based tool. That has now changed. Combined, see Fig. 6, Refs. [48, 79] demonstrate that the Roper resonance is indeed the proton's first radial excitation, and that its mass is far lighter than normal for such an excitation because the Roper obscures its dressed-quark-core with a dense cloud of pions and other mesons. Such feedback between QCD-based theory and reaction models is critical now and for the foreseeable future, especially since analyses of CLAS data on nucleon-resonance electrocouplings suggest strongly that this structure is typical; i.e., most low-lying N^*-states can best be understood as an internal quark-core dressed additionally by a meson cloud [97].

Additional analysis within the framework of Ref. [79] suggests a fascinating new possibility for the Roper, which is evident in Table. II. The nucleon ground state is dominated by the scalar diquark, with a significantly smaller but nevertheless important axial-vector diquark component. This feature persists in solutions obtained with more sophisticated Faddeev equation kernels (see, e.g., Table 2 in Ref. [115]). From the perspective of the nucleon's parity partner and its radial excitation, the scalar diquark component of the ground-state nucleon actually appears to be unnaturally large.

One can nevertheless understand the structure of the nucleon. As with so much else, the composition of the nucleon is intimately connected with DCSB. In a two-color version of QCD, the scalar diquark is a Goldstone mode, just like the pion [126]. (This is a long-known result of Pauli-Gürsey symmetry.) A "memory" of this persists in the three-color theory and is evident in many ways. Amongst them, through a large value of the canonically normalized Bethe-Salpeter amplitude and hence a strong quark+quark−diquark coupling within the nucleon. (A qualitatively identical effect explains the large value of the πN coupling constant.) There is no such enhancement mechanism associated with the axial-vector diquark. Therefore the scalar diquark dominates the nucleon. The effect on the Roper produced by a contact-interaction is striking, with orthogonality of the ground- and excited-states forcing the Roper to be constituted almost entirely from the axial-vector diquark correlation.

The computation of spectra is an important and necessary prerequisite to the calculation of nucleon transition form factors, the importance of which is difficult to overestimate given the potential of such form factors to assist in charting the long-range behavior of QCD's running

TABLE II: Diquark content of the baryons' dressed-quark cores, computed with a symmetry-preserving regularization of a vector × vector contact interaction [127].

	N	$N(1440)$	$N(1535)$	$N(1650)$	$\Delta(1232)$	$\Delta(1600)$	$\Delta(1700)$	$\Delta(1940)$
0^+	77%							
1^+	23%	100%			100%	100%		
0^-			51%	43%				
1^-			49%	57%			100%	100%

coupling. To place this in context, Refs. [79, 106, 118, 119] explored the sensitivity of a range of hadron properties to the running of the dressed-quark mass-function. These studies established conclusively that static properties are not a sensitive probe of the behavior in Figs. 24, 25; viz., regularized via a symmetry-preserving procedure, a vector × vector contact-interaction predicts masses, magnetic and quadrupole moments, and radii that are practically indistinguishable from results obtained with the most sophisticated QCD-based interactions available currently [92, 128]. The story is completely different, however, with the momentum-dependence of form factors; e.g., in the case of the pion, the difference between the form factor obtained with $M(p) =$ constant and that derived from $M(p^2)$ in Fig. 24 is dramatically apparent for $Q^2 > M^2(p = 0)$ [118]. The study of diquark form factors in Ref. [106] has enabled another reference computation to be undertaken; namely, nucleon elastic and nucleon-to-Roper transition form factors. This work is almost complete, with the result that axial-vector-diquark dominance of the Roper, Table II, has a material impact on the nucleon-to-Roper transition form factor.

E. Prospects

A compelling goal of the international theory effort that works in support of the N^*-program is to understand how the interactions between dressed-quarks and -gluons create nucleon ground- and excited-states, and how these interactions emerge from QCD. This document shows no single approach is yet able to provide a unified description of all N^* phenomena; and that intelligent reaction theory will long be necessary as a bridge between experiment and QCD-based theory. Nonetheless, material progress has been made since the release of the White Paper on "Theory Support for the Excited Baryon Program at the Jlab 12-GeV Upgrade" [129]: in developing strategies; methods; and approaches to the physics of nucleon resonances. Much of that achieved via the Dyson-Schwinger equations is indicated above. Additional contributions relevant to the N^* program are: verification of the accuracy of the diquark truncation of the quark-quark scattering matrix within the Faddeev equation [117]; and a computation of the $\Delta \to \pi N$ transition form factor [130].

We intend to continue working as part of the international effort to realize the goal of turning experiment into a probe of the dressed-quark mass function. In our view, precision data on nucleon-resonance transition form factors provides a realistic means by which to constrain the momentum evolution of the dressed-quark mass function and therefrom the infrared behavior of QCD's β-function; in particular, to locate unambiguously the transition boundary between the constituent- and current-quark domains that is signalled by the sharp drop apparent in Fig. 24. That can be related to an inflexion point in QCD's β-function. Contemporary theory indicates that

this transition boundary lies at $p^2 \sim 0.6\,\mathrm{GeV}^2$. Since a probe's input momentum Q is principally shared equally amongst the dressed-quarks in a transition process, then each can be considered as absorbing a momentum fraction $Q/3$. Thus in order to cover the domain $p^2 \in [0.5, 1.0]\,\mathrm{GeV}^2$ one requires $Q^2 \in [5, 10]\,\mathrm{GeV}^2$.

In concrete terms, work on a unified description of meson and baryon spectra is continuing; e.g., with the analysis of the contact-interaction in Ref. [79] being extended to include strange hadrons. This will be completed early in 2012, as will computation of the like-founded computation of the nucleon-to-Roper transition form factors. The latter will then be extended to provide a prediction for the $N \to N(1535)$ transition, for comparison with data [131] and other computations [132].

Following these efforts, the Faddeev equation framework of Ref. [115], will be applied to the $N \to N(1440)$ transition. The strong momentum dependence of the dressed-quark mass function is an integral part of this framework. Therefore, in this study it will be possible, e.g., to vary artificially the position of the marked drop in the dressed-quark mass function and thereby identify experimental signatures for its presence and location. In addition, it will provide a crucial check on the results in Table II. Such a study is expected to begin in mid-2012 and be completed by mid-2013. It is notable that DCSB produces an anomalous electromagnetic moment for the dressed-quark. This is known to produce a significant modification of the proton's Pauli form factor at $Q^2 \lesssim 2\,\mathrm{GeV}^2$ [133]. It is also likely to be important for a reliable description of F_2^* in the nucleon-to-Roper transition.

The Faddeev equation framework of Ref. [115] involves parametrizations of the dressed-quark propagators that are not directly determined via the gap equation. An important complement would be to employ the *ab initio* rainbow-ladder truncation approach of Ref. [116, 117] in the computation of properties of excited-state baryons, especially the Roper resonance. Even a result for the Roper's mass and its Faddeev amplitude would be useful, given the results in Table II. In order to achieve this, however, technical difficulties must be faced and overcome.

In parallel with the program outlined here an effort will be underway with the aim of providing the reaction theory necessary to make reliable contact between experiment and predictions based on the dressed-quark core. While rudimentary estimates can and will be made of the contribution from pseudoscalar meson loops to the dressed-quark core of the nucleon and its excited states, a detailed comparison with experiment will only follow when the DSE-based results are used to constrain the input for dynamical coupled channels calculations.

Acknowledgments We acknowledge valuable discussions with A. Bashir, C. Chen, B. El-Bennich, L. Chang, S.-x. Qin, H. L. L. Roberts and P. C. Tandy. Work supported by: U. S. Department of Energy, Office of Nuclear Physics, contract no. DE-AC02-06CH11357.

VI. N^* PHYSICS FROM LATTICE QCD: 2011

A. Introduction

Quantum chromodynamics (QCD), when combined with the electroweak interactions, underlies all of nuclear physics, from the spectrum and structure of hadrons to the most complex nuclear reactions. The underlying symmetries that are the basis of QCD were established long ago. Under very modest assumptions, these symmetries predict a rich and exotic spectrum of QCD bound states, few of which have been observed experimentally. While QCD predicts that quarks and gluons are the basic building blocks of nuclear matter, the rich structure that is exhibited by matter suggests there are underlying collective degrees of freedom. Experiments at nuclear and high-energy physics laboratories around the world measure the properties of matter with the aim to determine its underlying structure. Several such new experiments worldwide are under construction, such as the 12-GeV upgrade at Jefferson Lab's electron accelerator, its existing the experimental halls, as well as the new Hall D.

To provide a theoretical determination and interpretation of the spectrum, *ab initio* computations within lattice QCD have been used. Historically, the calculation of the masses of the lowest-lying states, for both baryons and mesons, has been a benchmark calculation of this discretized, finite-volume computational approach, where the aim is well-understood control over the various systematic errors that enter into a calculation; for a recent review, see [294]. However, there is now increasing effort aimed at calculating the excited states of the theory, with several groups presenting investigations of the low-lying excited baryon spectrum, using a variety of discretizations, numbers of quark flavors, interpolating operators, and fitting methodologies (Refs. [295–298]). Some aspects of these calculations remain unresolved and are the subject of intense effort, notably the ordering of the Roper resonance in the low-lying nucleon spectrum.

The Hadron Spectrum Collaboration, involving the Lattice Group at Jefferson Lab, Carnegie Mellon University, University of Maryland, University of Washington, and Trinity College (Dublin), is now several years into its program to compute the high-lying excited- state spectrum of QCD, as well as their (excited-state) electromagnetic transition form factors up to $Q^2 \sim 10$ GeV^2. This program has been utilizing "anisotropic" lattices, with finer temporal than spatial resolution, enabling the hadron correlation functions to be observed at short temporal distances and hence many energy levels to be extracted [299, 300]. Recent advances suggest that there is a rich spectrum of mesons and baryons, beyond what is seen experimentally. In fact, the HSC's calculation of excited spectra, as well as recent successes with GPUs, were featured in *Selected FY10 Accomplishments in Nuclear Theory in the FY12 Congressional Budget Request*.

B. Spectrum

The development of new operator constructions that follow from continuum symmetry constructions has allowed, for the first time, the reliable identification of the spin and masses of the single-particle spectrum at a statistical precision at or below about 1%. In particular, the excited spectrum of isovector as well as isoscalar mesons (Refs. [303–305]) shows a pattern of states, some of which are familiar from the $q\bar{q}$ constituent quark model, with up to total spin $J = 4$ and arranged into corresponding multiplets. In addition, there are indications of a rich spectrum of exotic J^{PC} states, as well as a pattern of states interpretable as non-exotic hybrids [306]. The pattern of these multiplets of states, as well as their relative separation in energy, suggest a phenomenology of constituent quarks coupled with effective gluonic degrees of freedom. In particular, the

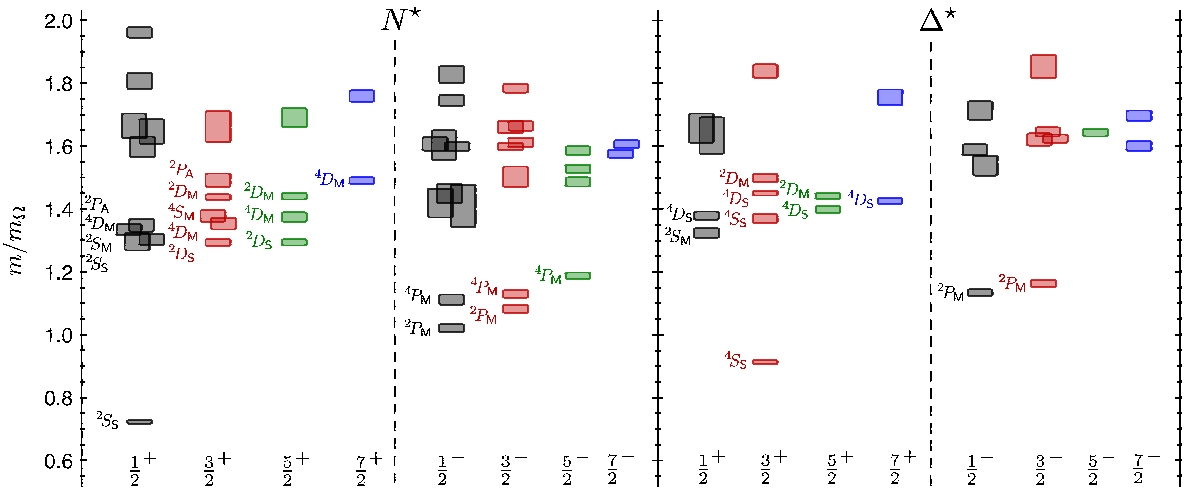

FIG. 29: Results from Ref. [301] showing the spin-identified spectrum of Nucleons and Deltas from the lattices at $m_\pi = 396$ MeV, in units of the calculated Ω mass. The states identified through their spectral overlaps are shown, and the full number of states expected from $SU(6) \otimes O(3)$ counting are found.

pattern of these exotic and non-exotic hybrid states appears to be consistent with a bag-model description and inconsistent with a flux-tube model [306].

Recently, this lattice program has been extended into the baryon spectrum, revealing for the first time, the excited-state single-particle spectrum of nucleons and Deltas along with their total spin up to $J = \frac{7}{2}$ in both positive and negative parity [301]. The results for the lightest-mass ensemble are shown in Fig. 29. There was found a high multiplicity of levels spanning across J^P which is consistent with $SU(6) \otimes O(3)$ multiplet counting, and hence with that of the non-relativistic qqq constituent quark model. In particular, the counting of levels in the low-lying negative-parity sectors are consistent with the non-relativistic quark model and with the observed experimental states [124]. The spectrum observed in the first-excited positive-parity sector is also consistent in counting with the quark model, but the comparison with experiment is less clear, with the quark model predicting more states than are observed experimentally, spurring phenomenological investigations to explain the discrepancies (e.g., see Refs. [124, 177, 229, 232, 307–309]).

In addition, it was found that there is significant mixing among each of the allowed multiplets, including the **20**-plet that is present in the non-relativistic qqq quark model but does not appear in quark-diquark models [307] (see in particular Ref. [310]). These results lend credence to the assertion that there is no "freezing" of degrees of freedom with respect to those of the non-relativistic quark model. These qualitative features of the calculated spectrum extend across all three of the quark-mass ensembles studied. Furthermore, no evidence was found for the emergence of parity-doubling in the spectrum [311].

The results for the baryon spectrum investigations from Ref. [301] suggest that to faithfully describe the excited spectrum requires the use of non-local operator constructions. Fig. 30 shows a comparison of the results for the Nucleon $J = \frac{1}{2}^+$ spectrum taken from Ref. [301] and with some other calculations in full QCD from Refs. [297, 302]. Up to some lattice scale ambiguity, it is clear there are a distinctly different number of states found at comparable pion masses. Namely, there are *four* nearly degenerate excited states found at approximately 2.2 GeV, and three nearly degenerate states near 2.8 GeV. The new results suggest the observed excited $J = \frac{1}{2}^+$ states are admixtures of radial excitations as well as D-wave and anti-symmetric P-wave structures, and the

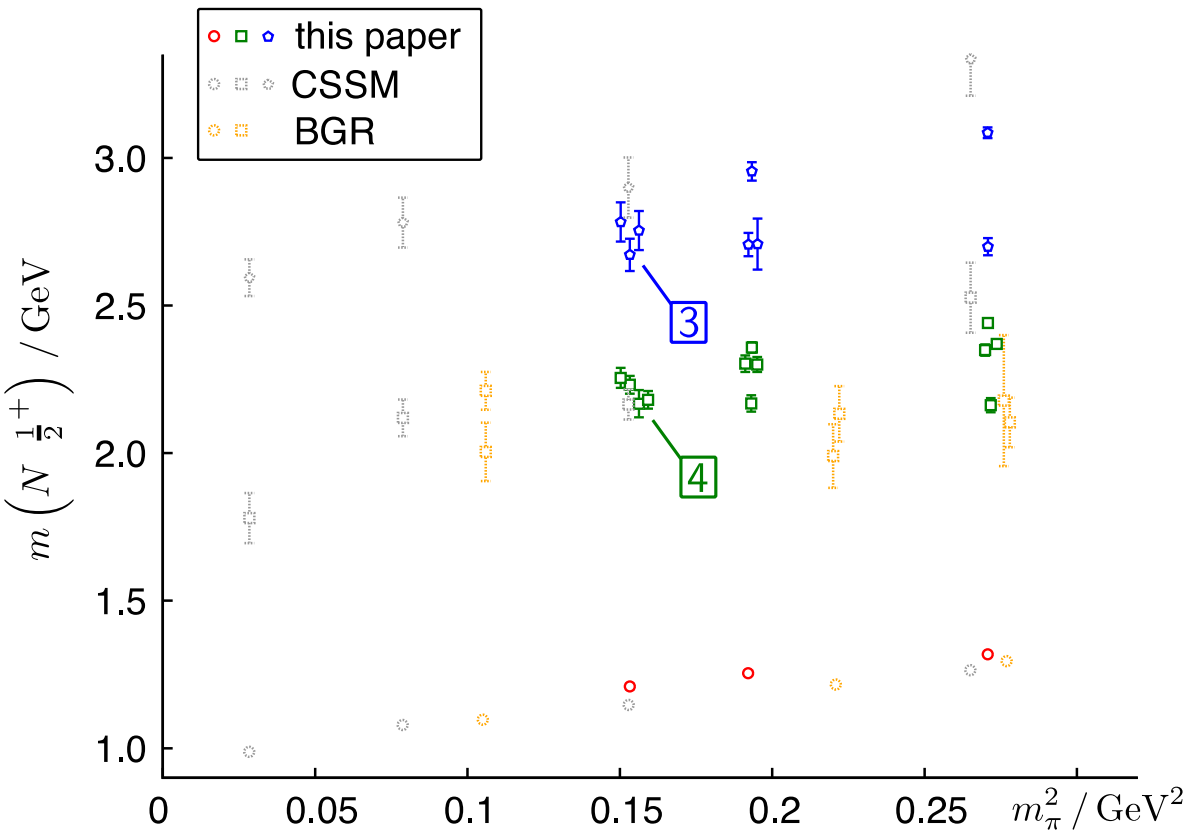

FIG. 30: Comparison of results for the nucleon $J = \frac{1}{2}^+$ channel. The results shown in grey are from Ref. [302], while those in orange are from Ref. [297]. Note that data are plotted using the scale-setting scheme in the respective papers. Results from Ref. [301] are shown in red (the ground state), green and blue. At the lightest pion mass, there is a clustering of four states as indicated near 2 GeV, while there are three nearly degenerate states 2.7 GeV. Operators featuring the derivative constructions discussed in Ref. [301] feature prominently in these excited states, suggesting previous results are insensitive to these excited states because the operator bases used were incomplete.

inclusion of operators featuring such structures is essential to resolve the degeneracy of states.

It was argued that the extracted N and Δ spectrum can be interpreted in terms of single-hadron states, and based on investigations in the meson sector [304] and initial investigations of the baryon sector at a larger volume [301], little evidence was found for multi-hadron states. To study multi-particle states, and hence the resonant nature of excited states, operator constructions with a larger number of fermion fields are needed. Such constructions are in progress [312], and it is believed that the addition of these operators will lead to a denser spectrum of states. With suitable understanding of the discrete energy spectrum of the system, the Lüscher formalism [313] and its inelastic extensions (for example, see Ref. [314]) can be used to extract the energy dependent phase shift for a resonant system, such as has been performed for the $I = 1$ ρ system [315]. The energy of the resonant state is determined from the energy dependence of the phase shift. It is this resonant energy that is suitable for chiral extrapolations. Suitably large lattice volumes and smaller pion masses are needed to adequately control the systematic uncertainties in these calculations.

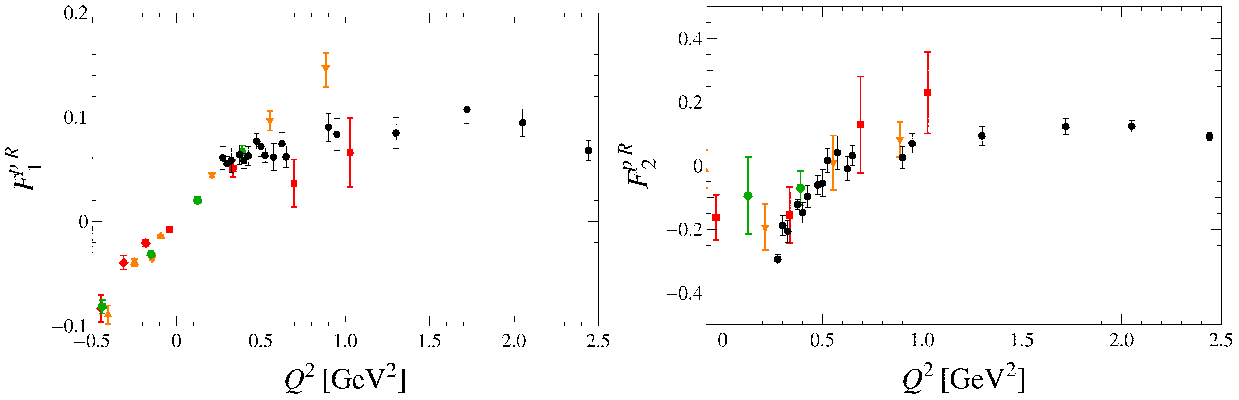

FIG. 31: Proton-Roper transition form factor $F_1^{pR}(Q^2)$ (left) and $F_2^{pR}(Q^2)$ (right) on the $N_f = 2+1$ anisotropic lattices with $M_\pi \approx 390$, 450, 875 MeV whose volumes are 3, 2.5, 2.5 fm, respectively.

C. Electromagnetic transition form factors

The measurement of the excited-to-ground state radiative transition form factors in the baryon sector provides a probe into the internal structure of hadrons. Analytically, these transition form factors can be expressed in terms of matrix elements between states $\langle N(p_f)|V_\mu(q)|N^*(p_i)\rangle$ where V_μ is a vector (or possibly axial-vector) current with some four-momentum $q = p_f - p_i$ between the final (p_f) and initial (p_i) states. This matrix element can be related to the usual form factors $F_1^*(q^2)$ and $F_2^*(q^2)$. However, the exact meaning as to the initial state $|N^*\rangle$ is the source of some ambiguity since in general it is a resonance. In particular, how is the electromagnetic decay disentangled from that of some $N\pi$ hadronic contribution?

Finite-volume lattice-QCD calculations are formulated in Euclidean space, and as such, one does not directly observe the imaginary part of the pole of a resonant state. However, the information is encoded in the volume and energy dependence of excited levels in the spectrum. Lüscher's formalism [313] and its many generalizations show how to relate the infinite-volume energy-dependent phase shifts in resonant scattering to the energy dependence of levels determined in a continuous but finite-volume box in Euclidean space. In addition, infinite-volume matrix elements can be related to those in finite-volume [316] up to a factor which can be determined from the derivative of the phase shift.

For the determination of transition form factors, what all this means in practice is that one must determine the excited-state transition matrix element from each excited level in the resonant region of a state, down to the ground state. The excited levels and the ground state might each have some non-zero momentum, arising in some Q^2 dependence. In finite volume, the transition form factors are both Q^2 and energy dependent, the latter coming from the discrete energies of the states within the resonant region. The infinite-volume form factors are related to these finite-volume form factors via the derivative of the phase shift as well as another kinematic function. Sitting close to the resonant energy, in the large volume limit the form factors become independent of the energy as expected.

The determination of transition form factors for highly excited states was first done in the charmonium sector with quenched QCD [317, 318]. Crucial to these calculations was the use of a large basis of non-local operators to form the optimal projection onto each excited level. In a quenched theory, the excited charmonium states are stable and have no hadronic decays, thus there is no correction factor.

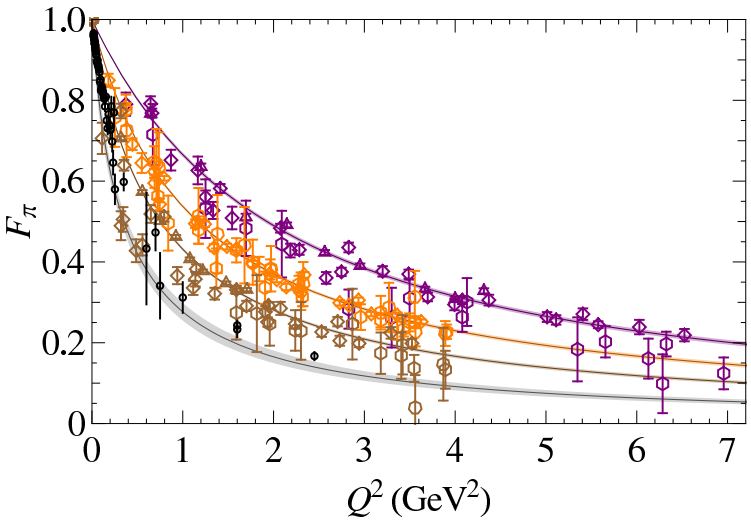

FIG. 32: Pion form factor utilizing an extended basis of smearing functions to increase the range of Q^2 with multiple pion masses at 580, 875, 1350 MeV. The experimental points are shown as (black) circles while the lowest gray band is the extrapolation to the physical pion mass using lattice points from Ref. [321].

The determination of the electromagnetic transitions in light-quark baryons will eventually require the determination of the transition matrix elements from multiple excited levels in the resonance regime, the latter determined through the spectrum calculations in the previous section. However, as a first step, the Q^2 dependence of transition form factors between the ground and first-excited state can be investigated within a limited basis. These first calculations of the $F_{1,2}^{pR}(Q^2)$ excited transition levels, in Refs. [319, 320] already have shown many interesting features.

The first calculations of the $P_{11} \to \gamma N$ transition form factors were performed a few years ago using the quenched approximation [319]. Since then, these calculations have been extended to full QCD with two light quarks and one strange quark ($N_f = 2 + 1$) using the same anisotropic lattice ensembles as for the spectrum calculations. Preliminary results [320] of the Q^2 dependence of the first-excited nucleon (the Roper) to the ground-state proton, $F_{1,2}^{pR}$, are shown in Fig. 31. These results focus on the low-Q^2 region. At the unphysical pion masses used, some points are in the time-like region. What is significant in these calculations with full-QCD lattice ensembles is that the sign of F_2 at low Q^2 has flipped compared to the quenched result, which had relatively mild Q^2 dependence at similar pion masses. These results suggest that at low Q^2 the pion-cloud dynamics are significant in full QCD.

The results so far are very encouraging, and the prospects are quite good for extending these calculations. The use of the larger operator basis employed in the spectrum calculations, supplemented with multi-particle operators, and including the correction factors from the resonant structure contained in phase shifts, should allow for the determination of multiple excited-level transition form factors up to about $Q^2 \approx 3$ GeV^2.

D. Form factors at $Q^2 \approx 6$ GeV^2

The traditional steps in a lattice form-factor calculation involve choosing suitable creation and annihilation operators with the quantum numbers of interest, and typically where the quark fields are spatially smeared so as to optimize overlap with the state of interest, often the ground state.

These smearing parameters are typically chosen to optimize the overlap of a hadron at rest or at low momentum. As the momentum is increased, the overlap of the boosted operator with the desired state in flight becomes small and statistically noisy. One method to achieve high Q^2 is to decrease the quark smearing, which has the effect of increasing overlap onto many excited states. By choosing a suitably large basis of smearing, one can then project onto the desired excited state at high(er) momentum. This technique can extend the range of Q^2 in form-factor calculations until lattice discretization effects become dominant. An earlier version of this technique (with smaller basis) was used for a quenched calculation of the Roper transition form factor reaching about 6 GeV^2 [319, 322]. Figure 32 shows an example from $N_f = 2 + 1$ at 580, 875, 1350 MeV pion masses using extended basis to extract pion form factors with Q^2 reaching nearly 7 GeV^2 [321] for the highest-mass ensemble. The extrapolated form factor at the physical pion mass shows reasonable agreement with JLab precision measurements. Future attempts will focus on decreasing the pion masses and exploring Q^2-dependence of pion form factors for yet higher Q^2.

As before, these form-factor calculations need to be extended to use a larger operator basis of single and multi-particle operators to overlap with the levels within the resonant region of the excited state, say the Roper. These operator constructions are suitable for projecting onto excited states with high momentum, as demonstrated in Ref. [312]. Future work will apply these techniques to form-factor calculations.

E. Form factors at high $Q^2 \gg 10$ GeV^2

At very high Q^2, lattice discretization effects can become quite large. A costly method to control these effects is to go to much smaller lattice spacing, basically $a \sim 1/Q$. An alternative method that was been devised long ago is to use renormalization-group techniques [323], and in particular, step-scaling techniques introduced by the ALPHA collaboration. The step-scaling method was initially applied to compute the QCD running coupling and quark masses. The technique was later extended to handle heavy-quark masses with a relativistic action [324, 325]. The physical insight is that the heavy-quark mass dependence of ratios of observables is expected to be milder than the observable itself. For form factors, the role of the large heavy-quark mass scale is now played by the large momentum scale Q. Basically, the idea is to construct ratios of observables (form factors) such that the overall Q^2 dependence is mild, and that suitable products of these ratios, evaluated at different lattice sizes and spacings, can be extrapolated to equivalent results at large volume and fine lattice spacing. The desired form factor is extracted from the ratios.

The technique, only briefly sketched here, is being used now in a USQCD lattice-QCD proposal by D. Renner (Ref. [326]) to compute the pion form-factor at large Q^2, and the technique is briefly discussed in Ref. [321]. In principle, the same technique can be used to compute excited-state transition form factors, and although feasibility has yet to be established, it seems worth further investigation.

F. Outlook

There has been considerable recent progress in the determination of the highly excited spectrum of QCD using lattice techniques. While at unphysically large pion masses and small lattice volumes, already some qualitative pictures of the spectrum of mesons and baryons is obtained. With the inclusion of multi-hadron operators, the outlook is quite promising for the determination of the excited spectrum of QCD. Anisotropic lattice configurations with several volumes are avail-

able now for pion masses down 230 MeV. Thus, it seems quite feasible to discern the resonant structure for at least a few low-lying states of mesons and baryons, of course within some systematic uncertainties, in the two-year timeframe. One of the more open questions is how to properly handle multi-channel decays which becomes more prevalent for higher-lying states. Some theoretical work has already been done using coupled-channel methods, but more work is needed and welcomed.

With the spectrum in hand, it is fairly straightforward to determine electromagnetic transition form factors for the lowest few levels of N^*, and up to some moderate Q^2 of a few GeV^2, in the two-year time-frame. Baryon form factors will probably continue to drop purely disconnected terms from the current insertion. Meson transition form factors, namely an exotic to non-exotic meson will be the first target in the short time-frame (less than two years), with the aim to determine photo-couplings. It might well be possible that with the new baryon operator techniques developed, the transition form factors can be extracted to $Q^2 \approx 6$ GeV^2. Going to an isotropic lattice with a small lattice spacing, it seems feasible to reach higher Q^2, say 10 GeV^2, and this could be available in less than five years. To reach $Q^2 \gg 10$ GeV^2 will probably require step-scaling techniques. The high-Q^2 limit is of considerable interest since it allows for direct comparisons with perturbative methods.

VII. ELECTROPRODUCTION OF N^* RESONANCES AT LARGE MOMENTUM TRANSFERS

We expect that at photon virtualities from 5 to 10 GeV^2 of CLAS12 the electroproduction cross sections of nuclear resonances will become amenable to the QCD description in terms of quark partons, whereas the description in terms of meson-baryon degrees of freedom becomes much less suitable than at smaller momentum transfers. The major challenge for theory is that quantitative description of form factors in this transition region must include nonperturbative contributions. In Ref. [132] we have suggested to use a combination of light-cone sum rules (LCSRs) and lattice calculations. To our opinion this approach presents a reasonable compromise between theoretical rigour and the necessity to make phenomenologically relevant predictions.

A. Light-cone wave functions and distribution amplitudes

The quantum-mechanical picture of a nucleon as a superposition of states with different number of partons assumes the infinite momentum frame or light-cone quantization. Although *a priori* there is no reason to expect that the states with, say, 100 partons (quarks and gluons) are suppressed as compared those with the three valence quarks, the phenomenological success of the quark model allows one to hope that only a first few Fock components are really necessary. In hard exclusive reactions which involve a large momentum transfer to the nucleon, the dominance of valence states is widely expected and can be proven, at least within QCD perturbation theory [327, 328].

The most general parametrization of the three-quark sector involves six scalar light-cone wave functions [329, 330] which correspond to different possibilities to couple the quark helicities λ_i and orbital angular momentum L_z to produce the helicity-$1/2$ nucleon state: $\lambda_1+\lambda_2+\lambda_3+L_z=1/2$. In particular if the quark helicities λ_i sum up to $1/2$, then zero angular momentum is allowed, $L=0$. The corresponding contribution can be written as [327–329]:

$$
\begin{aligned}
|N(p)^\uparrow\rangle^{L=0} \;=\; & \frac{\epsilon^{abc}}{\sqrt{6}}\int\frac{[dx][d^2\vec{k}]}{\sqrt{x_1x_2x_3}}\;\Psi_N(x_i,\vec{k}_i)|u_a^\uparrow(x_1,\vec{k}_1)\rangle \\
& \times\Big[\big|u_b^\downarrow(x_2,\vec{k}_2)\rangle|d_c^\uparrow(x_3,\vec{k}_3)\rangle-\big|d_b^\downarrow(x_2,\vec{k}_2)\rangle|u_c^\uparrow(x_3,\vec{k}_3)\rangle\Big]. \qquad (5)
\end{aligned}
$$

Here $\Psi_N(x_i,\vec{k}_i)$ is the light-cone wave function that depends on the momentum fractions x_i and transverse momenta $\vec{k}_i$ of the quarks. The integration measure is defined as

$$
\begin{aligned}
\int[dx] \;&=\; \int_0^1 dx_1dx_2dx_3\,\delta\big(\sum x_i-1\big)\,, \\
\int[d^2\vec{k}] \;&=\; (16\pi^3)^{-2}\int d\vec{k}_1d\vec{k}_2d\vec{k}_3\,\delta\big(\sum\vec{k}_i\big)\,. \qquad (6)
\end{aligned}
$$

In hard processes the contribution of $\Psi(x_i,\vec{k}_i)$ is dominant whereas the other existing three-quark wave functions give rise to a power-suppressed correction, i.e. a correction of higher twist.

The light-front description of a nucleon is very attractive for model building, but faces conceptual difficulties that do not allow the calculation of light-cone wave functions from first principles, at least at present. In particular there are subtle issues with renormalization and gauge dependence. An alternative approach has been to describe nucleon structure in terms of *distribution amplitudes*

(DA) corresponding to matrix elements of nonlocal gauge-invariant light-ray operators. The classification of DAs goes in twist rather than number of constituents as for the wave functions. For example the leading-twist-three nucleon (proton) DA is defined by the matrix element [331]:

$$\langle 0|\epsilon^{ijk}\Big(u_i^{\uparrow}(a_1n)C\not{n}u_j^{\downarrow}(a_2n)\Big)\not{n}d_k^{\uparrow}(a_3n)|N(p)\rangle = -\frac{1}{2}f_N\, p\cdot n\not{n}\, u_N^{\uparrow}(p)\int[dx]\, e^{-ip\cdot n\sum x_i a_i}\,\varphi_N(x_i)\,, \tag{7}$$

where $q^{\uparrow(\downarrow)} = (1/2)(1\pm\gamma_5)q$ are quark fields of given helicity, p_μ, $p^2 = m_N^2$, is the proton momentum, $u_N(p)$ the usual Dirac spinor in relativistic normalization, n_μ an auxiliary light-like vector $n^2 = 0$ and C the charge-conjugation matrix. The Wilson lines that ensure gauge invariance are inserted between the quarks; they are not shown for brevity. The normalization constant f_N is defined in such a way that

$$\int[dx]\,\varphi_N(x_i) = 1\,. \tag{8}$$

In principle, the complete set of nucleon DAs carries full information on the nucleon structure, same as the complete basis of light-cone wave functions. In practice, however, both expansions have to be truncated and usefulness of a truncated version, taking into account either a first few Fock states or a few lowest twists, depends on the physics application.

Using the wave function in Eq. (5) to calculate the matrix element in Eq. (7) it is easy to show that the DA $\varphi_N(x_i)$ is related to the integral of the wave function $\Psi_N(x_i,\vec{k}_i)$ over transverse momenta, which corresponds to the limit of zero transverse separation between the quarks in the position space [327]:

$$f_N(\mu)\,\varphi_N(x_i,\mu) \sim \int\limits_{|\vec{k}|<\mu}[d^2\vec{k}]\,\Psi_N(x_i,\vec{k}_i)\,. \tag{9}$$

Thus, the normalization constant f_N can be interpreted as the nucleon wave function at the origin (in position space).

Higher-twist three-quark DAs are related, in a loose sense, with similar integrals of the wave functions including extra powers of the transverse momentum, and with contributions of the other existing wave functions which correspond to nonzero quark orbital angular momentum.

As always in a field theory, extraction of the asymptotic behavior produces divergences that have to be regulated. As the result, the DAs become scheme- and scale-dependent. In the calculation of physical observables this dependence is cancelled by the corresponding dependence of the coefficient functions. The DA $\varphi_N(x_i,\mu)$ can be expanded in the set of orthogonal polynomials $\mathcal{P}_{nk}(x_i)$ defined as eigenfunctions of the corresponding one-loop evolution equation:

$$\varphi_N(x_i,\mu) = 120x_1x_2x_3\sum_{n=0}^{\infty}\sum_{k=0}^{N}c_{nk}^N(\mu)\mathcal{P}_{nk}(x_i)\,, \tag{10}$$

where

$$\int[dx]\,x_1x_2x_3\mathcal{P}_{nk}(x_i)\mathcal{P}_{n'k'} = \mathcal{N}_{nk}\delta_{nn'}\delta_{kk'} \tag{11}$$

and

$$c_{nk}^N(\mu) = c_{nk}^N(\mu_0)\left(\frac{\alpha_s(\mu)}{\alpha_s(\mu_0)}\right)^{\gamma_{nk}/\beta_0}. \tag{12}$$

Here $\mathcal{N}_{nk}$ are convention-dependent normalization factors, $\beta_0 = 11-\frac{2}{3}n_f$ and γ_{nk} the corresponding anomalous dimensions. The double sum in Eq. (10) goes over all existing orthogonal

polynomials $\mathcal{P}_{nk}(x_i)$, $k = 0, \ldots, n$, of degree n. Explicit expressions for the polynomials $\mathcal{P}_{nk}(x_i)$ for $n = 0, 1, 2$ and the corresponding anomalous dimensions can be found in Ref. [332].

In what follows we will refer to the coefficients $c_{nk}(\mu_0)$ as shape parameters. The set of these coefficients together with the normalization constant $f_N(\mu_0)$ at a reference scale μ_0 specifies the momentum fraction distribution of valence quarks on the nucleon. They are nonperturbative quantities that can be related to matrix elements of local gauge-invariant three-quark operators (see below).

In the last twenty years there had been mounting evidence that the simple-minded picture of a proton with the three valence quarks in an S-wave is insufficient, so that for example the proton spin is definitely not constructed from the quark spins alone. If the orbital angular momenta of quarks and gluons are nonzero, the nucleon is intrinsically deformed. The general classification of three-quark light-cone wave functions with nonvanishing angular momentum has been worked out in Refs. [329, 330]. In particular the wave functions with $L_z = \pm 1$ play a decisive role in hard processes involving a helicity flip, e.g. the Pauli electromagnetic form factor $F_2(Q^2)$ of the proton [333]. These wave functions are related, in the limit of small transverse separation, to the twist-four nucleon DAs introduced in Ref. [331]:

$$\begin{aligned}
\langle 0|\epsilon^{ijk}\Big(u_i^\uparrow(a_1 n) C\not{n} u_j^\downarrow(a_2 n)\Big)\not{p} d_k^\uparrow(a_3 n)|N(p)\rangle &= -\frac{1}{4}\, p\cdot n\, \not{p}\, u_{N^*}^\uparrow(p) \int [dx]\, e^{-ip\cdot n \sum x_i a_i} \\
&\quad \times \Big[f_N \Phi_4^{N,WW}(x_i) + \lambda_1^N \Phi_4^N(x_i)\Big]\,, \\
\langle 0|\epsilon^{ijk}\Big(u_i^\uparrow(a_1 n) C\not{n}\gamma_\perp\not{p} u_j^\downarrow(a_2 n)\Big)\, \gamma^\perp \not{n} d_k^\uparrow(a_3 n)|N(p)\rangle &= -\frac{1}{2}\, p\cdot n\, \not{n}\, m_N u_N^\uparrow(p) \int [dx]\, e^{-ip\cdot n \sum x_i a_i} \\
&\quad \times \Big[f_N \Psi_4^{N,WW}(x_i) - \lambda_1^N \Psi_4^N(x_i)\Big]\,, \\
\langle 0|\epsilon^{ijk}\Big(u_i^\uparrow(a_1 n) C\not{p}\not{n} u_j^\uparrow(a_2 n)\Big)\, \not{n} d_k^\uparrow(a_3 n)|N(p)\rangle &= \frac{\lambda_2^N}{12}\, p\cdot n\, \not{n}\, m_N u_N^\uparrow(p) \int [dx]\, e^{-ip\cdot n \sum x_i a_i} \\
&\quad \times\, \Xi_4^N(x_i)\,, \qquad (13)
\end{aligned}$$

where $\Phi_4^{N,WW}(x_i)$ and $\Psi_4^{N,WW}(x_i)$ are the so-called Wandzura-Wilczek contributions, which can be expressed in terms of the leading-twist DA $\varphi_N(x_i)$ [332]. The two new constants λ_1^N and λ_2^N are defined in such a way that the integrals of the "genuine" twist-4 DAs Φ_4, Ψ_4, Ξ_4 are normalized to unity, similar to Eq. (8). They are related to certain normalization integrals of the light-cone wave functions for the three-quark states with $L_z = \pm 1$, see Ref. [333] for details.

Light-cone wave functions and DAs of all baryons, including the nucleon resonances, can be constructed in a similar manner, taking into account spin and flavor symmetries. This extension is especially simple for the parity doublets of the usual $J^P = \frac{1}{2}^+$ octet since the nonlocal operators entering the definitions of nucleon DAs do not have a definite parity. Thus the same operators couple also to $N^*(1535)$ and one can define the corresponding leading-twist DA by the same expression as for the nucleon:

$$\langle 0|\epsilon^{ijk}\Big(u_i^\uparrow(a_1 n) C\not{n} u_j^\downarrow(a_2 n)\Big)\, \not{n} d_k^\uparrow(a_3 n)|N^*(p)\rangle = \frac{1}{2} f_{N^*}\, p\cdot n\, \not{n}\, u_{N^*}^\uparrow(p) \int [dx]\, e^{-ip\cdot n \sum x_i a_i}\, \varphi_{N^*}(x_i)\,, \qquad (14)$$

where, of course, $p^2 = m_{N^*}^2$. The constant f_{N^*} has a physical meaning of the wave function of $N^*(1535)$ at the origin. The DA $\phi_{N^*}(x_i)$ is normalized to unity (8) and has an expansion identical

to (10):

$$\varphi_{N^*}(x_i,\mu) = 120 x_1 x_2 x_3 \sum_{n=0}^{\infty}\sum_{k=0}^{N} c_{nk}^{N^*}(\mu)\mathcal{P}_{nk}(x_i)\,, \tag{15}$$

albeit with different shape parameters $c_{nk}^{N^*}$.

Similar as for the nucleon, there exist three independent subleading twist-4 distribution amplitudes for the $N^*(1535)$ resonance: $\Phi_4^{N^*}$, $\Psi_4^{N^*}$ and $\Xi_4^{N^*}$. Explicit expressions are given in Ref. [132].

B. Moments of distribution amplitudes from lattice QCD

The normalization constants f, λ_1, λ_2 and the shape parameters c_{nk} are related to matrix elements of local three-quark operators between vacuum and the baryon state of interest, and can be calculated using lattice QCD. Investigations of excited hadrons using this method are generally much more difficult compared to the ground states. On the other hand, the states of opposite parity can be separated rather reliably as propagating forwards and backwards in euclidian time. For this reason, for the time being we concentrate on the study of the ground state baryon octet $J^P = \frac{1}{2}^+$, and the lowest mass octet with negative parity, $J^P = \frac{1}{2}^-$, $N^*(1535)$ being the prime example.

Following the exploratory studies reported in Refs. [132, 334, 335] QCDSF collaboration is investing significant effort to make such calculations fully quantitative. The calculation is rather involved and requires the following steps: (1) Find lattice (discretized) operators that transform according to irreducible representations of spinorial group $\overline{H(4)}$; (2) Calculate non-perturbative renormalization constants for these operators; (3) Compute matrix elements of these operators on the lattice from suitable correlation functions, and (4) Extrapolate $m_\pi \to m_\pi^{\rm phys}$, lattice volume $V \to \infty$ and lattice spacing $a \to 0$.

Irreducibly transforming $\overline{H(4)}$ multiplets for three-quark operators have been constructed in Ref. [336]. Non-perturbative renormalization and one-loop scheme conversion factors RI-MOM$\to$ $\overline{\rm MS}$ have been calculated in Ref. [337]. A consistent perturbative renormalization scheme for the three-quarks operators in dimensional regularization has been found [338] and the calculation of two-loop conversion factors using this scheme is in progress.

The matrix elements of interest are calculated from correlation functions of the form $\langle \mathcal{O}_{\alpha\beta\gamma}(x)\bar{\mathcal{N}}(y)_\tau\rangle$, where $\mathcal{N}$ is a smeared nucleon interpolator and $\mathcal{O}$ is a local three-quark operator with up to two derivatives, and applying the parity "projection" operator $(1/2)(1 \pm m\gamma_4/E)$ [339]. In this way we get access to the normalization constants, the first and the second moments of the distribution amplitudes. Calculation of yet higher moments is considerably more difficult because one cannot avoid mixing with operators of lower dimension.

The correlation functions were evaluated using $N_f = 2$ dynamic Wilson (clover) fermions on several lattices and a range of pion masses $m_\pi \geq 180$ MeV. Our preliminary results for the wave functions the nucleon and $N^*(1535)$ at the origin are summarized in Fig. 33 [340]. The extrapolation of the results for the nucleon to the physical pion mass and infinite volume as well as the analysis of the related systematic errors are in progress. An example of such an analysis is shown in Fig. 34.

This analysis will be done using one-loop chiral perturbation theory. The necessary expressions have been worked out in Ref. [342]. Whereas the pion mass dependence of nucleon couplings is generally in agreement with expectations, we observe a large difference (up to a factor of three) in $N^*(1535)$ couplings calculated with heavy and light pions: All couplings drop significantly in

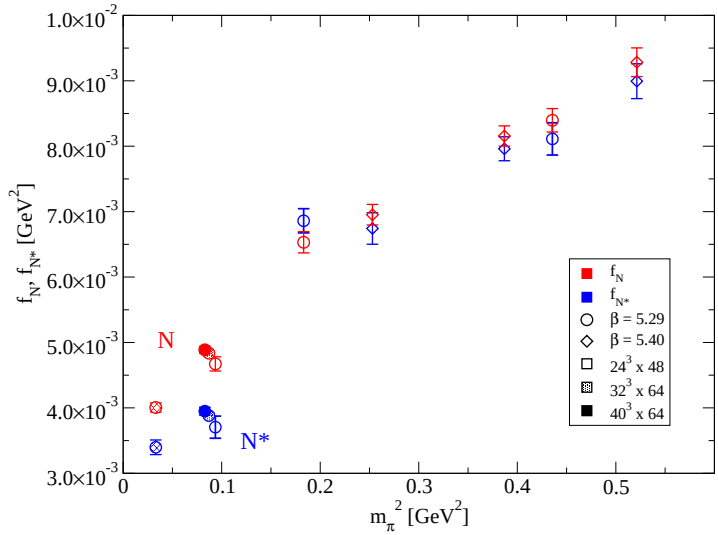

FIG. 33: Probability amplitude f_N, f_{N^*} to find the three valence quarks in the nucleon and $N^*(1535)$ at the same space-time point (wave function at the origin).

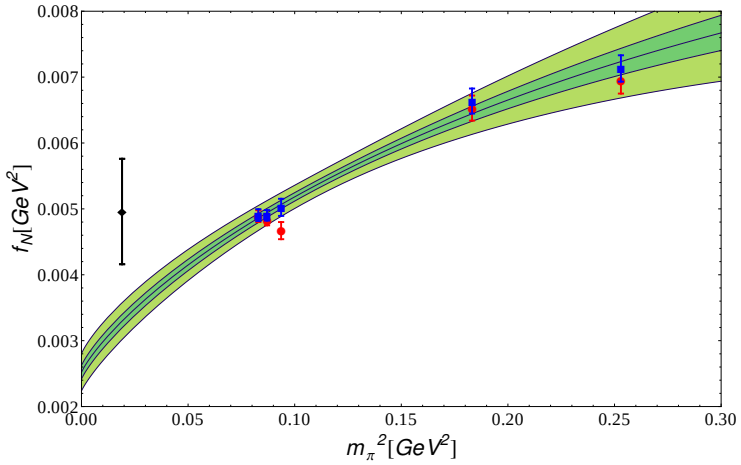

FIG. 34: The chiral extrapolation of f_N to the physical (light) quark masses. The red points are lattice data and the blue points are corrected for finite volume effects. The green bands are the 1- and 2-σ errors, respectively. The left-most black "data point" at the physical mass shows the recently updated estimate from QCD sum rule calculations [341].

the transition region where the decay $N^* \to N\pi$ opens up. This effect can be due to the change in the structure of the wave function, but also to contamination of our $N^*(1535)$ results by the contribution of the πN scattering state, or some other lattice artefact. This is one of the issues that have to be clarified in future.

We also find that the wave function of the $N^*(1535)$ resonance is much more asymmetric compared to the nucleon: nearly 50% of the total momentum is carried by the u-quark with the same helicity. This shape is illustrated in Fig. 35 where the leading-twist distribution amplitudes of the nucleon (left) and $N^*(1535)$ (right) are shown in barycentric coordinates $x_1 + x_2 + x_3 = 1$; x_i are the momentum fractions carried by the three valence quarks.

Our plans for the coming 2-3 years are as follows. The final analysis of the QCDSF lattice

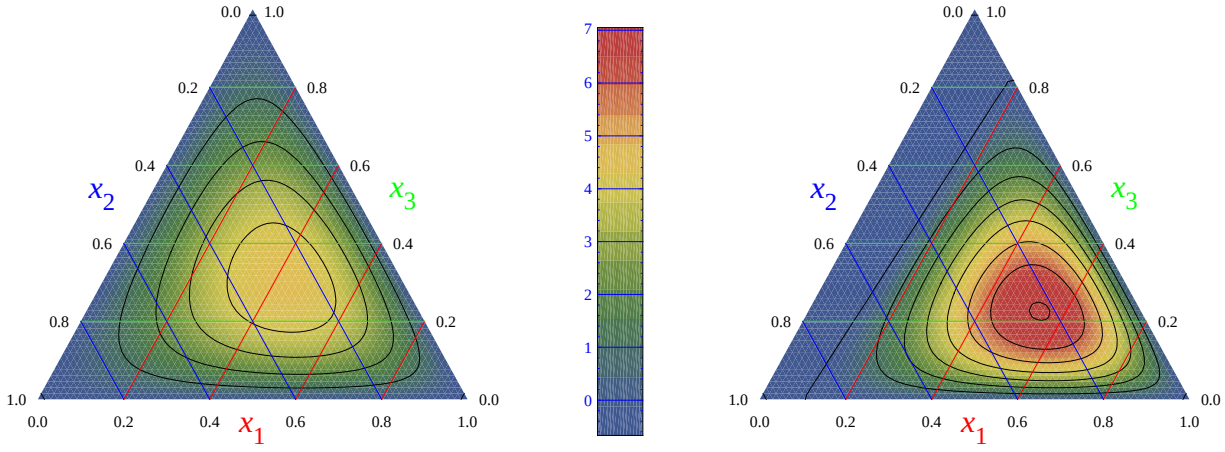

FIG. 35: Leading-twist distribution amplitudes of the nucleon (left) and $N^*(1535)$ (right) in barycentric coordinates $x_1 + x_2 + x_3 = 1$.

data using two flavors of dynamic fermions is nearly completed and in future we will go over to $N_f = 2 + 1$ studies, i.e. include dynamic strange quarks. The generation of the corresponding gauge configurations is in progress and first results are expected in one year from now. We will continue the studies of the lowest mass states in the $J^P = 1/2^+$ and $J^P = 1/2^-$ baryon octets. In particular the distribution amplitudes of the Λ and Σ baryons will be studied for the first time. At a later stage we hope to be able to do similar calculations for the $J^P = 3/2^\pm$ decuplets. We are working on the calculation of two-loop conversion factors RI-MOM$\to \overline{\rm MS}$ using the renormalization scheme suggested in [338] and plan to employ them in the future studies. Main attention will be payed to the analysis of various sources of systematic uncertainties. With the recent advances in the algorithms and computer hardware the quark mass and finite volume extrapolations of lattice data have become less of a problem, which allows us to concentrate on more subtle issues. Our latest simulations for small pion masses make possible, for the first time, to study the transition region where decays of resonances, e.g. $N^* \to N\pi$, become kinematically allowed. We have to understand the influence of finite resonance width on the calculation of operator matrix elements and to this end plan to consider ρ-meson distribution amplitudes as a simpler example. We will also make detailed studies of meson (pion) distribution amplutides in order to understand better the lattice discretization errors and work out a concrete procedure to minimize their effect. The full programm is expected to last five years and is part of the proposal for the renewal of the Transregional Collaborative Research Centre (SFB/Transregio 55 “Hadron Physics with Lattice QCD”) which will be submitted to the German Research Council (DFG) in April 2012.

C. Light-cone distribution amplitudes and form factors

The QCD approach to hard reactions is based on the concept of factorization: one tries to identify the short distance subprocess which is calculable in perturbation theory and take into account the contributions of large distances in terms of nonprerturbative parton distributions.

The problem is that in the case of the baryon form factors the hard perturbative QCD (pQCD) contribution is only the third term of the factorization expansion. Schematically, one can envisage

the expansion of, say, the Dirac electromagnetic nucleon form factor $F_1(Q^2)$ of the form

$$F_1(Q^2) \quad \sim \quad A(Q^2) + \left(\frac{\alpha_s(Q^2)}{\pi}\right) \frac{B(Q^2)}{Q^2} + \left(\frac{\alpha_s(Q^2)}{\pi}\right)^2 \frac{C}{Q^4} + \dots \tag{16}$$

where C is a constant determined by the nucleon DAs, while $A(Q^2)$ and $B(Q^2)$ are form-factor-type functions generated by contributions of low virtualities, see Fig. 36. The soft functions $A(Q^2)$ and $B(Q^2)$ are purely nonperturbative and cannot be further simplified e.g. factorized in terms of DAs. In the light-cone formalism, they are determined by overlap integrals of the soft parts of hadronic wave functions corresponding to large transverse separations. Various estimates suggest

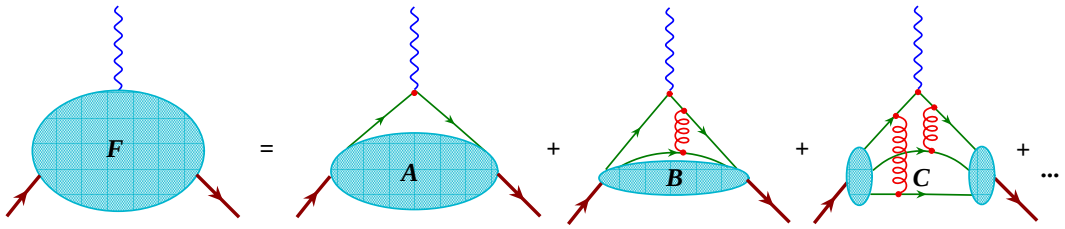

FIG. 36: Structure of QCD factorization for baryon form factors.

that $A(Q^2) \lesssim 1/Q^6$, $B(Q^2) \lesssim 1/Q^4$ and at very large Q^2 they are further suppressed by the Sudakov form factor. To be precise, in higher orders in $\alpha_s(Q)$ there exist double-logarithmic contributions $\sim 1/Q^4$ [343] that are not factorized in the standard manner; however, also they are suppressed by the Sudakov mechanism [343, 344]. Thus, the third term in (16) is formally the leading one at large Q^2 to power accuracy.

The main problem of the pQCD approach [327, 328] is a numerical suppression of each hard gluon exchange by the α_s/π factor which is a standard perturbation theory penalty for each extra loop. If, say, $\alpha_s/\pi \sim 0.1$, the pQCD contribution to baryon form factors is suppressed by a factor of 100 compared to the purely soft term. As the result, the onset of the perturbative regime is postponed to very large momentum transfers since the factorizable pQCD contribution $O(1/Q^4)$ has to win over nonperturbative effects that are suppressed by extra powers of $1/Q^2$, but do not involve small coefficients. There is an (almost) overall consensus that "soft" contributions play the dominant role at present energies. Indeed, it is known for a long time that the use of QCD-motivated models for the wave functions allows one to obtain, without much effort, soft contributions comparable in size to experimentally observed values. Also models of generalized parton distributions usually are chosen such that the experimental data on form factors are described by the soft contributions alone. A subtle point for these semi-phenomenological approaches is to avoid double counting of hard rescattering contributions "hidden" in the model-dependent hadron wave functions or GPD parametrizations.

One expects that the rapid development of lattice QCD will allow one to calculate several benchmark baryon form factors to sufficient precision from first principles. Such calculations are necessary and interesting in its own right, but do not add to our understanding of how QCD actually "works" to transfer the large momentum along the nucleon constituents, the quarks and gluons. The main motivation to study "hard"processes has always been to understand hadron properties in terms of quark and gluon degrees of freedom; for example, the rationale for the continuing measurements of the total inclusive cross section in deep inelastic scattering is to extract quark and gluon parton distributions. Similar, experimental measurements of the electroproduction of

nucleon resonances at large momentum transfers should eventually allow one to get insight in their structure on parton level, in particular momentum fraction distributions of the valence quarks and their orbital angular momentum encoded in DAs, and this task is obscured by the presence of large "soft" contributions which have to be subtracted.

Starting in Ref. [345] and in subsequent publications we have been developing an approach to hard exclusive processes with baryons based on light-cone sum rules (LCSR) [346, 347]. This technique is attractive because in LCSRs "soft" contributions to the form factors are calculated in terms of the same DAs that enter the pQCD calculation and there is no double counting. Thus, the LCSRs provide one with the most direct relation of the hadron form factors and distribution amplitudes for realistic momentum transfers of the order of $2-10$ GeV^2 that is available at present, with no other nonperturbative parameters. It is also sufficiently general and can be applied to many hard reactions.

The basic object of the LCSR approach is the correlation function

$$\int dx\, e^{iqx} \langle N^*(P)|T\{\eta(0) j(x)\}|0\rangle \tag{17}$$

in which j represents the electromagnetic (or weak) probe and η is a suitable operator with nucleon quantum numbers. The nucleon resonance in the final state is explicitly represented by its state vector $|N^*(P)\rangle$, see a schematic representation in Fig. 37. When both the momentum transfer Q^2

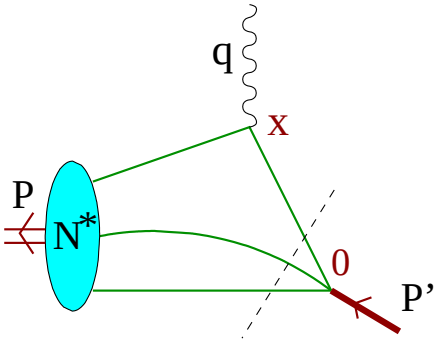

FIG. 37: Schematic structure of the light-cone sum rule for electroproduction of nucleon resonances.

and the momentum $(P')^2 = (P+q)^2$ flowing in the η vertex are large and negative, the asymptotic of the correlation function is governed by the light-cone kinematics $x^2 \to 0$ and can be studied using the operator product expansion (OPE) $T\{\eta(0) j(x)\} \sim \sum C_i(x) \mathcal{O}_i(0)$ on the light-cone $x^2 = 0$. The x^2-singularity of a particular perturbatively calculable short-distance factor $C_i(x)$ is determined by the twist of the relevant composite operator $\mathcal{O}_i$, whose matrix element $\langle N^*|\mathcal{O}_i(0)|0\rangle$ is given by an appropriate moment of the N^* DA. Next, one can represent the answer in form of the dispersion integral in $(P')^2$ and define the nucleon contribution by the cutoff in the quark-antiquark invariant mass, the so-called interval of duality s_0 (or continuum threshold). The main role of the interval of duality is that it does not allow large momenta $|k^2| > s_0$ to flow through the η-vertex; to the lowest order $O(\alpha_s^0)$ one obtains a purely soft contribution to the form factor as a sum of terms ordered by twist of the relevant operators and hence including both the leading- and the higher-twist nucleon DAs. Note that, in difference to the hard mechanism, the contribution of higher-twist DAs is only suppressed by powers of the interval of duality $s_0 \sim 2$ GeV^2 (or by powers of the Borel parameter if one applies some standard QCD sum rule machinery), but not by powers of Q^2. This feature is in agreement with the common wisdom that soft contributions are not constrained to small transverse separations.

We stress that LCSRs are not based on any nonperturbative model of the nucleon structure, but rather present a relation between the physical observables (form factors) and baryon wave functions at small transverse separation (distribution amplitudes).

Historically, LCSRs were developed in Refs. [346, 347] in an attempt to overcome difficulties of the Shifman-Vainstein-Zakharov QCD sum rule approach [348] for exclusive processes dominated by the light-cone kinematics. In the last 20 years LCSRs have been applied extensively to the exclusive B-decays and remain to be the only nonperturbative technique that allows one to calculate the corresponding form factors directly at large recoil. In fact the value of the CKM matrix element V_{ub} quoted by the Particle Data Group as the one extracted from exclusive semileptonic decay $B \to \pi\ell\nu_\ell$ is largely based on the recently updated LCSR calculations of the form factor $f_+^{B\to\pi}(0)$ [349, 350] (although the lattice QCD calculations have become competitive). Another important application of LCSRs was for calculation of the electromagnetic pion form factor. More references and further details can be found in the review articles [351, 352].

LCSRs for meson form factors have achieved a certain degree of maturity. One lesson is that they are fully consistent with pQCD and factorization theorems. In particular the LCSRs also contain terms generating the asymptotic pQCD contributions. In the pion case, it was explicitly demonstrated that the contribution of hard rescattering is correctly reproduced in the LCSR approach as a part of the $O(\alpha_s)$ correction. It should be noted that the diagrams of LCSR that contain the "hard" pQCD contributions also possess "soft" parts, i.e., one should perform a separation of "hard" and "soft" terms inside each diagram. As a result, the distinction between "hard" and "soft" contributions appears to be scale- and scheme-dependent. Most of the LCSRs for meson decays have been derived to the next-to-leading-order (NLO) accuracy in the strong coupling. The first NLO LCSR calculations were done in 1997–1998 and since then the NLO accuracy has become standard in this field. The size of NLO corrections depends on the form factor in question but typically is of the order of 20%, for the momentum transfers of interest.

Derivation of LCSRs for exclusive reactions involving baryons is, conceptually, a straightforward generalization of the LCSRs for mesons. On the other hand, there are a few new technical issues that had to be resolved, and also the calculations become much more challenging. The development so far was mainly to explore the existing possibilities and identify potential applications. Following the first application to the electromagnetic and axial form factors of the nucleon in Refs. [345, 353], LCSRs have been considered for the $\gamma^* N \to \Delta$ transition [354], heavy baryon decays (see [355] and references therein) and various transitions between baryons in the octet and the decuplet (e.g. [356]). In the work [132] we have suggested to use the same approach to the study of electroproduction of resonances at large momentum transfers and in particular $N^*(1535)$. Since the structure of sum rules for the nucleon elastic form factors and electroproduction of $N^*(1535)$ is very similar, the difference in form factors should expose directly the difference in the wave functions, which is of prime interest. The results for the helicity amplitudes $A_{1/2}(Q^2)$ and $S_{1/2}(Q^2)$ using the lattice results for the lowest moments of the $N^*(1535)$ DAs appear to be in a good agreement with the existing data, see Fig. 38.

All existing LCSRs for baryons are written to the leading order in the strong coupling which corresponds, roughly speaking, to the parton model level description of deep-inelastic scattering. Combined with realistic models of DAs the existing sum rules yield a reasonable description of the existing data to the expected 30-50% accuracy. In order to match the accuracy of the future experimental data and also of the next generation of lattice results, the LCSRs will have to be advanced to include NLO radiative corrections, as it has become standard for meson decays.

The first step towards LCSRs to the NLO accuracy was done in Ref. [357] where the $\mathcal{O}(\alpha_s)$ corrections are calculated for the (leading) twist-three contributions to the sum rules for electro-

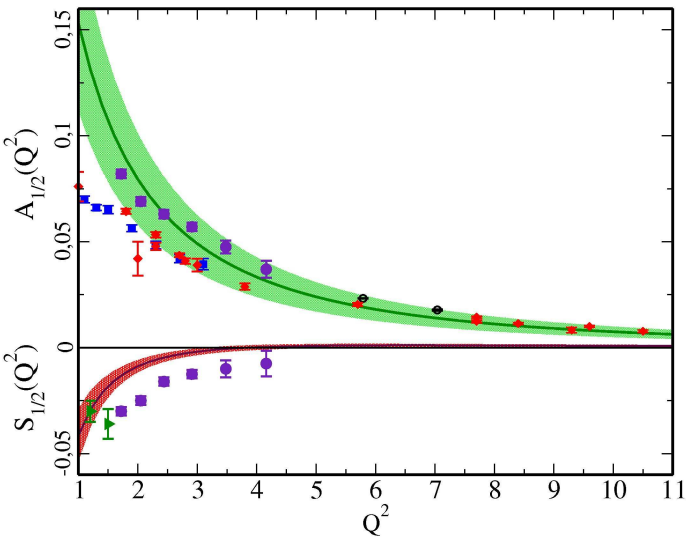

FIG. 38: The LCSR calculation for the helicity amplitudes $A_{1/2}(Q^2)$ and $S_{1/2}(Q^2)$ for the electroproduction of the $N^*(1535)$ resonance using the lattice results for the lowest moments of the $N^*(1535)$ DAs. The curves are obtained using the central values of the lattice parameters, and the shaded areas show the corresponding uncertainty. Figure taken from Ref. [132].

magnetic (elastic) nucleon form factors derived in [345, 353]. The results are shown in Fig. **??** and Fig. **??**. The NLO corrections are large and their effect *increases* with Q^2 which may be counter-intuitive. This behavior is, however, expected on general grounds because the leading regions for large momentum transfers corresponding to the ERBL (Efremov-Radyushkin-Brodsky-Lepage) collinear factorization appear at the NNLO level only, i.e. $\mathcal{O}(\alpha_s^2)$. The corrections for the G_E/G_M ratio are larger than for the magnetic form factor G_M itself, which is again expected since the electric form factor suffers from cancellations between chirality-conserving and chirality-violating contributions.

Large NLO corrections can be compensated by the change in the nucleon DA, similar as it happens with parton distributions — e.g. the small-x behavior of the LO and NLO gluon distribution is very different — but such an analysis would so far be premature since NLO corrections have not been calculated so far for the contributions of twist-four DAs that take into account the effects of orbital angular momentum.

In addition, it is necesary to develop a technique for the resummation of "kinematic" corrections to the sum rules that are due to nonvanishing masses of the resonances. The corresponding corrections to the total cross section of the deep-inelastic scattering are known as Wandzura-Wilczek corrections and can be resummed to all orders in terms of the Nachtmann variable; we are looking for a generalization of this method to non-forward kinematics which is also important in a broader context [358].

With these improvements, we expect that the LCSR approach can be used to constrain light-cone DAs of the nucleon and its resonances from the comparison with the electroproduction data. These constraints can then be compared with the lattice QCD calculations. In order to facilitate this comparison, a work is in progress to derive general expressions for the necessary light-cone sum rules to the NLO accuracy. The project is to have the LCSRs available as a computer code allowing one to calculate elastic electromagnetic and axial form factors and also a range of transition form factors involving nucleon resonances from a given set of distribution amplitudes. Although gross

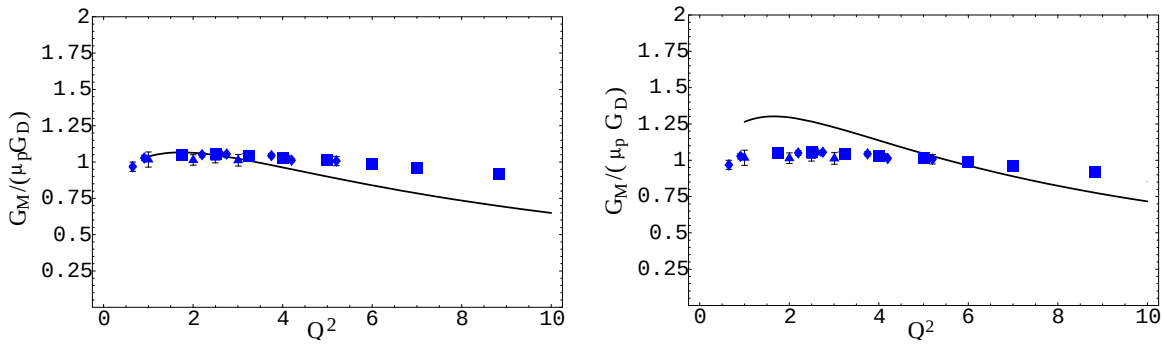

FIG. 39: LCSR results for the magnetic proton form factor (normalized to the dipole formula) for a realistic model of nucleon distribution amplitudes [353]. Left panel: Leading order (LO); right panel: next-to-leading order (NLO) for twist-three contributions. Figure adapted from Ref. [357].

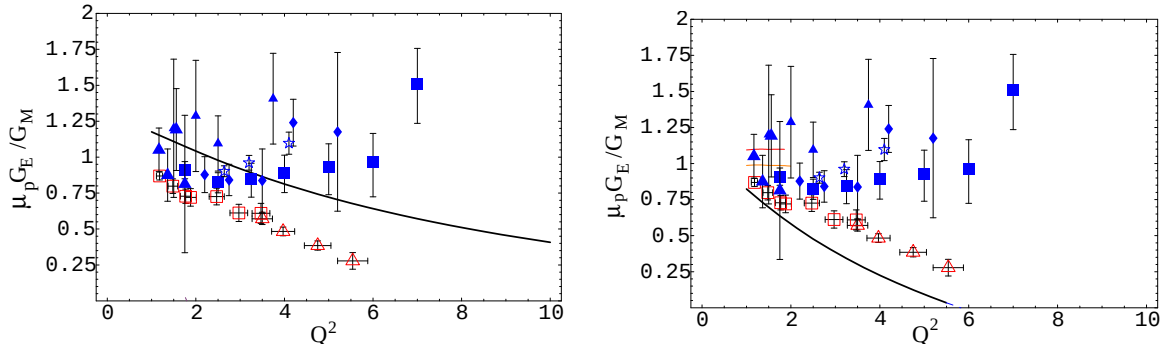

FIG. 40: LCSR results for the electric to magnetic proton form factor ratio for a realistic model of nucleon distribution amplitudes [353]. Left panel: Leading order (LO); right panel: next-to-leading order (NLO) for twist-three contributions. Figure adapted from Ref. [357].

features of the wave functions of resonances can definitely be extracted from such an analysis, the level of details "seen" in sum rule calculations will have to be tested on case by case basis. For this reason we are also working on similar calculations for the "gold-plated" decays like $\gamma^* \to \pi\gamma$, $\gamma^* \to \eta\gamma$, see [359], where the theoretical uncertainties are expected to be small.

VIII. THE N* ELECTROCOUPLING INTERPRETATION WITHIN THE FRAMEWORK OF CONSTITUENT QUARK MODELS

A. Introduction

The study of the electromagnetic excitation of the nucleon resonances is expected to provide a good test for our knowledge concerning the internal structure of baryons. From a fundamental point of view, the description of the resonance spectrum and excitation should be performed within a Quantum ChromoDynamics (QCD) approach, which, however, does not allow up to now to extract all the hadron properties in a systematic way. Therefore, one has to rely on models, eventually based on QCD or LQCD, such as the Constituent Quark Models (CQM). In CQMs quarks are considered as effective internal degrees of freedom and can acquire a mass and a finite size.

In the following we report some results of recent approaches using the CQ idea in the framework of various light front (LF) formulations of the quark wave function (Secs. II,III,IV) and a discussion on the use of CQM in the interpretation of high Q^2 helicity amplitudes with particular attention to some future perspectives (Sec. V).

B. Covariant quark-diquark model for the N and N^* electromagnetic transition form factors

The study of hadron structure using the fundamental theory, Quantum ChromoDynamics, can in practise be done only in the large Q^2 regime or, by means of lattice simulations, in the unphysical quark masses regime [134]. For this reason one has to rely on effective descriptions either with the degrees of freedom of QCD (quarks and gluons) within the Dyson-Schwinger (DS) framework [135], or in terms of the degrees of freedom observed at low Q^2, the meson cloud and the light baryon core, using a dynamical coupled-channels reaction (dynamical models or DM) framework [39, 136]. The DS framework helps to understand the transition between the perturbative regime of QCD and the low Q^2 regime, where the quarks acquire masses and structure dynamically due to the gluon dressing, although the meson degrees of freedom are not included till the moment [135]. Dynamical models, on the other hand, help to explain the transition between the low Q^2 picture, in terms of a finite size baryon and the surrounding meson cloud, and the intermediate region when $Q^2 > 2$ GeV^2, where the baryon core effects are dominant [39]. To complete the picture a parametrization of the structure of the baryon core is required, and a possibility is to use the meson-baryon dressing model to extract from the data the contributions of the core, that can be interpreted as a 3-valence quark system [44, 75]. Alternative descriptions comprise effective chiral perturbation theory, that can be used to interpolate lattice QCD results but is restricted to the low Q^2 regime, perturbative QCD that works only at very large Q^2 with a threshold that is still under discussion, QCD sum rules [137] and constituent quark models (QM) that can include also chiral symmetry and/or unquenched effects [138].

Constituent quark models (CQM) are inspired in QCD, in particular in the SU(6) symmetry, but include the gluon and quark-antiquark polarization in the quark substructure (that also generates the constituent quark mass) with effective interquark interactions [138]. There are different versions according to the interquark interaction potential and the kinematic considered (nonrelativistic, or relativistic). Among the relativistic descriptions there are, in particular, different implementations of relativity based on the Poincare invariance [138].

A particular CQM is the covariant spectator quark model. Contrarily to other CQMs, the spectator QM is not based on a wave equation determined by some complex and nonlinear potential,

that tries to emulate the QCD underlying interactions between quarks. For that reason, the model is not used to predict the baryonic spectrum. Instead, the wave functions are built from the baryon internal symmetries only, with the shape of the wave functions determined directly by the experimental data, or lattice data for some ground state systems [139].

In the covariant spectator theory (CST) [140] the 3-body baryon systems are described in terms of a vertex function Γ, where 2 quarks are on-mass-shell [141–143]. In CST confinement ensures that the vertex Γ vanishes when the 3 quarks are simultaneously on-mass-shell, and the singularities associated with the off-mass-shell quark is canceled by the vertex Γ [141, 142]. The baryon state can then be described by a wave function $\Psi(P,k) = (m_q - \not{k} - i\varepsilon)^{-1}\Gamma(P,k)$, where P is the baryon momentum, m_q the quark mass and k the quark momentum [142, 143]. Integrating over the two on-mass-shell quark momenta, one can reduce the 3-quark system to a quark-diquark system with an on-mass-shell effective diquark with an average mass m_D [142, 143]. In these conditions the baryon is described by a wave function for the quark-diquark, with individual states associated with the internal symmetries (color, flavor, spin, momentum, etc.). The electromagnetic interaction current is given in impulse approximation by the coupling of the photon with the off-mass-shell quark, while the diquark acts as a spectator on-mass-shell particle [139, 143, 144].

The photon-quark interaction is parametrized by using the vector meson dominance (VMD) mechanism, based on a combination of two poles associated with vector mesons: a light vector meson (mass $m_v = m_\rho \simeq m_\omega$) and an effective heavy meson with mass $M_h = 2M$, where M is the nucleon mass, which modulates the short range structure [139, 143, 144]. The free parameters of the current were calibrated for the SU(3) sector by nucleon electromagnetic form factor data [143] and with lattice QCD simulations associated with the baryon decuplet [144]. A parametrization based on VMD has the advantage in the generalization to the lattice QCD regime [144–147] and also for the timelike region ($Q^2 < 0$) [148].

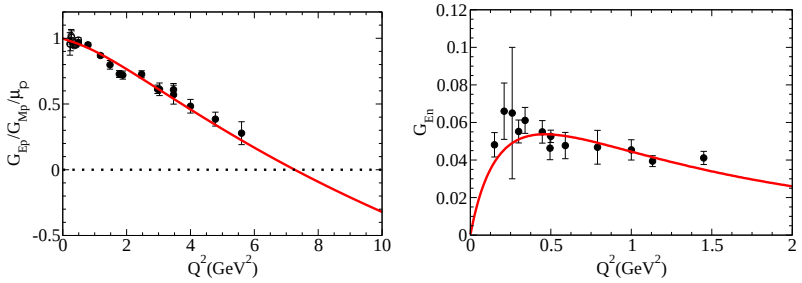

FIG. 41: Nucleon form factors. Model II of Ref. [143]. Left panel: $\mu_p\, G_{Ep}/G_{Mp}$ ratio, including the Jefferson Lab data. Right panel: neutron electric form form factor.

The covariant spectator quark model was applied to the description of the nucleon elastic form factors using a simple model where the quark-diquark motion is taken in the S-state approximation [143]. The nucleon data were used to fix the quark current as well as the radial wave function [143]. A specific model with no explicit pion cloud effects, except the effects included in the VMD parametrization is presented in Fig. 41. This parametrization, based only on the valence quark degrees of freedom, was extended successfully for the nucleon on the lattice regime [145].

The model was also applied to the first nucleon resonance the $\Delta(1232)$, in particular to the $\gamma N \to \Delta(1232)$ transition. Within a minimal model where the Δ is described as an S-state of 3-quarks with the total spin and isospin 3/2, one obtains, for dominant transition form factor $G_M^*(0) \leq 2.07\,\mathcal{I} \leq 2.07$, where $\mathcal{I} \leq 1$, is the overlap integral between the nucleon and Δ radial wave functions (both are S-states) in the limit $Q^2 = 0$ [149]. This simple relation, which is

a consequence of the normalization of the nucleon and Δ quark wave functions, illustrates the incapability in describing the $\gamma N \rightarrow \Delta(1232)$, with quark degrees of freedom only, since the experimental result is $G_M^*(0) \simeq 3$. The discrepancy, is common to all constituent quark models, and is also a manifestation of the importance of the pion excitation which contributes with about 30-40% of the strength of the reaction [39, 75, 136]. The model can however explain the quark core contribution in the transition, as extracted from the data using the EBAC model (Excited Baryon Analysis Center) [75], when the pion cloud is subtracted [149]. The comparison of the model with the EBAC estimate is presented in Fig. 42 (left panel, dashed line), and also with the G_M^* data, when a effective pion cloud is included (solid line). The model was also extended successfully to the reaction in the lattice regime [145, 146]. The description of the quadrupole form factors G_E^* (electric) and G_C^* (Coulomb) is also possible once small D state components are included [146, 150]. In that case, the lattice QCD data can be well described by an extension of the model with an admixture of D-states less than 1% [146], but the experimental data are fairly explained only when the pion cloud and valence quark degrees of freedom are combined [146]. Finally, the model was also applied to the first radial excitation of the $\Delta(1232)$, the $\Delta(1600)$ resonance [151]. In this case no extra parameters are necessary, and the pion cloud effects are largely dominant at low Q^2. The results for G_M^* are presented in the right panel of Fig. 42. In both systems the valence qu

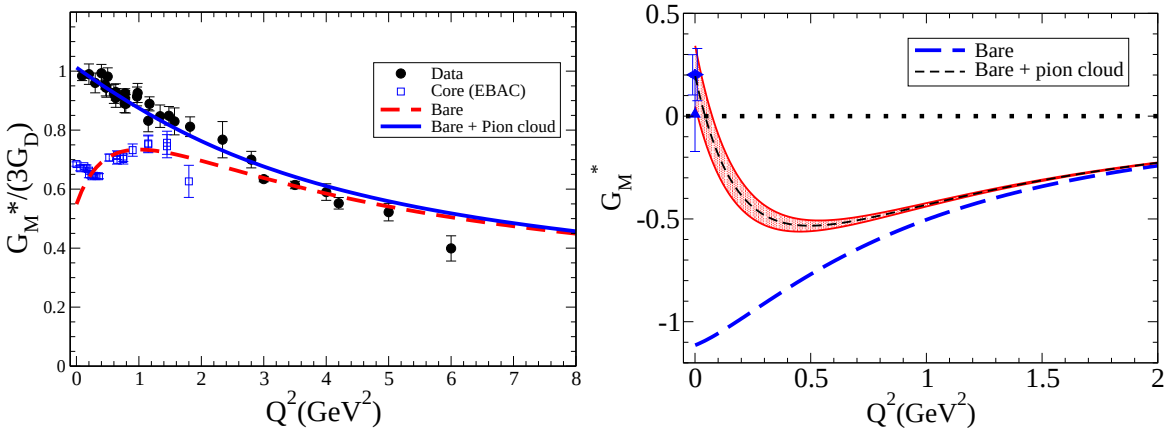

FIG. 42: Nucleon electromagnetic transition for spin 3/2 resonances. Left panel: $G_M^*/(3G_D)$ (G_D is the nucleon dipole form factor) for the $\gamma N \rightarrow \Delta(1232)$ reaction [150]. Right panel: G_M^* for the $\gamma N \rightarrow \Delta(1600)$ reaction [151]. In both cases the dashed line gives the valence quark contribution and the solid line the full result.

The model was also extended to the spin 1/2 state $N(1440)$ (Roper), interpreted as the first radial excitation of the nucleon [152]. The $N(1440)$ shared with the nucleon the spin and isospin structure, differing in the radial wave function. Under that assumption we calculated the transition form factors for the $\gamma N \rightarrow N(1440)$ reaction based exclusively on the valence quark degrees of freedom [152]. As an example, we present the Dirac-type form factor F_1^* in Fig. 43 (left panel). The model is also consistent with the lattice data [152]. The covariant spectator quark model was also applied to the chiral partner of the nucleon $N(1535)$ (negative parity) under two approximations: a pointlike diquark and a quark core restricted to spin 1/2 states [153]. Under these approximations the $\gamma N \rightarrow N(1535)$ transition form factors were calculated for the region $Q^2 \gg 0.23$ GeV^2 [153]. The result for F_1^* is presented in Fig. 43 (right panel). In both reactions the results are consistent with the data for $Q^2 > 1.5$ GeV^2 [152, 153], except for F_2^* for the

reaction with $N(1535)$. Our results support the idea that the valence quark dominance for the intermediate and high Q^2 region, but also the necessity of the meson excitations for the lower Q^2 region ($Q^2 < 2$ GeV^2). The form factor F_2^* for the $\gamma N \to N(1535)$ reaction is particularly interesting from the perspective of a quark model, since the data suggest that $F_2^* \approx 0$ for $Q^2 > 2$ GeV^2, contrarily to the result of the spectator quark model. These facts suggest that the valence quark and meson cloud contributions have opposite signs and cancel in the sum [153]. The direct consequence of the result for $F_2^* \approx 0$ is the proportionality between the amplitudes $A_{1/2}$ and $S_{1/2}$ for $Q^2 > 2$ GeV^2 [154].

Other applications of the covariant spectator quark model are the elastic electromagnetic form factors of the baryon octet (spin 1/2) [147, 155], and the baryon decuplet (spin 3/2) [144, 156–158], as well as the electromagnetic transition between octet and decuplet baryons, similarly to the $\gamma N \to \Delta(1232)$ reaction [159]. The study of the octet electromagnetic structure in the nuclear me

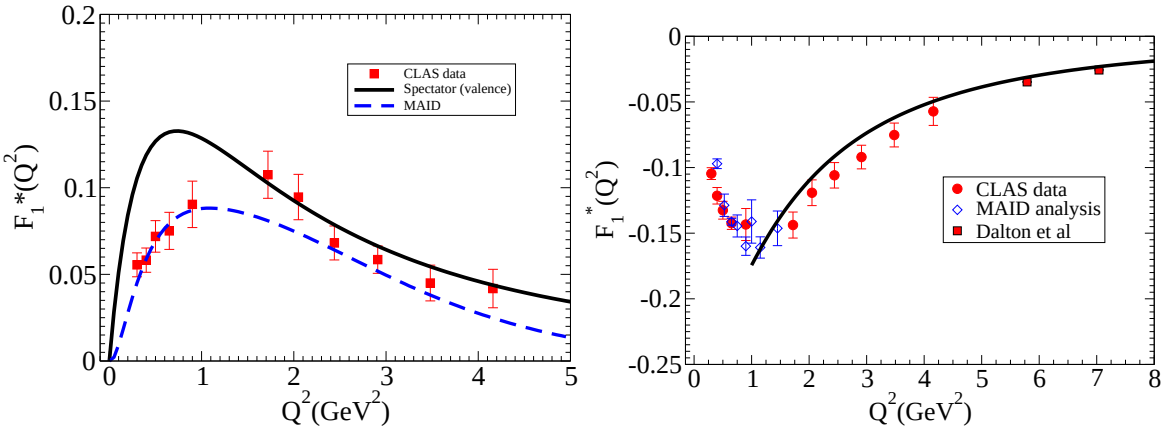

FIG. 43: Dirac-type form factors F_1^* for $\gamma N \to N^*$ transitions. Left panel: $\gamma N \to P_{11}(1440)$ reaction [152]. Right panel: $\gamma N \to S_{11}(1535)$ reaction [153].

Future developments include the calculation of the nucleon form factors with the inclusion of higher angular momentum states (P and D states). This work is in progress [161], and also will include the application of the deep inelastic scattering used to constrain the parameters in these states.

Extensions for higher resonances are underway for $P_{11}(1710)$, $D_{13}(1520)$ and $S_{11}(1650)$. The last two cases depend on the inclusion of an isospin 1/2, spin 3/2 core in a state of the total angular momentum 1/2. These states are expected to be the same as that in the part of the nucleon structure [161].

In future developments, the quality and quantity of the future lattice QCD studies will be crucial to constrain the parametrization of the wave functions, and clarify the effect of the valence quarks and meson cloud, following the successful applications to the lattice QCD regime for the nucleon [143, 147], $\gamma N \to \Delta(1232)$ transition [146] and Roper [152].

In parallel, the comparison with the estimate of the quark core contributions performed by the EBAC group preferentially for $Q^2 > 2$ GeV^2 [44, 75], will be also very useful in the next two years. To complement the quark models, the use of dynamical models and/or effective chiral models [162] to estimate the meson cloud effects are also very important. This is particularly relevant for the $\gamma N \to N(1535)$ reaction. From the experimental side, new accurate measurements in the low Q^2 region as well as the high Q^2 region, as will be measured in the future after the Jefferson

Lab 12 GeV upgrade, will be crucial, for the purposes of either to test the present parametrizations at high Q^2, or to calibrate the models for new calculations at even larger Q^2. The clarifications between the different analysis of the data such as EBAC, CLAS, SAID, MAID, Jülich and Bonn-Gatchina, will also have an important role [58, 59, 136, 163, 164, 166, 167].

C. Nucleon electromagnetic form factors and electroexcitation of low lying nucleon resonances up to $Q^2 = 12GeV^2$ in a light-front relativistic quark model

1. Introduction

In recent decade, with the advent of the new generation of electron beam facilities, there is dramatic progress in the investigation of the electroexcitation of nucleon resonances with significant extension of the range of Q^2. The most accurate and complete information has been obtained for the electroexcitation amplitudes of the four lowest excited states, which have been measured in a range of Q^2 up to 8 and 4.5 GeV^2 for the $\Delta(1232)P_{33}$, $N(1535)S_{11}$ and $N(1440)P_{11}$, $N(1520)D_{13}$, respectively (see reviews [168, 169]). At relatively small Q^2, nearly massless Goldstone bosons (pions) can produce significant pion-loop contributions. However it is expected that the corresponding hadronic component, including meson-cloud contributions, will be rapidly losing strength with increasing Q^2. The Jefferson Lab 12 GeV upgrade will open up a new era in the exploration of excited nucleons when the ground state and excited nucleon's quark core will be fully exposed to the electromagnetic probe.

Our goal is to predict $3q$ core contribution to the electroexcitation amplitudes of the resonances $\Delta(1232)P_{33}$, $N(1440)P_{11}$, $N(1520)D_{13}$, and $N(1535)S_{11}$. The approach we use is based on light-front (LF) dynamics which realizes Poincaré invariance and the description of the verteces $N(N^*) \to 3q, N\pi$ in terms of wave functions. The corresponding LF relativistic model for bound states is formulated in Refs. [170–172]. The parameters of the model for the $3q$ contribution have been specified via description of the nucleon electromagnetic form factors in the approach that combines $3q$ and pion-cloud contributions. The pion-loop contributions to nucleon electromagnetic form factors have been described according to the LF approach of Ref. [173].

2. Quark core contribution to transition amplitudes

The $3q$ contribution to the $\gamma^* N \to N(N^*)$ transitions has been evaluated within the approach of Refs. [171, 172] where the LF relativistic quark model is formulated in infinite momentum frame (IMF). The IMF is choosen in such a way, that the initial hadron moves along the z-axis with the momentum $P \to \infty$, the virtual photon momentum is $k^\mu = \left(\frac{m^2_{out}-m^2_{in}-\mathbf{Q}^2_\perp}{4P}, \mathbf{Q}_\perp, -\frac{m^2_{out}-m^2_{in}-\mathbf{Q}^2_\perp}{4P}\right)$, the final hadron momentum is $P' = P + k$, and $Q^2 \equiv -k^2 = \mathbf{Q}^2_\perp$; m_{in} and m_{out} are masses of the initial and final hadrons, respectively. The matrix elements of the electromagnetic current are related to the $3q$-wave functions in the following way:

$$\frac{1}{2P} < N(N^*), S'_z|J^{0,3}_{em}|N, S_z >|_{P\to\infty} = e\Sigma_i \int \Psi'^{+} Q_i \Psi d\Gamma, \tag{18}$$

where S_z and S'_z are the projections of the hadron spins on the z-direction, Q_i $(i = a, b, c)$ are the charges of the quarks in units of e, $e^2/4\pi = \alpha$, Ψ and Ψ' are wave functions in the verteces

$N(N^*) \to 3q$, and $d\Gamma$ is the phase space volume:

$$d\Gamma = (2\pi)^{-6} \frac{d\mathbf{q}_{b\perp} d\mathbf{q}_{c\perp} dx_b dx_c}{4 x_a x_b x_c}. \tag{19}$$

The quark momenta in the initial and final hadrons are parametrized via:

$$\mathbf{p}_i = x_i \mathbf{P} + \mathbf{q}_{i\perp}, \quad \mathbf{p}'_i = x_i \mathbf{P}' + \mathbf{q}'_{i\perp}, \tag{20}$$

$$\mathbf{P}\mathbf{q}_{i\perp} = \mathbf{P}'\mathbf{q}'_{i\perp} = 0, \quad \Sigma \mathbf{q}_{i\perp} = \Sigma \mathbf{q}'_{i\perp} = 0, \quad \mathbf{q}'_{i\perp} = \mathbf{q}_{i\perp} - y_i \mathbf{Q}_\perp, \tag{21}$$

$$\Sigma x_i = 1, \quad y_a = x_a - 1, \quad y_b = x_b, \quad y_c = x_c. \tag{22}$$

Here we have supposed that quark a is an active quark.

The wave function Ψ is related to the wave function in the c.m.s. of the system of three quarks through Melosh matrices [174]:

$$\Psi = U^+(p_a) U^+(p_b) U^+(p_c) \Psi_{fss} \Phi(\mathbf{q}_a, \mathbf{q}_b, \mathbf{q}_c), \tag{23}$$

where we have separated the flavor-spin-space part of the wave function Ψ_{fss} in the c.m.s. of the quarks and its spatial part $\Phi(\mathbf{q}_a, \mathbf{q}_b, \mathbf{q}_c)$. The Melosh matrices are defined by

$$U(p_i) = \frac{m_q + M_0 x_i + i\epsilon_{lm}\sigma_l q_{im}}{\sqrt{(m_q + M_0 x_i)^2 + \mathbf{q}^2_{i\perp}}}, \tag{24}$$

where m_q is the quark mass. The flavor-spin-space parts of the wave functions are constructed according to commonly used rules [76, 175]. To costruct these parts we need also the z-components of quark momenta in the c.m.s. of quarks. They are defined by:

$$q_{iz} = \frac{1}{2}\left(x_i M_0 - \frac{m_q^2 + \mathbf{q}^2_{i\perp}}{x_i M_0} \right), \quad q'_{iz} = \frac{1}{2}\left(x_i M'_0 - \frac{m_q^2 + \mathbf{q}'^2_{i\perp}}{x_i M'_0} \right), \tag{25}$$

where M_0 and M'_0 are invariant masses of the systems of initial and final quarks:

$$M_0^2 = \Sigma \frac{\mathbf{q}^2_{i\perp} + m_q^2}{x_i}, \quad M_0'^2 = \Sigma \frac{\mathbf{q}'^2_{i\perp} + m_q^2}{x_i}. \tag{26}$$

To study sensitivity to the form of the quark wave function, we employ two widely used forms of the spatial parts of wave functions:

$$\Phi_1 \sim exp(-M_0^2/6\alpha_1^2), \quad \Phi_2 \sim exp\left[-(\mathbf{q}_1^2 + \mathbf{q}_2^2 + \mathbf{q}_3^2)/2\alpha_2^2\right], \tag{27}$$

used, respectively, in Refs. [170–172] and [76].

3. Nucleon

The nucleon electromagnetic form factors were described by combining the $3q$-core and pion-cloud contributions to the nucleon wave function. With the pion loops evaluated according to Ref. [173], the nucleon wave function has the form:

$$|N> = 0.95|3q> + 0.313|N\pi>, \tag{28}$$

where the portions of different contributions were found from the condition the charge of the proton be unity: $F_{1p}(Q^2 = 0) = 1$. The value of the quark mass at $Q^2 = 0$ has been taken equal to $m_q(0) = 0.22$ GeV from the description of baryon and meson masses in the relativized quark model [176, 177]. Therefore, the only unknown parameters in the description of the $3q$ contribution to nucleon formfactors were the quantities α_1 and α_2 in Eqs. (27). These parameters were found equal to

$$\alpha_1 = 0.37 \text{ GeV}, \quad \alpha_2 = 0.405 \text{ GeV} \tag{29}$$

from the description of the magnetic moments at $Q^2 = 0$ (see Fig. 44). The parameters (29) give very close magnitudes for the mean values of invariant masses and momenta of quarks at $Q^2 = 0$: $< M_0^2 > \approx 1.35$ GeV^2 and $< \mathbf{q}_i^2 > \approx 0.1$ GeV^2, $i = a, b.c.$

The constant value of the quark mass gives rapidly decreasing form factors $G_{Ep}(Q^2)$, $G_{Mp}(Q^2)$, and $G_{Mn}(Q^2)$ (see Fig. 44). The wave functions (27) increase as m_q decreases. Therefore, to describe the experimental data we have assumed the Q^2-dependent quark mass. The quark masses that decrease with increasing Q^2:

$$m_q^{(1)}(Q^2) = \frac{0.22\text{GeV}}{1 + Q^2/60\text{GeV}}, \quad m_q^{(2)}(Q^2) = \frac{0.22\text{GeV}}{1 + Q^2/10\text{GeV}} \tag{30}$$

for the wave functions Φ_1 and Φ_2, respectively, allowed us to obtain good description of the nucleon electromagnetic form factors up to $Q^2 = 16$ GeV^2. From Fig. 45 it can be seen that at $Q^2 > 2$ GeV^2, these form factors are dominated by the $3q$-core contribution.

4. *Nucleon resonances* $\mathbf{\Delta}(1232)P_{33}$, $\mathbf{N}(1440)P_{11}$, $\mathbf{N}(1520)D_{13}$, *and* $\mathbf{N}(1535)S_{11}$

No calculations are available that allow for the separation of the $3q$ and $N\pi$ (or nucleon-meson) contributions to nucleon resonances. Therefore, the weights c^* ($c^* < 1$) of the $3q$ contributions to the resonances: $|N^* >= c^*|3q > +...$, are unknown. We determine these weights by fitting to experimental amplitudes at $Q^2 = 2 - 3$ GeV^2, assuming that at these Q^2 the transition amplitudes are dominated by the $3q$-core contribution, as is the case for the nucleon. Then we predict the transition amplitudes at higher Q^2 (see Figs. 46-49).

As it is shown in Refs. [202, 203], there are difficulties in the utilization of the LF approaches [76, 170–172] for the hadrons with spins $J \geq 1$. These difficulties can be avoided if Eq. (18) is used to calculate only those matrix elements that correspond to $S'_z = J$ [202]. This restricts the number of transition form factors that can be calculated for the resonances $\Delta(1232)P_{33}$ and $N(1520)D_{13}$, and only two transition form factors can be investigated for these resonances: $G_1(Q^2)$ and $G_2(Q^2)$ (the definitions can be found in review [168]). For these resonances we can not present the results for the transition helicity amplitudes. The results for the resonances with $J = \frac{1}{2}$: $N(1440)P_{11}$ and $N(1535)S_{11}$, are presented in terms of the transition helicity amplitudes.

5. *Discussion*

The important feature of the obtained predictions for the resonances is the fact that at $Q^2 > 2 - 3$ GeV^2 both investigated amplitudes for each resonance are described well by the $3q$ contribution by fitting the only parameter, that is the weight of this contribution to the resonance. These predictions need to be checked at higher Q^2.

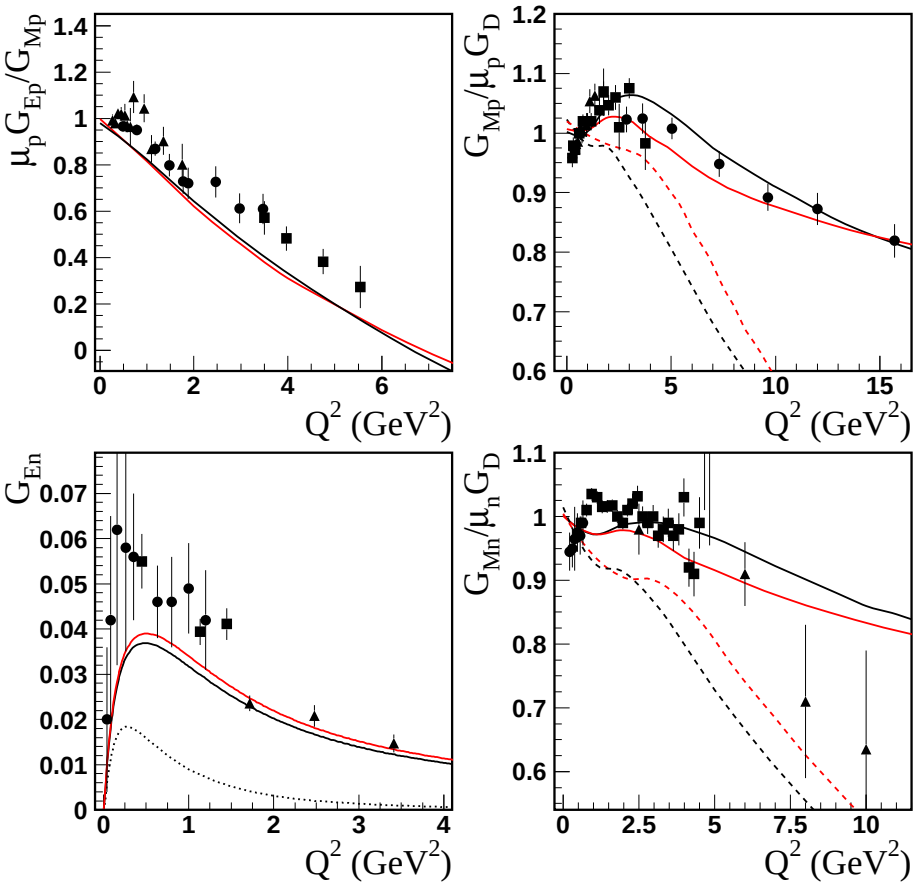

FIG. 44: Nucleon electromagnetic form factors. The solid curves correspond to the results obtained taking into account two contributions to the nucleon (Eq. 28): the pion-cloud [173] and the $3q$ core with the running quark masses (30) for the wave functions Φ_1 (black curves) and Φ_2 (red curves) in Eqs. (27). The black and red dashed curves are the results obtained for the nucleon taken as a pure $3q$ state with the parameters (29) and constant quark mass. Dotted curve for $G_{En}(Q^2)$ is the pion cloud contribution [173]. Data are from Refs. [178–186].

The results for the resonances allow us also to make conclusions on the size and form of expected pion-cloud and/or meson-baryon contributions to the amplitudes. According to our predictions for the $3q$ contributions, one can expect that pion-cloud contributions to the form factor $G_2(Q^2)$ for the $\Delta(1232)P_{33}$, to $S_{1/2}$ amplitude for the $N(1440)P_{11}$, and to the form factor $G_1(Q^2)$ for the $N(1520)D_{13}$ are small. Large contributions are expected to the longitudinal amplitude for the $N(1535)S_{11}$ and to the form factor $G_2(Q^2)$ for the $N(1520)D_{13}$. The expected pion-cloud contributions to the form factor $G_1(Q^2)$ for the $\Delta(1232)P_{33}$ and to $A_{1/2}$ amplitude for the $N(1535)S_{11}$ have Q^2 behaviour similar to that in the nucleon formfactors $G_{Mp(n)}(Q^2)$. In Fig. 47 by dotted curves we show estimated pion-cloud contribution to $A_{1/2}$ amplitude for the Roper resonance. It can be seen that non-trivial Q^2-dependence of this contribution can be expected.

The remarkable feature that follow from the description of the nucleon electromagnetic formfactors in our approach is the decreasing quark mass with increasing Q^2. This is in qualitative agreement with the QCD lattice calculations and with Dyson-Schwinger equations [90, 91, 204] where the running quark mass is generated dynamically. The mechanism that generates the run-

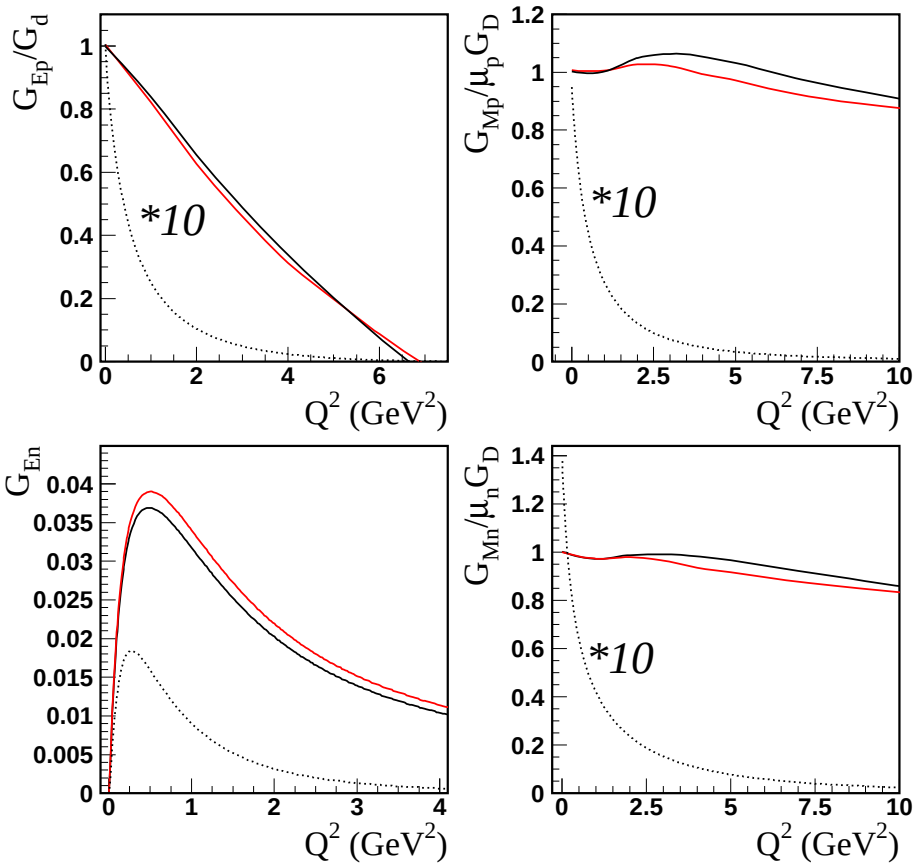

FIG. 45: Nucleon electromagnetic form factors. The legend for the black and red solid curves is as for Fig. 44. Dotted curves are the pion cloud contributions [173].

ning quark mass can generate also the quark anomalous magnetic moments and form factors. This should be incorporated in model calculations. Introducing quark form factors will cause a faster Q^2 fall-off of electromagnetic form factors in quark models. This will force $m_q(Q^2)$ to drop faster with Q^2 to describe the data.

D. Light-Front Holographic QCD

The relation between the hadronic short-distance constituent quark and gluon particle limit and the long-range confining domain is yet one of the most challenging aspects of particle physics due to the strong coupling nature of Quantum Chromodynamics, the fundamental theory of the strong interactions. The central question is how one can compute hadronic properties from first principles; i.e., directly from the QCD Lagrangian. The most successful theoretical approach thus far has been to quantize QCD on discrete lattices in Euclidean space-time. [205] Lattice numerical results follow from computation of frame-dependent moments of distributions in Euclidean space and dynamical observables in Minkowski space-time, such as the time-like hadronic form factors, are not amenable to Euclidean lattice computations. The Dyson-Schwinger methods have led to many important insights, such as the infrared fixed point behavior of the strong coupling constant, [206] but in practice, the analyses are limited to ladder approximation in Landau gauge. Baryon spec-

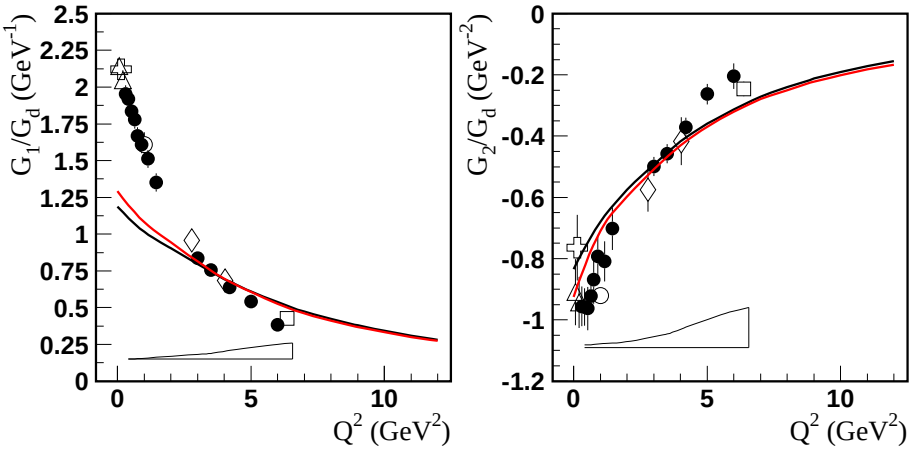

FIG. 46: The $\gamma^* p \to \Delta(1232)\mathrm{P}_{33}$ transition form factors; $G_1(Q^2) \sim G_M - G_E$. Weight factors are $c^{(1)}_{N^*} = 0.67 \pm 0.04$ and $c^{(2)}_{N^*} = 0.72 \pm 0.04$ for the wave functions Φ_1 (black curves) and Φ_2 (red curves) in Eqs. (27). Solid circles correspond to the amplitudes extracted from the CLAS data by JLab group [164], bands represent model uncertainties of these results. The results from other experiments are: open triangles [187–189]; open crosses [190–192]; open rhombuses [193]; open boxes [194]; and open circles [195, 196].

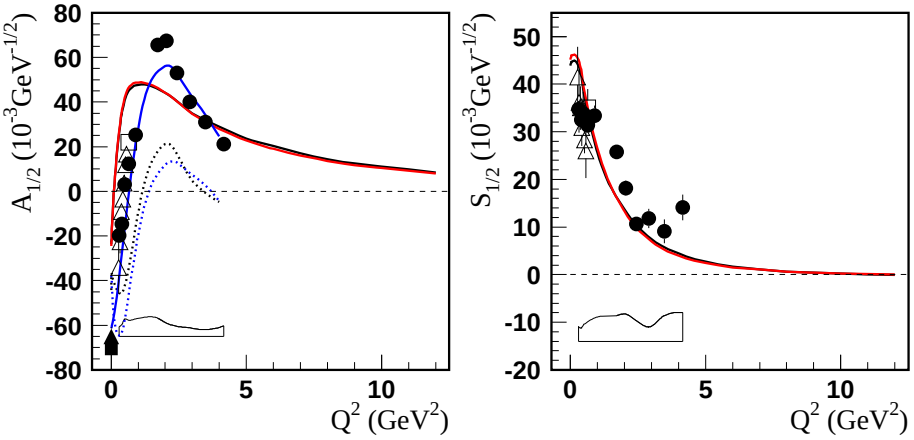

FIG. 47: The $\gamma^* p \to N(1440)\mathrm{P}_{11}$ transition amplitudes. Blue lines correspond to the MAID results [59]. Dotted curves are estimated pion-cloud contributions. $c^{(1)}_{N^*} = 0.73 \pm 0.05$, $c^{(2)}_{N^*} = 0.77 \pm 0.05$. The open triangles correspond to the amplitudes extracted from CLAS 2π electroproduction data [197]. Other legend is as for Fig. 46.

troscopy and the excitation dynamics of nucleon resonances encoded in the nucleon transition form factors can provide fundamental insight into the strong-coupling dynamics of QCD. New theoretical tools are thus of primary interest for the interpretation of the results expected at the new mass scale and kinematic regions accessible to the JLab 12 GeV Upgrade Project.

The AdS/CFT correspondence between gravity or string theory on a higher-dimensional anti–de Sitter (AdS) space and conformal field theories in physical space-time [207] has led to a semi-classical approximation for strongly-coupled QCD, which provides physical insights into its non-perturbative dynamics. The correspondence is holographic in the sense that it determines a duality

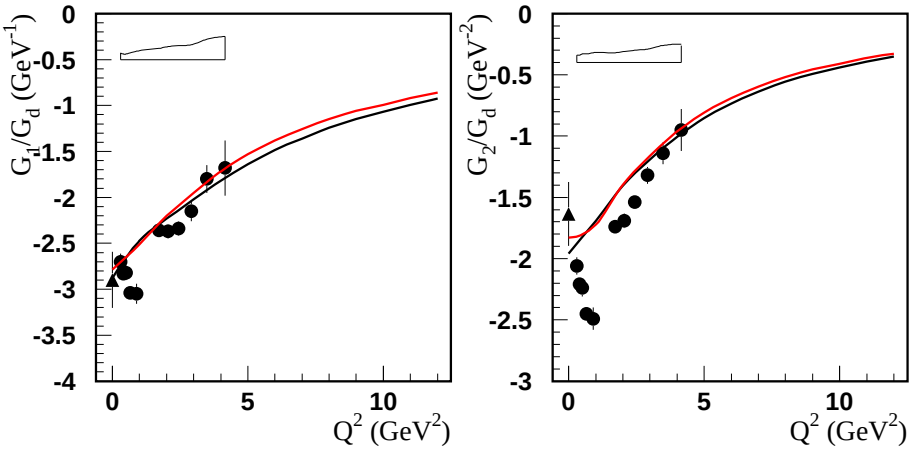

FIG. 48: The $\gamma^* p \to N(1520)\mathrm{D}_{13}$ transition form factors; $G_1(Q^2) \sim A_{1/2} - A_{3/2}/\sqrt{3}$. $c^{(1)}_{N^*} = 0.78 \pm 0.06$, $c^{(2)}_{N^*} = 0.82 \pm 0.06$. Other legend is as for Fig. 46.

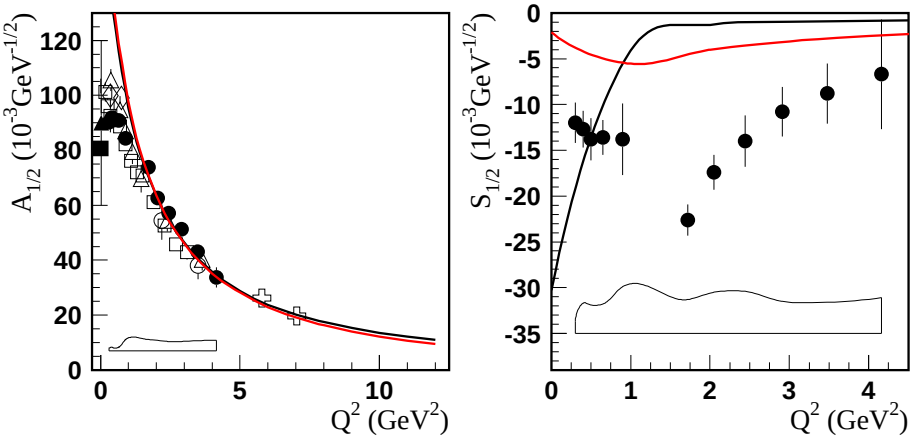

FIG. 49: The $\gamma^* p \to N(1535)\mathrm{S}_{11}$ transition amplitudes. The amplitudes extracted from the CLAS and JLab/Hall C data on $ep \to e\eta p$ are: the stars [198], the open boxes [131], the open circles [199], the crosses [200], and the rhombuses [60, 201]. $c^{(1)}_{N^*} = 0.88 \pm 0.03$, $c^{(2)}_{N^*} = 0.94 \pm 0.03$. Other legend is as for Fig. 46.

between theories in different number of space-time dimensions. This geometric approach leads in fact to a simple analytical and phenomenologically compelling nonperturbative approximation to the full light-front QCD Hamiltonian – "Light-Front Holography". [208] Light-Front Holography is in fact one of the most remarkable features of the AdS/CFT correspondence. [207] The Hamiltonian equation of motion in the light-front (LF) is frame independent and has a structure similar to eigenmode equations in AdS space. This makes a direct connection of QCD with AdS/CFT methods possible. [208] Remarkably, the AdS equations correspond to the kinetic energy terms of the partons inside a hadron, whereas the interaction terms build confinement and correspond to the truncation of AdS space in an effective dual gravity approximation. [208]

One can also study the gauge/gravity duality starting from the bound-state structure of hadrons in QCD quantized in the light-front. The LF Lorentz-invariant Hamiltonian equation for the rela-

tivistic bound-state system is

$$P_\mu P^\mu |\psi(P)\rangle = \left(P^+P^- - \mathbf{P}_\perp^2\right)|\psi(P)\rangle = M^2|\psi(P)\rangle, P^\pm = P^0 \pm P^3, \tag{31}$$

where the LF time evolution operator P^- is determined canonically from the QCD Lagrangian. [209] To a first semiclassical approximation, where quantum loops and quark masses are not included, this leads to a LF Hamiltonian equation which describes the bound-state dynamics of light hadrons in terms of an invariant impact variable ζ [208] which measures the separation of the partons within the hadron at equal light-front time $\tau = x^0 + x^3$. [210] This allows us to identify the holographic variable z in AdS space with an impact variable ζ. [208] The resulting Lorentz-invariant Schrödinger equation for general spin incorporates color confinement and is systematically improvable.

Light-front holographic methods were originally introduced [211, 212] by matching the electromagnetic current matrix elements in AdS space [213] with the corresponding expression using LF theory in physical space time. It was also shown that one obtains identical holographic mapping using the matrix elements of the energy-momentum tensor [214] by perturbing the AdS metric around its static solution. [215]

A gravity dual to QCD is not known, but the mechanisms of confinement can be incorporated in the gauge/gravity correspondence by modifying the AdS geometry in the large infrared (IR) domain $z \sim 1/\Lambda_{\rm QCD}$, which also sets the scale of the strong interactions. [216] In this simplified approach we consider the propagation of hadronic modes in a fixed effective gravitational background asymptotic to AdS space, which encodes salient properties of the QCD dual theory, such as the ultraviolet (UV) conformal limit at the AdS boundary, as well as modifications of the background geometry in the large z IR region to describe confinement. The modified theory generates the point-like hard behavior expected from QCD, [217, 219] instead of the soft behavior characteristic of extended objects. [216]

1. Nucleon Form Factors

In the higher dimensional gravity theory, hadronic amplitudes for the transition $A \to B$ correspond to the coupling of an external electromagnetic (EM) field $A^M(x,z)$ propagating in AdS space with a fermionic mode $\Psi_P(x,z)$ given by the left-hand side of the equation below

$$\int d^4x\, dz\, \sqrt{g}\, \bar{\Psi}_{B,P'}(x,z)\, e_M^A\, \Gamma_A\, A_q^M(x,z)\Psi_{A,P}(x,z) \;\sim$$
$$(2\pi)^4\delta^4\left(P' - P - q\right)\epsilon_\mu\langle\psi_B(P'),\sigma'|J^\mu|\psi_A(P),\sigma\rangle,$$

where the coordinates of AdS_5 are the Minkowski coordinates x^μ and z labeled $x^M = (x^\mu, z)$, with $M, N = 1, \cdots 5$, g is the determinant of the metric tensor and e_M^A is the vielbein with tangent indices $A, B = 1, \cdots, 5$. The expression on the right-hand side represents the QCD EM transition amplitude in physical space-time. It is the EM matrix element of the quark current $J^\mu = e_q\bar{q}\gamma^\mu q$, and represents a local coupling to pointlike constituents. Can the transition amplitudes be related for arbitrary values of the momentum transfer q? How can we recover hard pointlike scattering at large q from the soft collision of extended objects? [213] Although the expressions for the transition amplitudes look very different, one can show that a precise mapping of the J^+ elements can be carried out at fixed LF time, providing an exact correspondence between the holographic variable z and the LF impact variable ζ in ordinary space-time. [211]

A particularly interesting model is the "soft wall" model of Ref. [218], since it leads to linear Regge trajectories consistent with the light-quark hadron spectroscopy and avoids the ambiguities in the choice of boundary conditions at the infrared wall. In this case the effective potential takes the form of a harmonic oscillator confining potential $\kappa^4 z^2$. For a hadronic state with twist $\tau = N + L$ (N is the number of components and L the internal orbital angular momentum) the elastic form factor is expressed as a $\tau - 1$ product of poles along the vector meson Regge radial trajectory ($Q^2 = -q^2 > 0$) [212]

$$F(Q^2) = \frac{1}{\left(1 + \frac{Q^2}{M_\rho^2}\right)\left(1 + \frac{Q^2}{M_{\rho'}^2}\right)\cdots\left(1 + \frac{Q^2}{M_{\rho^{\tau-2}}^2}\right)}, \tag{32}$$

where $M_{\rho_n}^2 \to 4\kappa^2(n + 1/2)$. For a pion, for example, the lowest Fock state – the valence state – is a twist-2 state, and thus the form factor is the well known monopole form. The remarkable analytical form of Eq. (32), expressed in terms of the ρ vector meson mass and its radial excitations, incorporates the correct scaling behavior from the constituent's hard scattering with the photon [217, 219] and the mass gap from confinement.

2. *Computing Nucleon Form Factors in Light-Front Holographic QCD*

As an illustrative example we consider in this section the spin non-flip elastic proton form factor and the form factor for the $\gamma^* p \to N(1440)P_{11}$ transition measured recently at JLab. In order to compute the separate features of the proton an neutron form factors one needs to incorporate the spin-flavor structure of the nucleons, properties which are absent in the usual models of the gauge/gravity correspondence. This can be readily included in AdS/QCD by weighting the different Fock-state components by the charges and spin-projections of the quark constituents; e.g., as given by the $SU(6)$ spin-flavor symmetry.

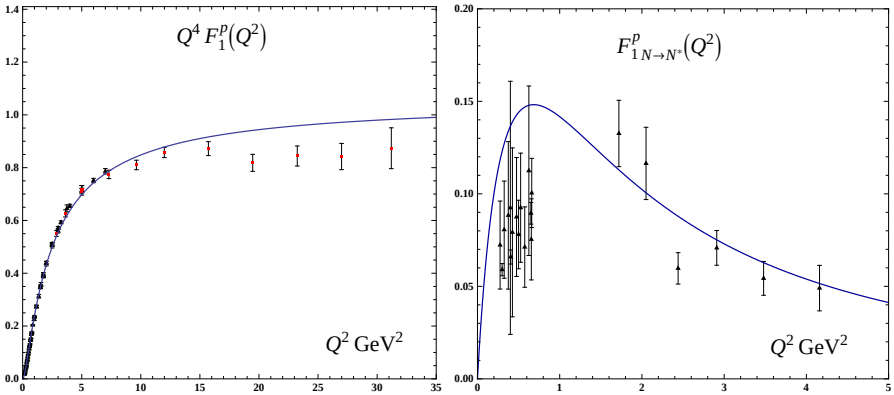

FIG. 50: Dirac proton form factors in light-front holographic QCD. Left: scaling of proton elastic form factor $Q^4 F_1^p(Q^2)$. Right: proton transition form factor $F_{1\,N\to N^*}^p(Q^2)$ for the $\gamma^* p \to N(1440)P_{11}$ transition. Data compilation from Diehl [220] (left) and CLAS π and 2π electroproduction data [164, 197, 221, 222] (right).

Using the $SU(6)$ spin-flavor symmetry the expression for the spin-non flip proton form factors for the transition $n, L \to n'L$ is [224]

$$F_{1\,n,L\to n',L}^p(Q^2) = R^4 \int \frac{dz}{z^4}\, \Psi_+^{n',L}(z) V(Q,z) \Psi_+^{n,L}(z), \tag{33}$$

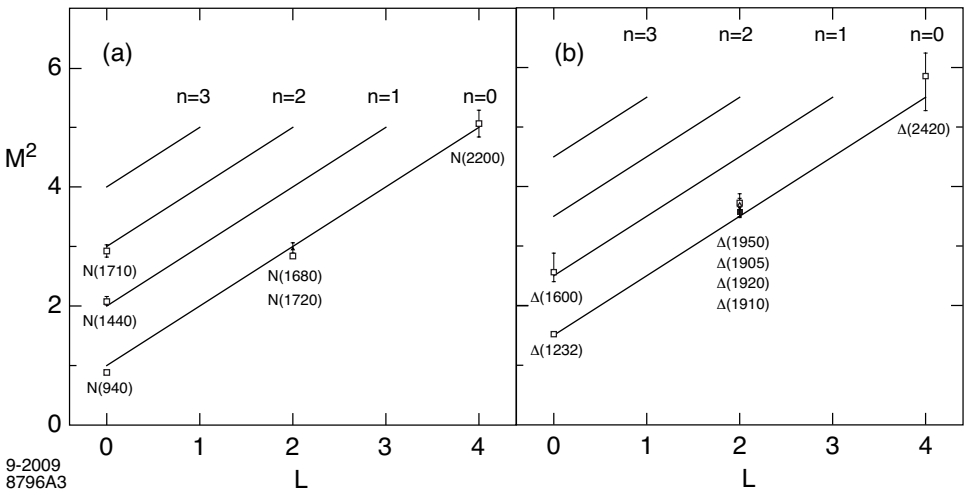

FIG. 51: Positive parity Regge trajectories for the N and Δ baryon families for $\kappa = 0.5$ GeV. Only confirmed PDG [223] states are shown.

where we have factored out the plane wave dependence of the AdS fields

$$\Psi_+(z) = \frac{\kappa^{2+L}}{R^2}\sqrt{\frac{2n!}{(n+L+1)!}}\, z^{7/2+L} L_n^{L+1}\left(\kappa^2 z^2\right) e^{-\kappa^2 z^2/2}. \tag{34}$$

The bulk-to-boundary propagator $V(Q,z)$ has the integral representation [225]

$$V(Q,z) = \kappa^2 z^2 \int_0^1 \frac{dx}{(1-x)^2}\, x^{\frac{Q^2}{4\kappa^2}} e^{-\kappa^2 z^2 x/(1-x)}, \tag{35}$$

with $V(Q=0,z) = V(Q,z=0) = 1$. The orthonormality of the Laguerre polynomials in (34) implies that the nucleon form factor at $Q^2 = 0$ is one if $n = n'$ and zero otherwise. Using (35) in (33) we find

$$F_1^p(Q^2) = \frac{1}{\left(1+\frac{Q^2}{M_\rho^2}\right)\left(1+\frac{Q^2}{M_{\rho'}^2}\right)}, \tag{36}$$

for the elastic proton Dirac form factor and

$$F_{1\,N\to N^*}^p(Q^2) = \frac{\sqrt{2}}{3}\frac{\frac{Q^2}{M_\rho^2}}{\left(1+\frac{Q^2}{M_\rho^2}\right)\left(1+\frac{Q^2}{M_{\rho'}^2}\right)\left(1+\frac{Q^2}{M_{\rho''}^2}\right)}, \tag{37}$$

for the EM spin non-flip proton to Roper transition form factor. The results (36) and (37), compared with available data in Fig. 50, correspond to the valence approximation. The transition form factor (37) is expressed in terms of the mass of the ρ vector meson and its first two radial excited states, with no additional parameters. The results in Fig. 50 are in good agreement with experimental data. The transition form factor to the $N(1440)P_{11}$ state shown in Fig. 50 corresponds to the first radial excitation of the three-quark ground state of the nucleon. In fact, the Roper resonance $N(1440)P_{11}$ and the $N(1710)P_{11}$ are well accounted in the light-front holographic framework as

the first and second radial states of the nucleon family, likewise the $\Delta(1600)P_{33}$ corresponds to the first radial excitation of the Δ family as shown in Fig. 51 for the positive-parity light-baryons. [226] In the case of massless quarks, the nucleon eigenstates have Fock components with different orbital angular momentum, $L = 0$ and $L = 1$, but with equal probability. In effect, in AdS/QCD the nucleonÕs angular momentum is carried by quark orbital angular momentum since soft gluons do not appear as quanta in the proton.

Light-front holographic QCD methods have also been used to obtain general parton distributions (GPDs) in Ref. [227], and a study of the EM nucleon to Δ transition form factors has been carried out in the framework of the Sakai and Sugimoto model in Ref. [228]. It is certainly worth to extend the simple computations described here and perform a systematic study of the different transition form factors measured at JLab. This study will help to discriminate among models and compare with the new results expected from the JLab 12 GeV Upgrade Project, in particular at photon virtualities $Q^2 > 5\ \mathrm{GeV}^2$, which correspond to the experimental coverage of the CLAS12 detector.

E. Constituent Quark Models and the interpretation of the nucleon form factors

Various Constituent Quark Models (CQM) have been proposed in the past decades after the pioneering work of Isgur and Karl (IK) [229]. Among them let us quote the relativized Capstick-Isgur model (CI) [177], the algebraic approach (BIL) [230], the hypercentral CQM (hCQM) [231], the chiral Goldstone Boson Exchange model (χCQM) [232] and the Bonn instanton model (BN) [233]. They are all able to fairly reproduce the baryon spectrum, which is the first test to be performed before applying any model to the description of other baryon properties. The models, although different, have a simple general structure, since, according to the prescription provided by the early Lattice QCD calculations [234], the three-quark interaction V_{3q} is split into a spin-flavour independent part V_{inv}, which is $SU(6)$-invariant and contains the confinement interaction, and a $SU(6)$-dependent part V_{sf}, which contains spin and eventually flavour dependent interactions

$$V_{3q} = V_{inv} + V_{sf} \tag{38}$$

In Tab. III, a summary of the main features of various Constituent Quark Models is reported.

After having checked that these models provide a reasonable description of the baryon spectrum, they have been applied to the calculation of many baryon properties, including electrocouplings. One should however not forget that in many cases the calculations referred to as CQM calculations are actually performed using a simple h.o. wave function for the internal quark motion either in the non relativistic (HO) or relativistic (relHO) framework. The former (HO) applies to the calculations of refs. [240] and [175], while the latter (relHO) is valid for ref. [76]. The relativized model (CI) of ref. [177] is used for a systematic calculation of the transition amplitudes in ref. [241] and, within a light front approach in refs. [242] and ref. [243] for the transitions to the Δ and Roper resonances respectively. In the algebraic approach [230], a particular form of the charge distribution along the string is assumed and used for both the elastic and transition form factors; the elastic form factors are fairly well reproduced, but there are problems with the transition amplitudes, specially at low Q^2. There is no helicity amplitude calculation with the GBE model, whereas the BN model has been also used for the helicity amplitudes [244], with particular attention to the strange baryons [245]. Finally, the hCQM has produced predictions for the transverse excitation of the negative parity resonances [246] and also for the main resonances, both for the longitudinal and transverse excitation [247].

TABLE III: Illustration of the features of various CQMs

CQM	Kin. Energy	V_{inv}	V_{sf}	ref.
Isgur-Karl	non rel.	h.o. + shift	OGE	[229]
Capstick-Isgur	rel	string +coul-like	OGE	[177]
$U(7)B.I.L.$	rel M^2	vibr + L	Gürsey-Rad	[230]
Hypercentral G.S.	non rel/ rel	$O(6)$: lin + hyp.coul	OGE	[231]
Glozman-Riska	rel	h.o. / linear	GBE	[232]
Bonn	rel	linear + 3 body	instanton	[233]

In some recent approaches the CQ idea is used to derive relations between the various electromagnetic form factors, relations which, after having fitted one selected quantity, say the elastic proton form factor (Sec. 2) or the helicity amplitude at intermediate Q^2 (Sec. 3), are used to predict the other quantities of interest. A remarkable prediction of both the proton elastic form factor and the proton transition to the Roper resonance is provided by the light-front holographic approach (Sec. 4).

The works briefly illustrated above have shown that the three-quark idea is able to fairly reproduce a large variety of observables, in particular the helicity amplitudes at medium Q^2, however, a detailed comparison with data shows that, besides the fundamental valence quarks, other issues are or presumably will be of relevant importance for the interpretation of the transition amplitudes. These issues are: relativity, pion cloud and quark-antiquark pair effects and quark form factors.

A consistent relativistic treatment is certainly important for the description of the elastic nucleon form factors. In fact, in the non-relativistic hCQM [231], the proton radius compatible with the spectrum is too low, about $0.5fm$, and the resulting form factors [248] are higher than data. However, the introduction of the Lorentz boosts improves the description of the elastic form factors [248] and determines a ratio $\mu_p G_e^p/G_M^p$ lower than 1 [249]. Using a relativistic formulation of the hCQM in the Point Form approach, in which again the unknown parameters are fitted to the spectrum, the predicted elastic nucleon form factors are nicely close to data [250]. Furthermore, if one introduces quark form factors, an accurate description of data is achieved [250]. Since such form factors are fitted, this means that they contain, in an uncontrolled manner, all the missing contributions.

For the excitation of higher resonances, the inclusion of relativity seems to be not crucial, since the Lorentz boosts affect only slightly the helicity amplitudes [251]. A quite different situation occurs for the excitation to the Δ, which is a spin-isospin excitation of the nucleon and as such it shares with the nucleon the spatial structure. In this case relativity is certainly important, however it does not seem to be sufficient even within LF approaches. In fact, the good results of the Rome group [242] are obtained introducing quark form factors, while in Sec. 2 the quark wave function fitted to the elastic nucleon form factor leads to a lack of strength at low Q^2 in the Δ excitation. In Sec. 3 a pion cloud term is present from the beginning in the nucleon form factor, nevertheless the transition to the Δ is too low at low Q^2.

Of course, the future data at high Q^2 will force, at least for consistency reasons, to use a relativistic approach also for the other resonances.

At medium-low Q^2 the behaviour of the helicity amplitudes is often described quite well, also in a non relativistic approach [247]. An example is provided by Fig. 52, where the hCQM results are compared with the more recent Jlab data. In Fig. 52 there are also the h.o. results, which do not seem to be able to reproduce the data. The good agreement achieved by the hCQM has a

dynamical origin. Let us remind that in hCQM the $SU(6)$-invariant part of the quark potential of Eq. (38) is

$$V_{inv}^{hCQM} = -\frac{\tau}{x} + \alpha x \tag{39}$$

($x = \sqrt{\rho^2 + \lambda^2}$ is the hyperradius) however the main responsible of the medium-high Q^2 behavior of the helicity amplitudes is the hypercoulomb interaction $-\frac{\tau}{x}$. In fact, in the analytical version of hCQM presented in ref. [252], it is shown that the helicity amplitudes provided by the $-\frac{\tau}{x}$ term are quite similar to the ones calculated with the full hCQM.

The main problem with the description provided by CQM (non relativistic or relativistic) is the lack of strength at low Q^2, which is attributed, with general consensus, to a missing pion cloud or quark-antiquark pair effect [246]. In fact, it has been shown within a dynamical model [59] that the one-pion contribution is relevant at low Q^2 and tends to compensate the lack of strength of unquenched three-quark models [253].

To conclude, a fully relativistic and unquenched hCQM is not yet available and work is now in progress in this direction, but certainly it will be a valuable tool for the interpretation of the helicity amplitudes at high Q^2.

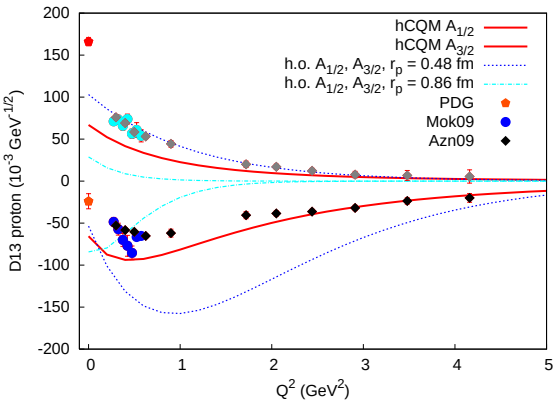

FIG. 52: The D13(1520) helicity amplitudes $A_{3/2}$ (upper part) and $A_{1/2}$ (lower part) predicted by the hCQM (full curves), in comparison with the data of refs. [197], [164] and the PDG values [124] at the photon point. The h.o.results for two different values of the proton r.m.s. radius ($0.5fm$ and $0.86fm$)Å are also shown.

However, also taking into account the one pion contribution there seems to be some problem. In Sec. 2, the quark wave function is chosen in order to reproduce the proton form factor, in this way all possible extra contributions (meson cloud, quark form factors,....) are implicitly included, but the description of the $N - \Delta$ transition needs an extra pion term. On the other hand, in Sec. 3 it is shown that the pion term explicitly included in the fit to the proton is not sufficient for the description of the $N - \Delta$ transition. In fact, the inclusion of a pion cloud term, either fitted or calculated (as e.g. in ref. [254]) seems to be too restrictive, since it is equivalent to only one quark-antiquark configuration. If one wants to include consistently all quark-antiquark effects, one has to proceed to unquenching the CQM, as it has been done in [255]. Such an unquenching is achieved by summing over all quark loops, that is over all intermediate meson-baryon states; the sum is in particular necessary in order to preserve the OZI rule.

This unquenching has been recently performed also for the baryon sector [256]. The state for a

baryon A is written as

$$|\Psi_A>= N\left[|A>+\sum_{BClj}\int d\vec{k}\,|BC\vec{k}lJ>\frac{<BC\vec{k}lJ|T^\dagger|A>}{M_A-E_B-E_C}\right] \tag{40}$$

where B (C) is any intermediate baryon (meson), $E_B(E_C)$ are the corresponding energies, M_A is the baryon mass, $T^\dagger$ is the $^3P_0$ pair creation operator and $\vec{k}$, $\vec{l}$ and $\vec{J}$ are the relative momentum, the orbital and total angular momentum, respectively. Such unquenched model, with the inclusion of the quark-antiquark pair creation mechanism, will allow to build up a consistent description of all the baryon properties (spectrum, form factors,...). There are already some applications [256], in particular it has been checked that, thanks to the summation over all the intermediate states prescribed in Eq. (40), the good account of the baryon magnetic moments provided by the standard CQM is not vanified [256]. Using an interaction containing the quark-antiquark production the resonances acquire a finite width, at variance with what happens in all CQMs, allowing a consistent description of both electromagnetic and strong vertices.

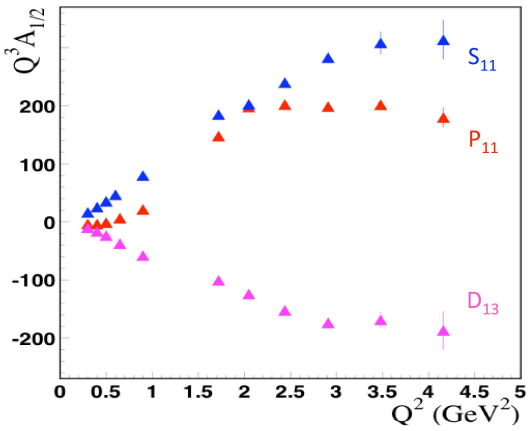

FIG. 53: The experimental values [164] of $Q^3A^p_{1/2}$ for the resonances P11(1440), D13(1520) and S11(1525)

The structure of the state in Eq. (40) is more general than the one containing a single pion contribution. The influence of the quark-antiquark cloud will be certainly important at low Q^2, but one can also expect that the multiquark components, which are mixed with the standard 3q states as in Eq. (40), may have a quite different behavior [257] in the medium-high Q^2 region, leading therefore to some new and interesting behavior also at short distances. Actually, there are some clues that this may really happen. First, it has been shown in [258] that the quantity $Q^3A^p_{1/2}$ seems to become flat in the range around $4\ GeV^2$ (see Fig. 53), while the CQM calculations do not show any structure.

A second important issue is the ratio $R_p = \mu_p G^p_e/G^p_M$ between the proton form factors. A convenient way of understanding its behavior is to consider the ratio $Q^2F^p_2/F^P_1$, which is expected to saturate at high Q^2 [259], while it should pass through the value $4M^2_p/\kappa_p$ in correspondence of a zero for R_p [260]. The predictions of the hCQM [250] are compared with the Jlab data [178, 179, 261] in Fig. 54. For a pure three-quark state, even in presence of quark form factors

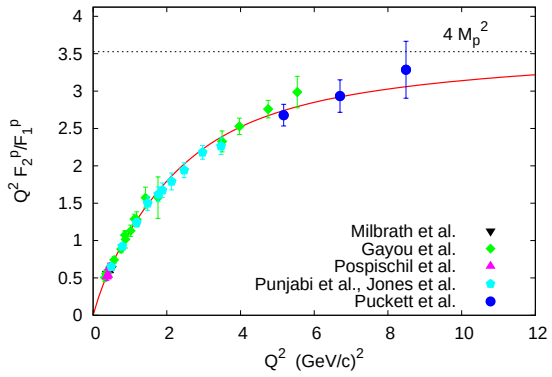

FIG. 54: (Color on line) The ratio F_p at high Q^2 calculated using the theoretical form factors of Ref. [250].

as in [250] the occurence of a zero seems to be difficult, while an interference between three- and multi-quark configurations may be a possible candidate for the generation of a dip in the electric form factors [260].

Once the quark-antiquark pair creation effects have been included consistently in the CQM, it will be possible to disentangle the quark forms factors from the other dynamic mechanisms. The presence of structures with a finite dimension has been shown in a recent analysis of deep inelastic electron-proton scattering [262].

[1] M. R. Pennington, The 8th International Workshop on the Physics of Excited Nucleons, NSTAR2011, May 17-20, 2011, Newport News, VA, USA, ed. by V. Burkert, M. Jones, M. Pennington, D. Richards, AIP Conf. Proc, **1432**, 176.

[2] C. D. Roberts, The 8th International Workshop on the Physics of Excited Nucleons, NSTAR2011, May 17-20, 2011, Newport News, VA, USA, ed. by V. Burkert, M. Jones, M. Pennington, D. Richards, AIP Conf. Proc, **1432**, 19.

[3] J. J. Dudek and R. G. Edwards, Phys. Rev. D **85**, 054016 (2012).

[4] R. W. Gothe, The 8th International Workshop on the Physics of Excited Nucleons, NSTAR2011, May 17-20, 2011, Newport News, VA, USA, ed. by V. Burkert, M. Jones, M. Pennington, D. Richards, AIP Conf. Proc, **1432**, 26.

[5] I. Aznauryan, et al., "Theory Support for the Excited Baryon Program at the JLAB 12 GeV Upgrade", arXiv:0907.1903[nucl-th]. $www.jlab.org/exp\_prog/12GEV\_EXP$

[6] R. Gothe, V. Mokeev, et al., Jlab experiment E12-09-003, "Nucleon Resonance Studies with CLAS12". $www.jlab.org/exp\_prog/12GEV\_EXP$

[7] I. G. Aznauryan, V. D. Burkert, T-S. H. Lee and V. I. Mokeev, J. Phys: Conf. Ser. **299**, 012008 (2011).

[8] I. G. Aznauryan and V. D. Burkert, Prog. Part. Nucl. Phys. **67**, 1 (2012).

[9] V. D. Burkert," The JLAB 12 GeV Upgrade and the Initial Science Program", arXiv:1203.2373[nucl-ex].

[10] G. V. Fedotov et al., CLAS Collaboration, Phys. Rev. C **79**, 015204 (2009).

[11] M. Ripani et al., CLAS Collaboration, Phys. Rev. Lett. **91**, 022002 (2003).

[12] H. Denizli et al., CLAS Collaboration, Phys. Rev. C **76**, 015204 (2007).

[13] D. S Carman et al., CLAS Collaboration, Phys. Rev. C **79**, 065205 (2009).

[14] P. Ambrozewicz, D. S Carman et al., CLAS Collaboration, Phys. Rev. C **75**, 045203 (2007).

[15] K. Nakamura et al., J. Phys. G, **37**, 075021 (2010).

[16] M. Dugger et al., CLAS Collaboration, Phys. Rev. C **79**, 065206 (2009).

[17] S. Capstick and B. D. Keister, Phys. Rev. D **51**, 3598 (1995).

[18] I. G. Aznauryan, Phys. Rev. C **76**, 025212 (2007).

[19] B. Julia-Diaz et al., Phys. Rev. C **77**, 045205 (2008).

[20] M. Aiello, M. M. Giannini and E. Santopinto, J. Phys. G **24**, 753 (1998).

[21] C. D. Roberts, Prog. Part. Nucl. Phys. C **61**, 50 (2008); M. Bhagwat and P. C. Tandy, AIP Conf. Proc. **842**, 225 (2006).

[22] P. O. Bowman et al., Phys. Rev. D **71**, 054507 (2005).

[23] C. D. Roberts, arXiv:1204.2553[nucl-th].

[24] H-W. Lin and S. D. Cohen, The 8th International Workshop on the Physics of Excited Nucleons, NSTAR2011, May 17-20, 2011, Newport News, VA, USA, ed. by V. Burkert, M. Jones, M. Pennington, D. Richards, AIP Conf. Proc, **1432**, 305.

[25] I. G. Aznauryan et al., CLAS Collaboration, Phys. Rev. C **80**, 055203 (2009).

[26] V. I. Mokeev et al., CLAS Collaboration, arXiv:1205.3948[nucl-ex].

[27] V. I. Mokeev, The 8th International Workshop on the Physics of Excited Nucleons, NSTAR2011, May 17-20, 2011, Newport News, VA, USA, ed. by V. Burkert, M. Jones, M. Pennington, D. Richards, AIP Conf. Proc, **1432**, 68.

[28] H. Kamano, arXiv:1206.3374

[29] N. Suzuki, T. Sato, and T.-S. H. Lee, Phys. Rev. C**82**, 045206 (2010).

[30] G. Gilfoyle, et al., Jlab experiment E12-07-104.

[31] E. Brash, et al., Jlab experiment E12-07-109.

[32] B. Wojstekhowski, et al., Jlab experiment E12-09-019.

[33] B. Wojstekhowski, et al., Jlab experiment E12-09-016.
[34] B. Moffit, et al., Jlab experiment E12-11-105.
[35] D. Gaskell, G. Huber, et al., Jlab experiment E12-06-101.
[36] M. Battaglieri, et al., Jlab experiment E12-11-005.
[37] Electromagnetic N-N^* Transition Form Factor Workshop, October 13-15 2008, Newport News, USA $www.jlab.org/conferences/EmNN$.
[38] Nucleon Resonance Structure in Exclusive Electroproduction at High Photon Virtualities Workshop, May 16 2011, Newport News, USA $www.jlab.org/conferences/electroproduction/index.html$.
[39] V. Burkert and T.-S. H. Lee, Int. J. of Mod. Phys. E **13**, 1035 (2004).
[40] T.-S. H. Lee and L.C. Smith, J. Phys. G **34**, 1 (2007).
[41] A. Matsuyama, T. Sato, and T.-S. H. Lee, Phys. Rep. **439**, 193 (2007).
[42] B. Juliá-Díaz, T.-S. H. Lee, A. Matsuyama, and T. Sato, Phys. Rev. C **76**, 065201 (2007).
[43] B. Julia-Diaz, T.-S. H. Lee,A. Matsuyama, T. Sato and L. C. Smith, Phys. Rev. C **77**, 045205 (2008).
[44] B. Julia-Diaz, H. Kamano, T.-S. H. Lee, A. Matsuyama, T. Sato, N. Suzuki, Phys. Rev. C **80**, 025207 (2009)
[45] H. Kamano, B. Julia-Diaz, T.-S. H. Lee, A. Matsuyama, and T. Sato, Phys. Rev. C **79**, 025206 (2009).
[46] H. Kamano, B. Juliá-Díaz, T.-S. H. Lee, A. Matsuyama, and T. Sato, Phys. Rev. C **80**, 065203 (2009).
[47] N. Suzuki, T. Sato, T.-S. H. Lee, Phys. Rev. C **79**, 025205 (2009)
[48] N. Suzuki, B. Julia-Diaz, H. Kamano, T.-S. H. Lee, A. Matsuyama, T. Sato, Phys. Rev. Lett. **104**, 042302 (2010),arXiv:0909.1356
[49] N. Suzuki, T. Sato, T.-S.H. Lee, Phys. Rev. C **82**, 045206 (2010),arXiv:1006.2196
[50] H. Kamano, S.X. Nakamura, T.-S.H. Lee, T. Sato Phys.Rev. C **81**, 065207 (2010)
[51] Wen-Tai Chiang and Frank Tabakin, Phys. Rev. C **55** (1997) 2054.
[52] M. Goldberger and K. Watson, *Collision Theory* (Wiley, New York, 1964)
[53] A.M. Sandorfi, S. Holbit, H. Kamano, T.-S. H. Lee, J. Phys. G **38**, 053001 (2011)
[54] R. E. Cutkosky, C. P. Forsyth, R. E. Hendrick, and R. L. Kelly, Phys. Rev. D **20**, 2839 (1979); R. E. Cutkosky and S. Wang, Phys. Rev. D **42**, 235 (1990).
[55] M. Batinic, I. Slaus, A. Svarc, and B. M. K. Nefkens, Phys. Rev. C **51**, 2310 (1995); M. Batinic, I. Dadic, I. Slaus, A. Svarc, B. M. K. Nefkens, and T.-S. H. Lee, Phys. Scr. **58**, 15 (1998); S. Ceci, A. Svarc, B. Zauner, Phys. Rev. Lett. **97**, 062002 (2006).
[56] T. P. Vrana, S. A. Dytman, T.-S. H. Lee, Phys. Rept. **328**, 181 (2000).
[57] D. M. Manley, E. M. Saleski, Phys. Rev. D **45**, 4002 (1992).
[58] R. A. Arndt, J. M. Ford, and L. D. Roper, Phys. Rev. D **32**, 1085 (1985); R. A. Arndt, W. J. Briscoe, I. I. Strakovsky, and R. L. Workman, Phys. Rev. C **74**, 045205 (2006) (other references therein).
[59] D. Drechsel, O. Hanstein, S.S. Kamalov, and L. Tiator, Nucl. Phys. A **645**, 145 (1999); S.S. Kamalov, S. N. Yang, D. Drechsel, O. Hanstein, and L. Tiator, Phys, Rev, C **64**, 032201(R) (2001).
[60] I. G. Aznauryan, Phys. Rev. C **68**, 065204 (2003).
[61] Feuster and U. Mosel, Phys. Rev. C **58**, 457 (1998); Phys. Rev. C **59**, 460-491 (1999); V. Shklyar, H. Lenske, U. Mosel, G. Penner, Phys. Rev. C **71**, 055206 (2005).
[62] A. Usov and O. Scholten, Phys. Rev. C **72**, 025205 (2005).
[63] A.V. Anisovich, A.V. Sarantsev, O. Bartholomy, E. Klempt, V.A. Nikonov, and U. Thoma, Eur. Phys. J. A **25**, 427 (2005); A. V. Sarantsev *et al.*, Phys. Lett. B **659**, 94 (2008).
[64] M. Döring, C. Hanhart, F. Huang, S. Krewald, and U.-G. Meißner, Nucl. Phys. A **829**, 170 (2009)
[65] B.C. Pearce and B.K. Jennings, Nucl. Phys. A **528**, 655 (1991).
[66] F. Gross and Y. Surya, Phys. Rev. C **47**, 703 (1993).
[67] T. Sato, T.-S. H. Lee, Phys. Rev. C **54**, 2660 (1996)

[68] T. Sato and T.-S. H. Lee, Phys. Rev. C **63**, 055201 (2001).
[69] V. Pascalutsa and J. Tjon, Phys. Rev. C **61**, 054003 (2000); G. Caia, L. Wright, and V. Pascalutsa, Phys. Rev. C **72**, 035203 (2005)
[70] Y. Elmessirri and M.G. Fuda, Phys. Rev. C **60**, 044001 (1999); M.G. Fuda and H. Alharbi, Phys. Rev. C **68**, 064002 (2003).
[71] C.C. Lee, S.N. Yang, and T.-S. H. Lee, J. Phys. G **17** L131 (1991); C.T. Hung, S.N. Yang, and T.-S. H. Lee, Phys. Rev. C **64**, 034309 (2001).
[72] R. Machleidt, p. 189, Vol. 19, (1989),*Advances in Nuclear Physics* (Plenum Press),Editted by J.W. Negele and Erich Vogt.
[73] G. Hohler, F. Kaiser, R. Koch, and E. Pietarinen, Handbook of Pion Nucleon Scattering, Physics Data Vol.12 (Karlsruhe, 1979); G. Höhler, *Pion-nucleon scattering* (Springer-Verlag, Berlin 1983), Vol. I/92. ; G. Hoehler and A. Schulte, πN Newsletter **7** (1992) 94; G. Hoehler, πN Newsletter **9** (1993) 1.
[74] Herman Feshbach, *Theoretical Nuclear Physics, Nuclear Reactions* (Wiley, New York, 1992)
[75] B. Julia-Diaz, T.-S.H. Lee, T. Sato, L.C. Smith Phys.Rev. C **75**, 015205 (2007)
[76] S. Capstick and B. D. Keister, Phys. Rev. D **51**, 3598 (1995)
[77] B. Julia-Diaz and D. O. Riska, Nucl. Phys. A **757**, 441 (2005); B. Julia-Diaz, D. O. Riska, and F. Coester, Phys. Rev. C **69**, 035212 (2004).
[78] C. Alexandrou et al., Phys. ReV. D **69**, 114506 (2004); C. Alexandrou, Forcrand, H. Neff, J.W. Negele, W. Schroers, A. Tsapalis, Phys. Rev. Lett. **94**, 021601 (2005), C. Alexandrou,T. Leontious,J.W. Negele, A. Tsapalis, hep-lat/0608051.
[79] Hannes L.L. Roberts, Lei Chang, Ian C. CloÃńt and Craig D. Roberts Few Body Syst. **51**, 1 (2011)
[80] Gunnar S. Bali, Hartmut Neff, Thomas Duessel, Thomas Lippert, and Klaus Schilling. Observation of string breaking in QCD. *Phys. Rev.*, D **71**, 114513, 2005.
[81] Lei Chang, Ian C. Cloët, Bruno El-Bennich, Thomas Klahn, and Craig D. Roberts. Exploring the light-quark interaction. *Chin. Phys.*, C **33**, 1189–1196, 2009.
[82] Ph. Boucaud et al. The Infrared Behaviour of the Pure Yang-Mills Green Functions. arXiv:1109.1936 [hep-ph].
[83] Craig D. Roberts, Anthony G. Williams, and G. Krein. On the implications of confinement. *Int. J. Mod. Phys.*, A **7**, 5607–5624, 1992.
[84] C. D. Roberts. Hadron Properties and Dyson-Schwinger Equations. *Prog. Part. Nucl. Phys.*, **61**, 50–65, 2008.
[85] V. N. Gribov. The theory of quark confinement. *Eur. Phys. J.*, C **10**, 91–105, 1999.
[86] H. J. Munczek and A. M. Nemirovsky. The Ground State q anti-q Mass Spectrum in QCD. *Phys. Rev.*, D **28**, 181, 1983.
[87] M. Stingl. A schematic model of mesons based on analytic propagators. *Phys. Rev.*, D **29**,2105, 1984.
[88] R. T. Cahill. Hadronization of QCD. *Austral. J. Phys.*, **42**,171–186, 1989.
[89] J. Glimm and A. Jaffee. *Quantum Physics. A Functional Point of View*. Springer-Verlag, New York, 1981.
[90] M. S. Bhagwat and P. C. Tandy. Analysis of full-QCD and quenched-QCD lattice propagators. *AIP Conf. Proc.*, **842**, 225–227, 2006.
[91] Patrick O. Bowman et al. Unquenched quark propagator in Landau gauge. *Phys. Rev.*, D **71**, 054507, 2005.
[92] Si-xue Qin, Lei Chang, Yu-xin Liu, Craig D. Roberts, and David J. Wilson. Interaction model for the gap equation. *Phys. Rev.*, C(R), 2011.
[93] Stanley J. Brodsky, Guy F. de Teramond, and Alexandre Deur. Nonperturbative QCD Coupling and its β function from Light-Front Holography. *Phys. Rev.*, D **81**, 096010, 2010.

[94] A. C. Aguilar, D. Binosi, and J. Papavassiliou. QCD effective charges from lattice data. *JHEP*, **07**, 002, 2010.

[95] Craig D. Roberts. Opportunities and Challenges for Theory in the N* program. arXiv:1108.1030 [nucl-th].

[96] Ralf W. Gothe. Experimental Challenges of the N* Program. arXiv:1108.4703 [nucl-ex].

[97] I. G. Aznauryan, V. D. Burkert, and V. I. Mokeev. Nucleon Resonance Electrocouplings from the CLAS Meson Electroproduction Data arXiv:1109.1294. 2011.

[98] A. Bender, Craig D. Roberts, and L. Von Smekal. Goldstone Theorem and Diquark Confinement Beyond Rainbow- Ladder Approximation. *Phys. Lett.*, B **380**, 7–12, 1996.

[99] Patrick O. Bowman, Urs M. Heller, Derek B. Leinweber, Maria B. Parappilly, and Anthony G. Williams. Unquenched gluon propagator in Landau gauge. *Phys. Rev.*, D **70**, 034509, 2004.

[100] A. C. Aguilar, D. Binosi, J. Papavassiliou, and J. Rodriguez-Quintero. Non-perturbative comparison of QCD effective charges. *Phys. Rev.*, D **80**, 085018, 2009.

[101] Jonivar I. Skullerud, Patrick O. Bowman, Ayse Kizilersu, Derek B. Leinweber, and Anthony G. Williams. Nonperturbative structure of the quark gluon vertex. *JHEP*, **04**, 047, 2003.

[102] M. S. Bhagwat and P. C. Tandy. Quark-gluon vertex model and lattice-QCD data. *Phys. Rev.*, D **70**, 094039, 2004.

[103] Craig D. Roberts and Bruce H. J. McKellar. Critical coupling for dynamical chiral symmetry breaking. *Phys. Rev.*, D **41**, 672, 1990.

[104] Jacques C. R. Bloch. Multiplicative renormalizability and quark propagator. *Phys. Rev.*, D **66**, 034032, 2002.

[105] A. Bashir and M. R. Pennington. Gauge independent chiral symmetry breaking in quenched QED. *Phys. Rev.*, D **50**, 7679–7689, 1994.

[106] H. L. L. Roberts, A. Bashir, L. X. Gutierrez-Guerrero, C. D. Roberts, and D. J. Wilson. pi- and rho-mesons, and their diquark partners, from a contact interaction. *Phys. Rev.*, C **83**, 065206, 2011.

[107] Lei Chang and Craig D. Roberts. Sketching the Bethe-Salpeter kernel. *Phys. Rev. Lett.*, **103**, 081601, 2009.

[108] Lei Chang and Craig D. Roberts. Tracing masses of ground-state light-quark mesons. arXiv:1104.4821 [nucl-th].

[109] Si-xue Qin, Lei Chang, Yu-xin Liu, Craig D. Roberts, and David J. Wilson. Commentary on rainbow-ladder truncation for excited states and exotics. arXiv:1109.3459 [nucl-th].

[110] V. V. Flambaum, A. Holl, P. Jaikumar, C. D. Roberts, and S. V. Wright. Sigma terms of light-quark hadrons. *Few Body Syst.*, **38**, 31–51, 2006.

[111] R. D. Young and A. W. Thomas. Octet baryon masses and sigma terms from an SU(3) chiral extrapolation. *Phys. Rev.*, D **81**, 014503, 2010.

[112] Yoichiro Nambu and G. Jona-Lasinio. Dynamical model of elementary particles based on an analogy with superconductivity. I. *Phys. Rev.*, **122**, 345–358, 1961.

[113] Pieter Maris and Peter C. Tandy. The pi, K+, and K0 electromagnetic form factors. *Phys. Rev.*, C **62**, 055204, 2000.

[114] M. S. Bhagwat and P. Maris. Vector meson form factors and their quark-mass dependence. *Phys. Rev.*, C **77**, 025203, 2008.

[115] I. C. Cloët, G. Eichmann, B. El-Bennich, T. Klähn, and C. D. Roberts. Survey of nucleon electromagnetic form factors. *Few Body Syst.*, **46**, 1–36, 2009.

[116] G. Eichmann, I. C. Cloët, R. Alkofer, A. Krassnigg, and C. D. Roberts. Toward unifying the description of meson and baryon properties. *Phys. Rev.*, C **79**, 012202(R), 2009.

[117] Gernot Eichmann. Nucleon electromagnetic form factors from the covariant Faddeev equation. *Phys.*

Rev., D **84**, 014014, 2011.

[118] L. X. Gutierrez-Guerrero, A. Bashir, I. C. Cloët, and C. D. Roberts. Pion form factor from a contact interaction. *Phys. Rev.*, C **81**, 065202, 2010.

[119] H. L. L. Roberts, C. D. Roberts, A. Bashir, L. X. Gutierrez-Guerrero, and P. C. Tandy. Abelian anomaly and neutral pion production. *Phys. Rev.*, C **82**, 065202, 2010.

[120] Lei Chang, Yu-Xin Liu, and Craig D. Roberts. Dressed-quark anomalous magnetic moments. *Phys. Rev. Lett.*, **106**, 072001, 2011.

[121] R. T. Cahill, Craig D. Roberts, and J. Praschifka. Baryon structure and QCD. *Austral. J. Phys.*, **42**, 129–145, 1989.

[122] R. T. Cahill, Craig D. Roberts, and J. Praschifka. Calculation of diquark masses in QCD. *Phys. Rev.*, D **36**, 2804, 1987.

[123] A. M. Gasparyan, J. Haidenbauer, C. Hanhart, and J. Speth. Pion nucleon scattering in a meson exchange model. *Phys. Rev.*, C **68**, 045207, 2003.

[124] K. Nakamura et al. Review of particle physics. *J. Phys.*, G **37**, 075021, 2010.

[125] Lei Chang, Craig D. Roberts, and Peter C. Tandy. Selected highlights from the study of mesons. *Chin. J. Phys.*, **49**, 955–1004, 2011.

[126] Craig D. Roberts. Confinement, diquarks and Goldstone's theorem. nucl-th/9609039.

[127] Craig D. Roberts, Ian C. Cloët, Lei Chang, and Hannes L. L. Roberts. Dressed-quarks and the Roper resonance. arXiv:1108.1327 [nucl-th].

[128] Pieter Maris and Peter C. Tandy. Bethe-Salpeter study of vector meson masses and decay constants. *Phys. Rev.*, C **60**, 055214, 1999.

[129] I. Aznauryan et al. Theory Support for the Excited Baryon Program at the Jlab 12 GeV Upgrade. arXiv:0907.1901 [nucl-th].

[130] Valentin Mader, Gernot Eichmann, Martina Blank, and Andreas Krassnigg. Hadronic decays of mesons and baryons in the Dyson-Schwinger approach. *Phys.Rev.*, D **84**, 034012, 2011.

[131] H. Denizli et al. Q*2 dependence of the S(11)(1535) photocoupling and evidence for a P-wave resonance in eta electroproduction. *Phys.Rev.*, C **76**, 015204, 2007.

[132] V.M. Braun, M. Gockeler, R. Horsley, T. Kaltenbrunner, A. Lenz, et al. Electroproduction of the N*(1535) resonance at large momentum transfer. *Phys.Rev.Lett.*, **103**, 072001, 2009.

[133] L. Chang, I. C. Cloët, C. D. Roberts, and H. L. L. Roberts. T(r)opical Dyson-Schwinger Equations. *AIP Conf. Proc.*, **1354**, 110–117, 2011.

[134] R. Edwards and W.H. Lin arXiv:0907.1901 [nucl-th], chapter II; R. Edwards, this document, chapter II.

[135] I. Clöet and C. D. Roberts, arXiv:0907.1901 [nucl-th], chapter III; C. Roberts, this document, chapter III.

[136] T.-S. H. Lee, arXiv:0907.1901 [nucl-th], chapter VIII; R. Gothe, this document, chapter VIII.

[137] V. Braun, arXiv:0907.1901 [nucl-th], chapter IV; V. Braun, this document, chapter IV.

[138] S. Capstick, M. Giannini, E. Santopinto, Q. Zhao and B. Zau, arXiv:0907.1901 [nucl-th], chapter IV; This document, chapter IV.

[139] G. Ramalho, F. Gross, M. T. Peña and K. Tsushima, Proceedings of Exclusive Reactions at High Momentum Transfer IV, 287 (2011) [arXiv:1008.0371 [hep-ph]].

[140] F. Gross, Phys. Rev. **186**, 1448 (1969); F. Gross, J. W. Van Orden and K. Holinde, Phys. Rev. C **45**, 2094 (1992).

[141] A. Stadler, F. Gross and M. Frank, Phys. Rev. C **56**, 2396 (1997).

[142] F. Gross and P. Agbakpe, Phys. Rev. C **73**, 015203 (2006).

[143] F. Gross, G. Ramalho and M. T. Peña, Phys. Rev. C **77**, 015202 (2008).

[144] G. Ramalho, K. Tsushima and F. Gross, Phys. Rev. D **80**, 033004 (2009).
[145] G. Ramalho and M. T. Peña, J. Phys. G **36**, 115011 (2009).
[146] G. Ramalho and M. T. Peña, Phys. Rev. D **80**, 013008 (2009).
[147] G. Ramalho and K. Tsushima, arXiv:1107.1791 [hep-ph], to appear in Phys. Rev. D.
[148] G. Ramalho and M. T. Peña, work in preparation.
[149] G. Ramalho, M. T. Peña and F. Gross, Eur. Phys. J. A **36**, 329 (2008).
[150] G. Ramalho, M. T. Peña and F. Gross, Phys. Rev. D **78**, 114017 (2008).
[151] G. Ramalho and K. Tsushima, Phys. Rev. D **82**, 073007 (2010).
[152] G. Ramalho and K. Tsushima, Phys. Rev. D **81**, 074020 (2010).
[153] G. Ramalho and M. T. Peña, Phys. Rev. D **84**, 033007 (2011).
[154] G. Ramalho and K. Tsushima, Phys. Rev. D **84**, 051301 (2011).
[155] F. Gross, G. Ramalho and K. Tsushima, Phys. Lett. B **690**, 183 (2010).
[156] G. Ramalho, M. T. Peña and F. Gross, Phys. Lett. B **678**, 355 (2009).
[157] G. Ramalho, M. T. Peña and F. Gross, Phys. Rev. D **81**, 113011 (2010).
[158] G. Ramalho and M. T. Peña, Phys. Rev. D **83**, 054011 (2011).
[159] G. Ramalho and K. Tsushima, work in preparation.
[160] G. Ramalho, K. Tsushima, and A. W. Thomas, work in preparation.
[161] F. Gross, G. Ramalho and M. T. Peña, work in preparation.
[162] D. Jido, M. Doering and E. Oset, Phys. Rev. C **77**, 065207 (2008).
[163] I. G. Aznauryan and V. I. Mokeev, arXiv:0907.1901 [nucl-th], chapter VII; V. I. Mokeev, this document, chapter VII.
[164] I. G. Aznauryan *et al.* [CLAS Collaboration], Phys. Rev. C **80**, 055203 (2009).
[165] D. Drechsel, S. S. Kamalov and L. Tiator, Eur. Phys. J. A **34**, 69 (2007).
[166] M. Döring, C. Hanhart, F. Huang, S. Krewald and U. G. Meissner, Phys. Lett. B **681**, 26 (2009).
[167] A. V. Anisovich, E. Klempt, V. A. Nikonov, M. A. Matveev, A. V. Sarantsev and U. Thoma, Eur. Phys. J. A **44**, 203 (2010).
[168] I. G. Aznauryan, V. D. Burkert, arXiv:1109,1720, 2011.
[169] L. Tiator, D. Drechsel, S.S. Kamalov, and M. Vanderhaeghen, arXiv:1109,6745, 2011.
[170] V. B. Berestetskii and M. V. Terent'ev, Sov. J. Nucl. Phys., **24**, 1044 (1976); **25**, 347 (1977).
[171] I. G. Aznauryan, A. S. Bagdasaryan, and N. L. Ter-Isaakyan, Phys. Lett. B **112**, 393 (1982); Yad. Fiz. **36**, 1278 (1982).
[172] I. G. Aznauryan, Phys. Lett. B **316**, 391 (1993); Z. f*ü*r Phys. A **346**, 297 (1993).
[173] G. A. Miller, Phys. Rev. C **66**, 032201 (2002).
[174] H. J. Melosh, Phys. Rev. D **9**, 1095 (1974).
[175] R. Koniuk and N. Isgur, Phys. Rev. D **21**, 1868 (1980).
[176] S. Godfrey and N. Isgur, Phys. Rev. D **32**, 189 (1985).
[177] S. Capstick and N. Isgur, Phys. Rev. D **34**, 2809 (1986).
[178] M. K. Jones et al., Phys. Rev. Lett. **84**, 1398 (2000).
[179] O. Gayou et al., Phys. Rev. Lett. **88**, 092301 (2002).
[180] A. F. Sill et al., Phys. Rev. D **48**, 29 (1993).
[181] W. Bartel et al., Nucl. Phys. B **58**, 429 (1973).
[182] R. Madey et al., Phys. Rev. Lett. **91**, 122002 (2003).
[183] S. Riordan et al., Phys. Rev. Lett. **105**, 262302 (2010).
[184] B. Anderson et al., Phys. Rev. C **75**, 043003 (2007).
[185] J. Lachniet et al., Phys. Rev. Lett. **102**, 192001 (2009).
[186] S. Rock et al., Phys. Rev. Lett. **49**, 1139 (1982).

[187] S. Stave et al., Eur. Phys. J. A **30** 471 (2006).
[188] N.F. Sparveris et al., Phys. Lett. B **651** 102 (2007).
[189] S. Stave et al., Phys. Rev. C **78** 025209 (2008).
[190] C. Mertz et al., Phys. Rev. Lett. **86** 2963 (2001).
[191] C. Kunz et al., Phys. Lett. B **564** 21 (2003).
[192] N.F. Sparveris et al., Phys. Rev. Lett. **94** 022003 (2005).
[193] V.V. Frolov et al., Phys. Rev. Lett. **82** 45 (1999).
[194] A.N. Villano et al., Phys. Rev. C **80** 035203 (2009).
[195] J. J. Kelly et al., Phys. Rev. Lett. **95** 102001 (2005).
[196] J. J. Kelly et al., Phys. Rev. C **75** 025201 (2007).
[197] V.I. Mokeev et al., Phys. Rev. C **80** 045212 (2009).
[198] R. Thompson et al., CLAS Collaboration, Phys. Rev. Lett. **86**, 1702 (2001).
[199] C.S. Armstrong et al., Phys. Rev. D **60** 052004 (2009).
[200] M.M. Dalton et al., Phys. Rev. C **80** 015205 (2009).
[201] I.G. Aznauryan, V.D. Burkert, H. Egiyan, et al., Phys. Rev. C **71** 015201 (2005).
[202] I. G. Aznauryan and A. S. Bagdasaryan, Sov. J. Nucl. Phys. **41**, 158 (1985).
[203] B. D. Keister, Phys. Rev. D **49**, 1500 (1994).
[204] M.S. Bhagwat et al., Phys. Rev. C **68** 015203 (2003).
[205] K. G. Wilson, Phys. Rev. D **10**, 2445 (1974).
[206] J. M. Cornwall, Phys. Rev. D **26**, 1453 (1982).
[207] J. M. Maldacena, Int. J. Theor. Phys. **38**, 1113 (1999) [arXiv:hep-th/9711200].
[208] G. F. de Teramond and S. J. Brodsky, Phys. Rev. Lett. **102**, 081601 (2009) [arXiv:0809.4899 [hep-ph]].
[209] S. J. Brodsky, H. C. Pauli and S. S. Pinsky, Phys. Rept. **301**, 299 (1998) [arXiv:hep-ph/9705477].
[210] P. A. M. Dirac, Rev. Mod. Phys. **21**, 392 (1949).
[211] S. J. Brodsky and G. F. de Teramond, Phys. Rev. Lett. **96**, 201601 (2006) [arXiv:hep-ph/0602252].
[212] S. J. Brodsky and G. F. de Teramond, Phys. Rev. D **77**, 056007 (2008) [arXiv:0707.3859 [hep-ph]].
[213] J. Polchinski and M. J. Strassler, JHEP **0305**, 012 (2003) [arXiv:hep-th/0209211].
[214] S. J. Brodsky and G. F. de Teramond, Phys. Rev. D **78**, 025032 (2008) [arXiv:0804.0452 [hep-ph]].
[215] Z. Abidin and C. E. Carlson, Phys. Rev. D **77**, 095007 (2008), [arXiv:0801.3839 [hep-ph]].
[216] J. Polchinski and M. J. Strassler, Phys. Rev. Lett. **88**, 031601 (2002) [arXiv:hep-th/0109174].
[217] S. J. Brodsky and G. R. Farrar, Phys. Rev. Lett. **31**, 1153 (1973).
[218] A. Karch, E. Katz, D. T. Son and M. A. Stephanov, Phys. Rev. D **74**, 015005 (2006) [arXiv:hep-ph/0602229].
[219] V. A. Matveev, R. M. Muradian and A. N. Tavkhelidze, Lett. Nuovo Cim. **7**, 719 (1973).
[220] M. Diehl, Nucl. Phys. Proc. Suppl. **161**, 49 (2006) [arXiv:hep-ph/0510221].
[221] I. G. Aznauryan, V. D. Burkert, G. V. Fedotov, B. S. Ishkhanov, V. I. Mokeev, Phys. Rev. C **72**, 045201 (2005) [hep-ph/0508057].
[222] I. G. Aznauryan *et al.* [CLAS Collaboration], Phys. Rev. C **78**, 045209 (2008) [arXiv:0804.0447 [nucl-ex]].
[223] C. Amsler *et al.* (Particle Data Group), Phys. Lett. B **667**, 1 (2008).
[224] S. J. Brodsky and G. F. de Teramond, World Scientific Subnuclear Series, **45**, 139 (2007) [arXiv:0802.0514 [hep-ph]].
[225] H. R. Grigoryan, A. V. Radyushkin, Phys. Rev. D **76**, 095007 (2007) [arXiv:0706.1543 [hep-ph]].
[226] G. F. de Teramond and S. J. Brodsky, Nucl. Phys. B, Proc. Suppl. **199**, 89 (2010) [arXiv:0909.3900 [hep-ph]].

[227] A. Vega, I. Schmidt, T. Gutsche, V. E. Lyubovitskij, Phys. Rev. D **83**, 036001 (2011) [arXiv:1010.2815[hep-ph]].
[228] H. R. Grigoryan, T.-S. H. Lee, H.-U. Yee, Phys. Rev. D **80**, 055006 (2009) [arXiv:0904.3710 [hep-ph]].
[229] N. Isgur and G. Karl, *Phys. Rev.* D **18**, 4187 (1978); *Phys. Rev.* D **19**, 2653 (1979).
[230] R. Bijker, F. Iachello and A. Leviatan, Ann. Phys. (N.Y.) **236**, 69 (1994)
[231] M. Ferraris, M.M. Giannini, M. Pizzo, E. Santopinto and L. Tiator, Phys. Lett. B **364**, 231 (1995).
[232] L. Ya. Glozman and D.O. Riska, Phys. Rep. C **268**, 263 (1996); L.Ya. Glozman, W. Plessas, K. Varga, R.F. Wagenbrunn, Phys. Rev. D **58**, 094030 (1998).
[233] U. Löring, K. Kretzschmar, B. Ch. Metsch, H. R. Petry, Eur. Phys. J. A **10**, 309 (2001); U. Löring, B.Ch. Metsch, H. R. Petry, Eur. Phys.J. A **10**, 395 (2001); 447 (2001).
[234] A. De RúIJjula, H. Georg, S.L. Glashow, Phys. Rev. D **12**, 147 (1975).
[235] F. Güersey and L.A. Radicati, Phys. Rev. Lett. **13**, 173 (1964).
[236] Gunnar S. Bali et al., Phys. Rev. D **62**, 054503 (2000); Gunnar S. Bali, Phys. Rep. **343**, 1 (2001).
[237] C. Alexandrou, P. de Forcrand, O. Jahn, Nucl. Phys. Proc. Suppl. **119**, 667 (2003).
[238] H. Suganuma, T.T. Takahashi, F. Okiharu, H. Ichie, hep-lat/0407014.
[239] K. Glantschnig, R. Kainhofer, W. Plessas, B. Sengl, R.F. Wagenbrunn, Eur.Phys.J.A **23**, 507 (2005).
[240] L. A. Copley, G. Karl and E. Obryk, Phys. Lett. **29**, 117 (1969).
[241] S. Capstick, Phys. Rev. D **46**, 2864 (1992).
[242] F. Cardarelli, E. Pace, G. Salmè, S. Simula, Phys. Lett. B **371**, 7 (1996).
[243] F. Cardarelli, E. Pace, G. Salmè, S. Simula, Phys. Lett. B **397**, 13 (1997).
[244] D. Merten, U. Loring, K. Kretzschmar, B. Metsch and H. R. Petry, Eur. Phys. J. A **14** (2002) 477.
[245] T. Van Cauteren, J. Ryckebusch, B. Metsch, H-R. Petry, Eur.Phys. J. A **26**, 339 (2005).
[246] M. Aiello, M. M. Giannini, E. Santopinto, J. Phys. G: Nucl. Part. Phys. **24**, 753 (1998).
[247] E. Santopinto and M.M. Giannini, A systematic study of longitudinal and transverse helicity amplidutes in the hypercentral Constituent Quark Model, in preparation.
[248] M. De Sanctis, E. Santopinto, M.M. Giannini, Eur. Phys. J. A **1**, 187 (1998).
[249] M. De Sanctis, M.M. Giannini, L. Repetto, E. Santopinto, Phys. Rev. C **62**, 025208 (2000).
[250] M.De Sanctis, M.M. Giannini, E. Santopinto, A. Vassallo, Phys. Rev. C **76**, 062201 (2007).
[251] M. De Sanctis, E. Santopinto, M.M. Giannini, Eur. Phys. J. A **2**, 403 (1998).
[252] E. Santopinto, F. Iachello and M.M. Giannini, Nucl. Phys. A **623**, 100c (1997); Eur. Phys. J. A **1**, 307 (1998).
[253] L. Tiator, D. Drechsel, S. Kamalov, M.M. Giannini, E. Santopinto, A. Vassallo, Eur. Phys. J. A **19** (Suppl.1), 55 (2004).
[254] D. Y. Chen, Y. B. Dong, M. M. Giannini, E. Santopinto, Nucl. Phys. A **782**, 62 (2007).
[255] P. Geiger and N. Isgur, Phys. Rev. Lett. **67**, 1066 (1991); Phys. Rev. D **44**, 799 (1991); Phys. Rev. **D 47**, 5050 (1993); P. Geiger and N. Isgur, Phys. Rev. D **55**, 299 (1997).
[256] R. Bijker and E. Santopinto, AIP Conf. Proc. **947**, 168 (2007); Phys.Rev. C **80**, 065210 (2009); AIP Conf.Proc.**1116**, 93 (2009) and **1265**, 240 (2010); E. Santopinto and R.Bijker, Few Body Syst. **44**, 95 (2008); AIP Conf.Proc. **1056**, 95 (2008) and **1354**, 135 (2011); Phys.Rev. C **82**, 062202 (2010); E. Santopinto, R.Bijker and J. Ferretti, Few Body Syst. **50**, 199 (2011).
[257] C.S. An, Q.B. Li, D.O. Riska, B.S. Zou, Phys. Rev. C **74**, 055205 (2006), Erratum-ibid. C **75**, 069901 (2007); C. S. An, B. Zou, Eur. Phys. J. A **39**, 195 (2009); B.Julia-Diaz, D.O.Riska, Nucl. Phys. A **780**, 175 (2006).
[258] V. Mokeev, Invited talk at the 8th International Workshop on the Physics of Excited Nucleons May 17-20, 2011 Thomas Jefferson National Accelerator Facility Newport News, Virginia USA

[259] S. J. Brodsky and G. R. Farrar, Phys. Rev. D **11**, 1309 (1975); G. P. Lepage and S. J. Brodsky, Phys. Rev. Lett. **43**, 545 (1979).
[260] E. Santopinto, A. Vassallo, M.M. Giannini, M. De Sanctis, Phys. Rev. C **82**, 065204 (2010).
[261] O. Gayou *et al.* , Phys. Rev. C **64**, 038202 (2001);
B. D. Milbrath *et al.*, Phys. Rev. Lett. **80** (1998) 452 [Erratum-ibid. **82** (1999) 2221]; T. Pospischil *et al.*; V. Punjabi *et al.*, Phys. Rev. C **71**, 055202 (2005); A.J.R. Puckett et al. Phys. Rev. Lett. **104**, 242301 (2010).
[262] R. Petronzio, S. Simula, G. Ricco, Phys. Rev. D **67**, (2003) 094004.
[263] R. Gothe, V. Mokeev, et al., Jlab experiment E1209003, "Nucleon Resonance Studies with CLAS12", $www.jlab.org/exp\_prog/12GEV\_EXP$
[264] V. D. Burkert et al., J. Phys: Conf. Ser. **299**, 012008 (2011).
[265] I. G. Aznauryan and V. D. Burkert, arXiv:1109.1220.
[266] I. G. Aznauryan, V. D. Burkert, and V. I. Mokeev, arXiv:1108.1125 [nucl-ex].
[267] I. G. Aznauryan, Phys. Rev. C **76**, 025212 (2007).
[268] I. T. Obukhovky et al., Phys. Rev. D **84**, 014004 (2011).
[269] H. Kamano and T-S.H.Lee, arXiv:1108.0324[nucl-th].
[270] I. G. Aznauryan, Phys. Rev. C **67**, 0152009 (2003).
[271] R. L. Walker, Phys. Rev. **182**, 1729 (1969).
[272] M. Guidal, J.-M. Laget, and M. Vanderhaeghen, Nucl. Phys. A **627**, 645 (1997).
[273] M. Guidal, J.-M. Laget, and M. Vanderhaeghen, Phys. Lett. B **400**, 6 (1997).
[274] K. Park et al., CLAS Collaboration, Phys. Rev. C **77**, 015208 (2008).
[275] G. V. Fedotov et al., CLAS Collaboration, Phys. Rev. C **79**, 015204 (2009).
[276] M. Ripani et al., CLAS Collaboration, Phys. Rev. Lett. **91**, 022002 (2003)
[277] I. J. R. Aitchison, Nucl. Phys. A **189**, 417 (1972).
[278] M. Ripani et al., Nucl. Phys. A **672**, 220 (2000).
[279] V. I. Mokeev et al., Phys. of Atom. Nucl. **70**, 427 (2007).
[280] V. I. Mokeev et al., in "Proc. of the Workshop on the Physics of Excited Nucleon. NSTAR2005", ed. by S.Capstick, V.Crede, P.Eugenio, World Scientific Publishing Co.,hep-ph/0512164, p. 47.
[281] V. I. Mokeev et al., in "Proceedings of the 11th Workshop on the Physics of Excited Nucleons. NSTAR2007", Springer 2008, ed. by H-W. Hammer, V.Kleber, U.Thoma, H. Schmieden, p. 76.
[282] I. J. R Aitchison and J. J. Brehm, Phys. Rev. D **17**, 3072 (1978).
[283] V. I. Mokeev, N^* electrocouplings and $N\pi\pi$ hadronic decay widths from phenomenological analysis of the CLAS $\pi^+\pi^- p$ electroproduction data, the invited talk at Sixth International Workshop on Pion-Nucleon Partial -Wave Analysis and the Interpretation of Baryon Resonances, 23-27 May, 2011, Washington, DC, USA, $gwdac.phys.gwu.edu/pwa2011/PWAhome.htm$
[284] M. Dugger et al., CLAS Collaboration, Phys. Rev. C **79**, 065206 (2009).
[285] V. D. Burkert et al., Phys. Rev. C **67**, 035204 (2003).
[286] E. L. Isupov, Two pion cross sections from e1-6 data, CLAS Hadron Spectroscopy Group Meeting, $wwwold.jlab.org/Hall-B/claschair/agendas/clasagenda\_march10.html$
[287] S. V. Goloskokov, P. Kroll, Eur. Phys. J. C **53**, 367 (2008) [arXiv:0708.3569 [hep-ph]].
[288] S. V. Goloskokov, P. Kroll, Eur. Phys. J. C **65**, 137-151 (2010). [arXiv:0906.0460 [hep-ph]].
[289] S. V. Goloskokov, P. Kroll, Eur. Phys. J. A **47**, 112 (2011). [arXiv:1106.4897 [hep-ph]].
[290] P. .Hagler *et al.* [LHPC Collaboration], Phys. Rev. D **77**, 094502 (2008) [arXiv:0705.4295 [hep-lat]].
[291] H. Moutarde and F. Sabatié, private communication
[292] K. Goeke, M. V. Polyakov, M. Vanderhaeghen, Prog. Part. Nucl. Phys. **47**, 401-515 (2001). [hep-ph/0106012].

[293] A. V. Belitsky, A. V. Radyushkin, Phys. Rept. **418**, 1-387 (2005). [hep-ph/0504030].
[294] H.-W. Lin (2011), 1106.1608.
[295] M. Mahbub, W. Kamleh, D. B. Leinweber, A. O Cais, and A. G. Williams, Phys.Lett. B **693**, 351 (2010), 1007.4871.
[296] M. Mahbub, A. O. Cais, W. Kamleh, D. B. Leinweber, and A. G. Williams, Phys.Rev. D **82**, 094504 (2010), 1004.5455.
[297] G. P. Engel, C. Lang, M. Limmer, D. Mohler, and A. Schafer (BGR [Bern-Graz-Regensburg] Collaboration), Phys.Rev. D **82**, 034505 (2010), 1005.1748.
[298] N. Mathur, Y. Chen, S. Dong, T. Draper, I. Horvath, et al., Phys.Lett. B **605**, 137 (2005), hep-ph/0306199.
[299] R. G. Edwards, B. Joo, and H.-W. Lin, Phys. Rev. D **78**, 054501 (2008), arXiv:0803.3960.
[300] H.-W. Lin et al. (Hadron Spectrum), Phys. Rev. D **79**, 034502 (2009), arXiv:0810.3588.
[301] R. G. Edwards, J. J. Dudek, D. G. Richards, and S. J. Wallace (2011), to be published in Phys. Rev. D., 1104.5152.
[302] M. S. Mahbub, W. Kamleh, D. B. Leinweber, P. J. Moran, and A. G. Williams (2010), 1011.5724.
[303] J. J. Dudek, R. G. Edwards, M. J. Peardon, D. G. Richards, and C. E. Thomas, Phys. Rev. Lett. **103**, 262001 (2009), 0909.0200.
[304] J. J. Dudek et al., Phys. Rev. D **82**, 034508 (2010), 1004.4930.
[305] J. J. Dudek, R. G. Edwards, B. Joo, M. J. Peardon, D. G. Richards, et al., Phys.Rev. D **83**, 111502 (2011), 1102.4299.
[306] J. J. Dudek (2011), to be published in Phys. Rev. D., 1106.5515.
[307] M. Anselmino, E. Predazzi, S. Ekelin, S. Fredriksson, and D. B. Lichtenberg, Rev. Mod. Phys. **65**, 1199 (1993).
[308] S. Capstick and W. Roberts, Prog. Part. Nucl. Phys. 45, S **241** (2000), nucl-th/0008028.
[309] J. L. Goity, C. Schat, and N. N. Scoccola, Phys. Lett. B **564**, 83 (2003), hep-ph/0304167.
[310] D. B. Lichtenberg and L. J. Tassie, Phys. Rev. **155**, 1601 (1967).
[311] L. Glozman, Phys.Lett. B **475**, 329 (2000), hep-ph/9908207.
[312] C. E. Thomas, R. G. Edwards, and J. J. Dudek (2011), to be published in Phys. Rev. D., 1107.1930.
[313] M. Luscher, Nucl. Phys. B **364**, 237 (1991).
[314] M. Lage, U.-G. Meissner, and A. Rusetsky, Phys. Lett. B **681**, 439 (2009), 0905.0069.
[315] X. Feng, K. Jansen, and D. B. Renner (2010), 1011.5288.
[316] C. Kim, C. Sachrajda, and S. R. Sharpe, Nucl.Phys. B **727**, 218 (2005), hep-lat/0507006.
[317] J. J. Dudek, R. G. Edwards, N. Mathur, and D. G. Richards, Phys. Rev. D **77**, 034501 (2008), arXiv:0707.4162.
[318] J. J. Dudek, R. Edwards, and C. E. Thomas, Phys. Rev. D **79**, 094504 (2009), 0902.2241.
[319] H.-W. Lin, S. D. Cohen, R. G. Edwards, and D. G. Richards, Phys.Rev. D **78**, 114508 (2008), 0803.3020.
[320] H.-W. Lin and S. D. Cohen (2011), 1108.2528.
[321] H.-W. Lin and S. D. Cohen (2011), 1104.4319.
[322] H.-W. Lin, S. D. Cohen, R. G. Edwards, K. Orginos, and D. G. Richards, PoS LATTICE2008, **140** (2008), 0810.5141.
[323] S. Caracciolo, R. G. Edwards, A. Pelissetto, and A. D. Sokal, Phys.Rev.Lett. **75**, 1891 (1995), hep-lat/9411009.
[324] M. Guagnelli, F. Palombi, R. Petronzio, and N. Tantalo, Phys.Lett. B **546**, 237 (2002), hep-lat/0206023.
[325] D. Guazzini, R. Sommer, and N. Tantalo, JHEP 0801, **076** (2008), 0710.2229.

[326] D. Renner (2011), uSQCD proposal.
[327] G. P. Lepage, S. J. Brodsky, Phys. Rev. D **22**, 2157 (1980).
[328] V. L. Chernyak, A. R. Zhitnitsky, Phys. Rept. **112**, 173 (1984).
[329] X. -d. Ji, J. -P. Ma, F. Yuan, Nucl. Phys. B **652**, 383-404 (2003).
[330] X. -d. Ji, J. -P. Ma, F. Yuan, Eur. Phys. J. C **33**, 75-90 (2004).
[331] V. Braun, R. J. Fries, N. Mahnke, E. Stein, Nucl. Phys. B **589**, 381-409 (2000).
[332] V. M. Braun, A. N. Manashov, J. Rohrwild, Nucl. Phys. B **807**, 89-137 (2009).
[333] A. V. Belitsky, X. -d. Ji, F. Yuan, Phys. Rev. Lett. **91**, 092003 (2003). [hep-ph/0212351].
[334] M. Gockeler, R. Horsley, T. Kaltenbrunner, Y. Nakamura, D. Pleiter, P. E. L. Rakow, A. Schafer, G. Schierholz *et al.*, Phys. Rev. Lett. **101**, 112002 (2008).
[335] V. M. Braun *et al.* [QCDSF Collaboration], Phys. Rev. D **79**, 034504 (2009).
[336] T. Kaltenbrunner, M. Gockeler, A. Schafer, Eur. Phys. J. C **55**, 387-401 (2008).
[337] M. Gockeler *et al.* [QCDSF and UKQCD Collaborations], Nucl. Phys. B **812**, 205-242 (2009).
[338] S. Krankl, A. Manashov, Phys. Lett. B **703**, 519-523 (2011).
[339] F. X. Lee, D. B. Leinweber, Nucl. Phys. Proc. Suppl. **73**, 258-260 (1999).
[340] R. W. Schiel *et al.* [QCDSF Collaboration], arXiv:1112.0473 [hep-lat].
[341] M. Gruber, Phys. Lett. B **699**, 169 (2011).
[342] P. Wein, P. C. Bruns, T. R. Hemmert, A. Schafer, [arXiv:1106.3440 [hep-ph]].
[343] A. Duncan, A. H. Mueller, Phys. Rev. D **21**, 1636 (1980).
[344] N. Kivel, M. Vanderhaeghen, Phys. Rev. D **83**, 093005 (2011).
[345] V. M. Braun, A. Lenz, N. Mahnke, E. Stein, Phys. Rev. D **65**, 074011 (2002).
[346] I. I. Balitsky, V. M. Braun, A. V. Kolesnichenko, Nucl. Phys. B **312**, 509 (1989).
[347] V. L. Chernyak, I. R. Zhitnitsky, Nucl. Phys. B **345**, 137 (1990).
[348] M. A. Shifman, A. I. Vainshtein, V. I. Zakharov, Nucl. Phys. B **147**, 385 (1979).
[349] P. Ball and R. Zwicky, Phys. Rev. D **71**, 014015 (2005).
[350] G. Duplancic, A. Khodjamirian, T. Mannel, B. Melic and N. Offen, JHEP **0804**, 014 (2008).
[351] V. M. Braun, arXiv:hep-ph/9801222.
[352] P. Colangelo and A. Khodjamirian, arXiv:hep-ph/0010175.
[353] V. M. Braun, A. Lenz, M. Wittmann, Phys. Rev. D **73**, 094019 (2006).
[354] V. M. Braun, A. Lenz, G. Peters and A. V. Radyushkin, Phys. Rev. D **73**, 034020 (2006).
[355] A. Khodjamirian, C. .Klein, T. .Mannel and Y. -M. Wang, arXiv:1108.2971 [hep-ph].
[356] T. M. Aliev, K. Azizi and M. Savci, Eur. Phys. J. A **47**, 125 (2011).
[357] K. Passek-Kumericki, G. Peters, Phys. Rev. D **78**, 033009 (2008).
[358] V. M. Braun, A. N. Manashov, Phys. Rev. Lett. **107**, 202001 (2011).
[359] S. S. Agaev, V. M. Braun, N. Offen and F. A. Porkert, Phys. Rev. D **83**, 054020 (2011).